Northeast Atlantic Late Quaternary planktic Foraminifera as primary productivity and water mass indicators

Shirley A. van Kreveld

Kreveld, S.A. van. Northeast Atlantic Late Quaternary planktic Foraminifera as primary productivity and water mass indicators. — Scripta Geol., 113: 23-91, 18 figs., 12 pls, Leiden, December 1996.
S.A. van Kreveld, Center for Marine Earth Sciences, Institute of Earth Sciences, Free University, De Boelelaan 1085, 1081 HV Amsterdam, The Netherlands.

Keywords: Planktic Foraminifera, palaeo primary productivity, water mass, Northeast Atlantic.
Primary productivity and water mass reconstructions based on planktic Foraminifera reveal distinct interglacial/glacial variations for the past 208 ka in a mid-latitude Northeast Atlantic piston core. Average total planktic foraminiferal absolute frequencies and accumulation rates, which are interpreted to reflect primary productivity, are higher in interglacial than in glacial sediments. Low total planktic foraminiferal absolute frequencies and accumulation rates in 'Heinrich layers' are likewise interpreted to show low production of Foraminifera due to low surface ocean fertility.
'Heinrich layers' are enriched in ice-rafted debris, recording periods of massive iceberg production and rapid melting in the Northeast Atlantic. The dominance of *Neogloboquadrina pachyderma* (sinistral) in these layers reflects an extension of cold low salinity polar waters. The fresh water along with turbidity caused by melting icebergs may account for the low productivity during these events.
In contrast, the dominance of *Globigerina bulloides, Neogloboquadrina incompta, Globorotalia scitula, Globigerinita glutinata,* and *Globorotalia inflata* group in interglacial sediments is interpreted to reflect conditions comparable with the present day North Atlantic Current (NAC) waters in the area. In the modern ocean, the Gulf Stream and its extension, the NAC, are driven by seasonally strong westerly winds which induce mixing, supplying nutrients from deep to surface waters. Enough food and sufficient light combine to provide for pulses of algal blooms which support large populations of Foraminifera.
The important planktic foraminiferal test contributors in glacial sediments are not only *Turborotalita quinqueloba,* a subpolar species, but also polar and NAC indicator species. Primary productivity is inferred to be extremely seasonal, with low productivity during winter when there was little sunlight and partial ice cover.
Planktic Foraminifera are good primary productivity indicators in this carbonate-dominated, open-ocean Northeast Atlantic site. In contrast, organic carbon, which is directly linked to primary productivity and is extensively used as a proxy in upwelling areas, is unsuitable in this site because of the very low organic carbon content of the sediments and the contamination by terrigenous organic matter.

Contents

Introduction

The observed variability in atmospheric CO_2 concentrations during the Late Quaternary (Delmas et al., 1980; Barnola et al., 1987; Neftel et al., 1988) is attributed, at least in part, to changes in surface water productivity and ocean circulation (Broecker, 1992). Primary producers, such as coccolithophorids, can act as a 'biological pump' (Berger et al., 1987) by drawing down both surface water and atmospheric CO_2. Since biological productivity and ocean circulation are important in redistributing carbon in the ocean, palaeo primary productivity and surface water mass changes are reconstructed during the last glacial cycle in a mid-latitude open-ocean site. Although productivity is lower than in coastal upwelling areas, the large areal coverage of the open-ocean makes it an important factor in the global carbon budget (Milliman, 1993). These reconstructions are valuable in constraining global carbon cycle models.

This paper aims to reconstruct glacial to interglacial palaeo primary productivity and surface water mass variations in mid-latitude Northeast Atlantic using planktic foraminiferal accumulation rates and relative frequencies, respectively. For this purpose, I studied piston core T88-9P because it has a 208 ka sediment record and was unaffected by dissolution as it was recovered way above the lysocline. Moreover, this core is ideal for this study because it was recovered in mid-ocean where extensive coccolithophorid blooms presently occur (Brown & Yoder, 1994a), outside the influence of turbidity currents and at an optimum position for receiving debris discharged during iceberg melting.

Planktic Foraminifera can be used to reconstruct palaeo primary productivity variations from deep-sea cores because their fluxes are strongly correlated with surface ocean productivity (Thunell & Reynolds, 1984). Additionally, foraminiferal assemblages characterise distinct biogeographic zones which are intimately linked to particular water masses (Boltovskoy, 1959, 1962; Bé & Tolderlund, 1971; Vincent & Berger, 1981; Ottens, 1991), and as the tests of foraminiferal species are preserved in the sediments, they can be used to reconstruct past water mass changes. These were reconstructed by grouping the relative frequencies of the planktic foraminiferal species using cluster and correspondence analyses and then comparing these groups to present day plankton distribution and their associated water masses. Diversity indices were also calculated to aid in water mass reconstructions.

Aside from planktic Foraminifera, the organic carbon content of the sediments, which is primarily derived from biological production in surface waters, has also been extensively used as a primary productivity indicator (Müller & Suess, 1979; Betzer et al., 1984; Stein & Stax, 1991; Thunell et al., 1992; Sarnthein et al., 1992). In this paper, the usefulness of organic carbon as a fertility proxy in an open-ocean, mid-latitude Northeast Atlantic site is assessed.

Planktic foraminiferal assemblages preserved in deep-sea sediments have been extensively used to reconstruct (ecologic) water mass movements (CLIMAP, 1976, 1984). They were also used as a primary productivity proxy. For example, high frequency of *Globigerina bulloides* was utilised as an index for high productivity (Prell, 1984a) whilst the ratio of *Neogloboquadrina dutertrei* to *Pulleniatina obliquiloculata* was used as a qualitative fertility indicator (Berger & Killingley, 1977). Mix (1989) and Sarnthein et al. (1992) extended the one species based index to all the planktic Foraminifera by using transfer functions to arrive at quantitative estimates of primary production. The above proxies only use relative frequencies of planktic Foraminifera. This study is among the few providing data on planktic foraminiferal accumulations rates which can directly be compared with sediment trap flux data.

Other organisms, including benthic Foraminifera (Thomas et al., 1995; Herguera & Berger, 1991; Herguera, 1992, 1994; Berger et al., 1994), coccolithophorids (Pujos, 1992; Giraudeau & Rogers, 1994), diatoms (Sancetta, 1992; Schrader, 1992; Abrantes et al., 1994; Takahashi, 1994), and dinoflagellates (Lourens et al., 1992; Dale & Fjellsa, 1994; Versteegh, 1995), also serve as primary productivity proxies. Aside from microfossils, chemical tracers, such as carbonate (Brummer & van Eijden, 1992; van Kreveld et al., 1996), opal (Mortlock et al., 1991), barium (Dymond et al., 1992), and oxygen and carbon isotopes in planktic Foraminifera (Steens et al., 1992) have been also utilised as indicators of past surface water productivity.

Hydrography

The present day circulation of the North Atlantic is characterised by the southward flow of the cold East Greenland Current and the Labrador Current and the northeastern flow of the Gulf Stream (Fig. 1). The cold, low saline Labrador Current joins the warm saline extension of the Gulf Stream off Newfoundland to form the North Atlantic Current (NAC) (Dietrich et al., 1975; Krauss, 1986). The northern NAC component crosses the Mid-Atlantic Ridge at 52°N into the Northeast Atlantic (Krauss, 1986) (Fig. 1). The southern branch of the NAC heads towards the Azores and continues to Madeira (Mann, 1967; Käse & Siedler, 1984; Siedler et al., 1985). A transitional zone separates the anticyclonic (clockwise) gyre of subtropical waters to the south from the cyclonic (counterclockwise) gyre in the north (Krauss, 1986).

The surface water circulation is associated with polar, subpolar, NAC, transitional, and subtropical water masses (Fig. 1) (Krauss, 1986). The southern limit of the East Greenland Current approximately marks the present day polar front. The northern limit of the NAC approximates the subpolar front while its southern limit is associated with a transition zone, separating the subtropical waters to the south from the northern water mass (Krauss, 1986).

In contrast to modern times, oceanic surface water reconstructions for the last glacial maximum (Ruddiman & McIntyre, 1976; CLIMAP, 1981), show that ice-bear-

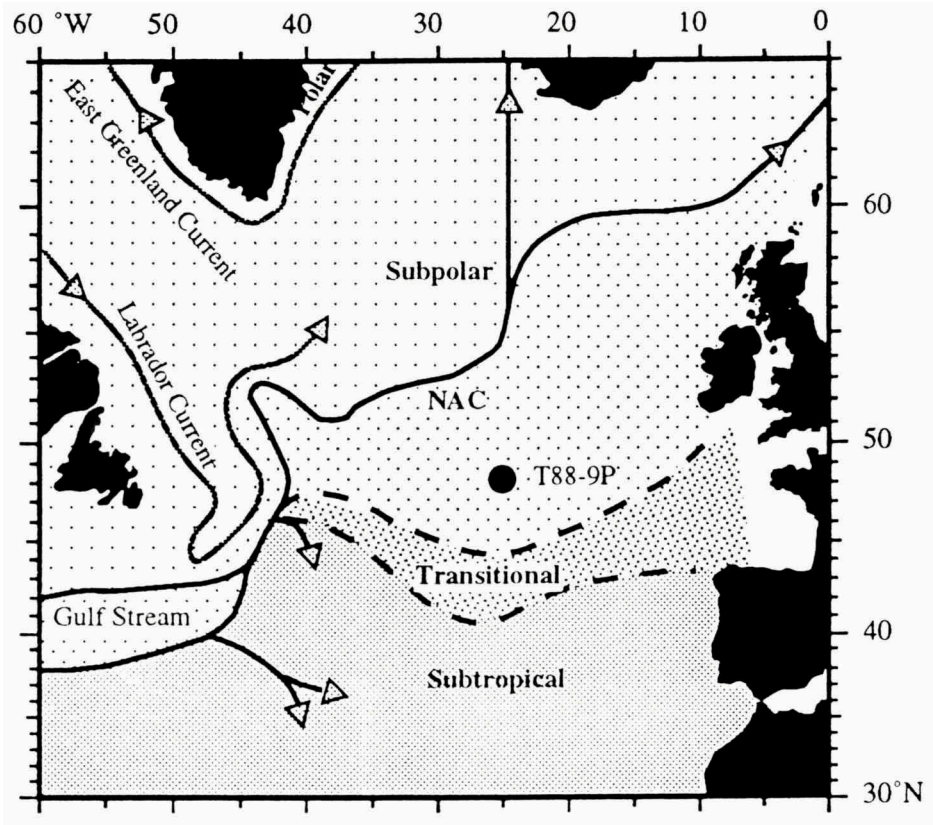

Fig. 1. Oceanographic map of the Northeast Atlantic Ocean depicting present day surface currents (Krauss, 1986) and their associated water masses. Filled circle shows the position of piston core T88-9P (48°23'2" N, 25°05'6" W; water depth = 3193 m; core length = 7.90 m). NAC stands for North Atlantic Current.

ing polar water covered the North Atlantic above latitude 45°N in a cold counterclockwise gyre (Fig. 2). A west-east oriented subpolar front developed at this latitude parallel to the eastern path of the Gulf Stream (equivalent to NAC) which was compressed to a narrow band between the clockwise subtropical gyre and the counterclockwise polar gyre (Fig. 2).

Material and methods

Piston core T88-9P (48°23'2" N, 25°05'6" W; recovery 790 cm) (Fig. 1) provides a good planktic foraminiferal record for the last 208 ka since it is well- preserved, continuous, and recovered well above the lysocline at 3193 m water depth. This core has undergone minimal carbonate dissolution as shown by the presence of aragonitic pteropod shells as well as fragile and juvenile planktic Foraminifera specimens with spines occasionally preserved, even during isotopic stage 2 when carbonate dissolu-

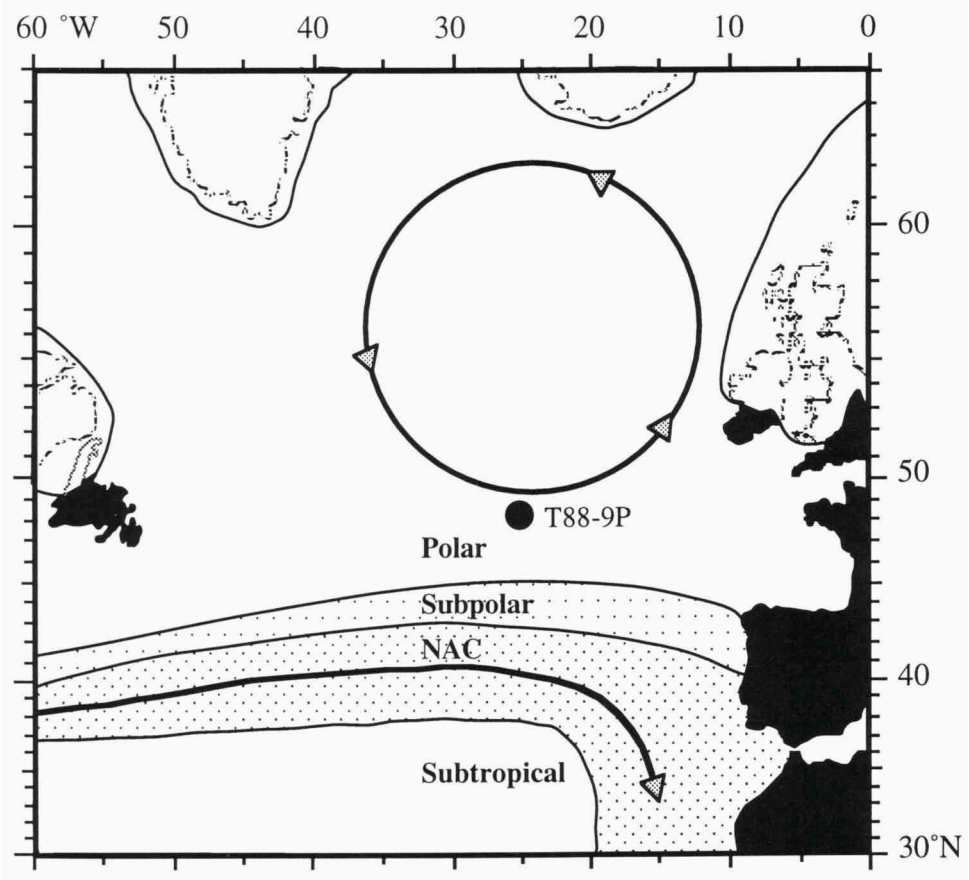

Fig. 2. Palaeoceanographic map of the Northeast Atlantic ocean showing inferred surface currents and water masses during the last glacial maximum (redrawn from Ruddiman & McIntyre, 1976 and CLIMAP, 1981). Bold lines show the ice extent.

tion was high (Crowley, 1981).

The core was collected in April, 1988 during the 'Actuomicropalaeontology Palaeoceanography North Atlantic Project' (APNAP- II) R/V Tyro cruise. It was sampled every 5 cm in the upper 50 cm and then at about 10 cm intervals. These 10 cm^3, 1 cm thick samples, totalling 83, were sieved through 125 µm mesh screens and the fractions were weighed. The >125 µm fraction was repeatedly split to obtain an aliquot of c. 300 specimens of planktic Foraminifera. There were 16 species found and the most common species are illustrated in plates 1-12. One sample (238 cm) did not contain any planktic Foraminifera.

The weight % carbonate of the bulk sediment was analysed with a ±2% precision by a modified Scheibler-type gasometric technique (Bruin, 1937).

Gray reflectance profiles were obtained by digitally scanning and measuring the relative reflectivity of the coloured core photograph (courtesy of L. Labeyrie and E. Cortijo, Centre des Faibles Radioactivités, Laboratoire mixte CNRS-CEA, Gif sur Yvette Cedex, France).

Dry bulk density was determined by weighing 5 cm^3 of sediment after drying at 50°C.

Three samples weighing c. 15 mg of >250 µm sized mixed planktic Foraminifera were dated by radiocarbon measurements using accelerator mass spectrometry (AMS).

Forty-six bulk samples were analysed in duplicate for organic carbon content using a Carlo Erba NA-1500 elemental analyser according to the method described by Nieuwehuize et al. (in press). These samples were oven-dried at 60 °C, then homogenised by thorough grounding in an agate mortar mill to reduce variability between duplicates. The organic carbon content was measured after removal of the inorganic carbon by acidification using 25% HCl in silver sample cups. Duplicate measurements were within ± 0.06%.

The accumulation rates of planktic Foraminifera were calculated using the following formulas:

(1) pfTAR = S*DBD*pf/g
(2) pfSAR = S*DBD*pf species/g

whereby:

pf/g=planktic Foraminifera per gram dry weight (no./g);
pfTAR=total planktic foraminiferal accumulation rate (no./cm^2ka);
pfSAR=planktic foraminiferal species accumulation rate (no./cm^2ka);
S=sedimentation rate (cm/ka);
DBD=dry bulk density; dry weight per wet volume (g/cm^3);

Cluster and correspondence analyses were used on the planktic Foraminifera relative frequency data matrix to determine systematic faunal changes through time. Both samples and species relative frequency were clustered separately using a weighted pair group cluster method on a correlation matrix (Davis, 1986).

Correspondence analysis (Hill, 1974; Davis, 1986; Bénzecri, 1992) is one of several ordination methods which reduces the dimensionality of large data matrices. It extracts eigenvectors from a chi-square weighted distance matrix calculated from the relative frequencies of the planktic foraminiferal species and the samples which are taken from different depth intervals in the core. Correspondence analysis has the advantage that samples and species scores are scaled so that both can be plotted in one graph, thus facilitating interpretation.

Diversity indices were calculated to document diversity trends through time. Simple diversity gives the number of species in a sample, the Shannon diversity index expressed as ($H'=-\sum p_i * \ln p_i$) takes into account the relative proportion of each species (p_i) in a sample (Shannon, 1949), and equitability ($E'=e^{H'}/s$ in which s is the number of species in a sample) measures the evenness of the species distribution in a sample (Buzas & Gibson, 1969). When one species dominates the foraminiferal assemblage, equitability approaches zero, while it is one when all species are present in equal proportions.

Results

Stratigraphy

The interglacial sediments of piston core T88-9P are coccolith and foraminiferal oozes whilst the glacial sediments are mostly calcareous sand, silt and clay (Fig. 3A).

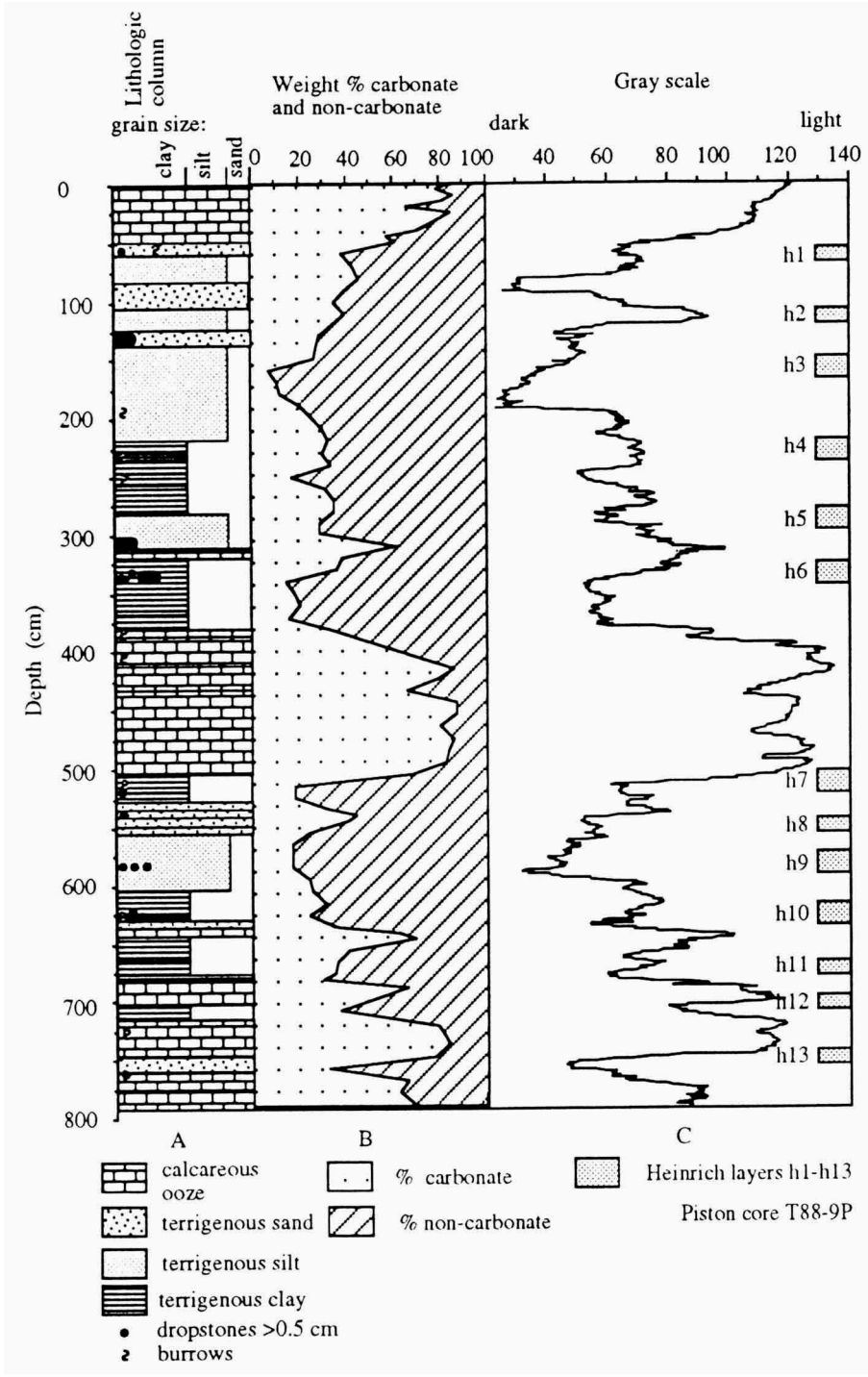

Fig. 3. Core T88-9P (A) lithologic column based on visual core description, (B) weight % carbonate content of the bulk sample and (C) gray reflectance profile plotted against depth. Light-coloured sediments have higher gray reflectances than dark-coloured ones, as shown by the higher numbers. Rectangles h1- h13 are intervals interpreted as Heinrich layers.

Thus, the former generally have a higher weight % bulk carbonate (up to 87%) while it can be as low as 7% in the latter (Fig. 3B). As a result of the varying carbonate content, the interglacial layers are cream to brown coloured and usually have higher gray reflectances than glacial layers which are olive gray to gray (Fig. 3C).

'Heinrich layers' are considered to record massive influxes of icebergs into the North Atlantic (Heinrich, 1988; Broecker et al., 1992; Bond et al., 1992; Grousset et al., 1993). Van Kreveld et al. (1996) identified thirteen intervals in the core which were interpreted as Heinrich layers based mainly on the high ice-rafted debris content and the presence of detrital carbonate. These layers also have very low planktic foraminiferal accumulation rates (>125 μm) with *N. pachyderma* sinistral (s) dominating the foraminiferal assemblage (van Kreveld et al., 1996). Most of these layers contain dropstones and have high dry bulk densities.

The Heinrich layers in core T88-9P were successively numbered from top to bottom and designated with a small letter h. The upper six correspond to those identified by Heinrich (1988). However, the lower seven identified in isotopic stages 6-7 are different from those of Heinrich (1988) which are in stage 5. Van Kreveld et al. (1996) discuss the differences in the timing of the Heinrich layers identified in nearby cores.

Heinrich layers h1, h2, h4 and h5 have higher gray reflectances than h3 (Fig. 3C), due to their higher detrital carbonate content. The detrital carbonate originates from limestone and dolomite bedrocks in eastern Canada (Andrews & Tedesco, 1992; Grousset et al., 1993).

Age model

The ages are based on three radiocarbon dates, on two ash layers and on the correlation of the oxygen isotope curves of *Globigerina bulloides* and *Globorotalia inflata* with the chronostratigraphy of Martinson et al. (1987) (Fig. 4A-C) (van Kreveld et al., 1996). The radiocarbon age of the surface sample was calibrated to a calendar date using the program Calib 3.0 (Stuiver & Reimer, 1993) which is based on the marine bidecadal data set of Stuiver & Braziunas (1993) while those of samples 128 cm (21 100 ± 300 years BP) and 148 cm (23 900 ± 300 years BP) were calibrated using Th-U ages obtained by mass spectrometry on corals (Bard et al., 1990, 1993) after subtracting 400 ^{14}C years for reservoir correction (Bard, 1988).

The chronology of the core was supplemented by the carbonate content percentage, *N. pachyderma* (s) frequency, coccolith abundance and gray scale records to identify isotopic stage boundaries 5/4 and 4/3. I also used the strong gradient in the carbon isotope curves of both *Globigerina bulloides* and *Globorotalia inflata* to identify the 5/4 boundary (Fig. 5A).

The depth to age conversion was modelled by linearly interpolating between the age control points by assuming uniform sedimentation rates to obtain the date for each sample (Fig. 5B). The sedimentation rates, which are generally higher for glacial than for interglacial sediments, vary from 2.2 cm/ka to 7.5 cm/ka. I assume that the Heinrich layers have the same sedimentation rate as the surrounding glacial sediments, therefore the planktic foraminiferal accumulation rate in Heinrich layers is a minimum estimate while it is a maximum estimate for glacial sediments. This

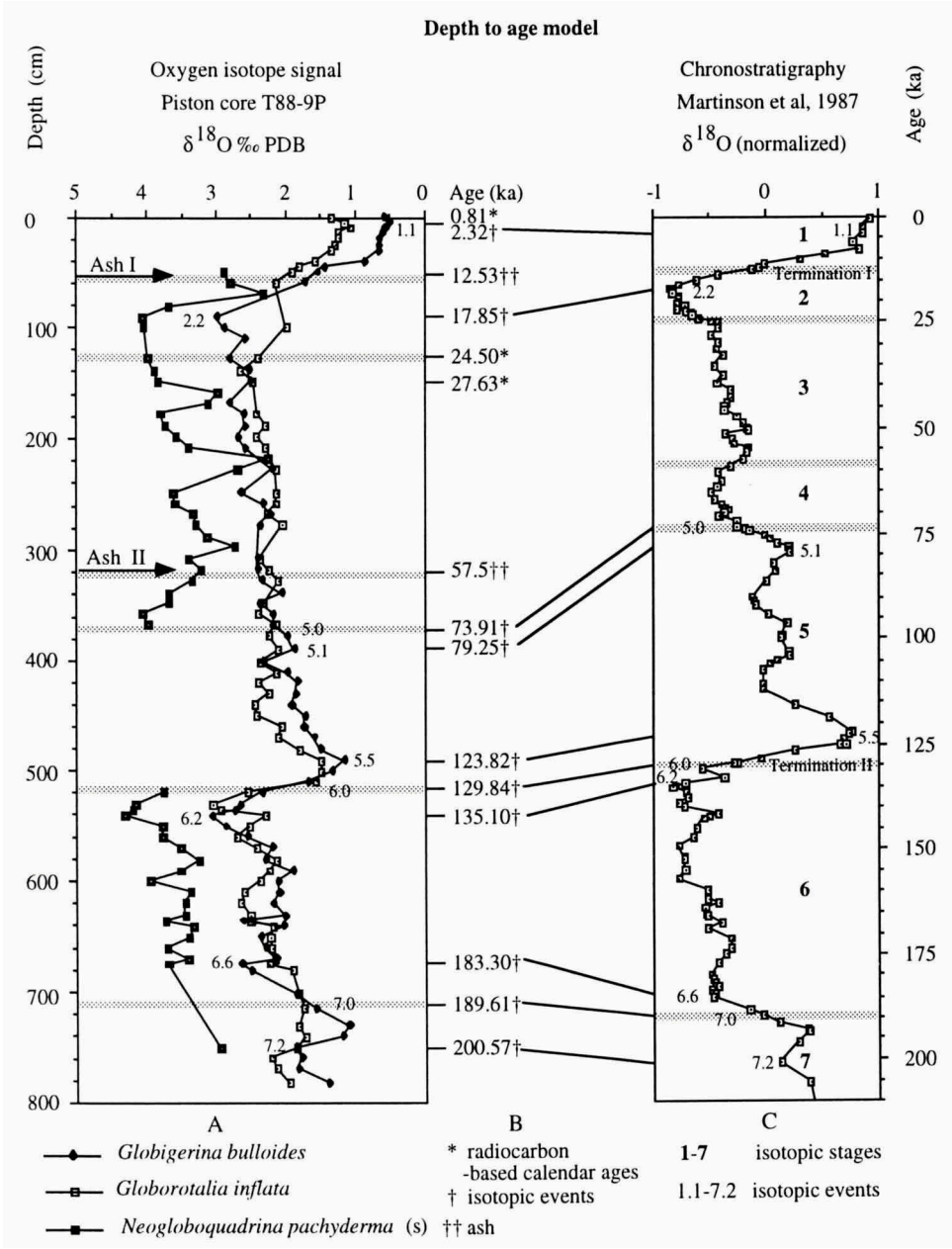

Fig. 4. (A) *Globigerina bulloides*, *Globorotalia inflata* and *Neogloboquadrina pachyderma* (s) oxygen isotope ratios. (B) Control points for depth to age transformation are mainly based on calendar-calibrated radiocarbon ages, ash layers and isotope stratigraphy. (C) Orbitally-based chronostratigraphy of Martinson et al. (1987), with the events and boundaries used for the age model. Stippled lines mark the isotopic stage boundaries.

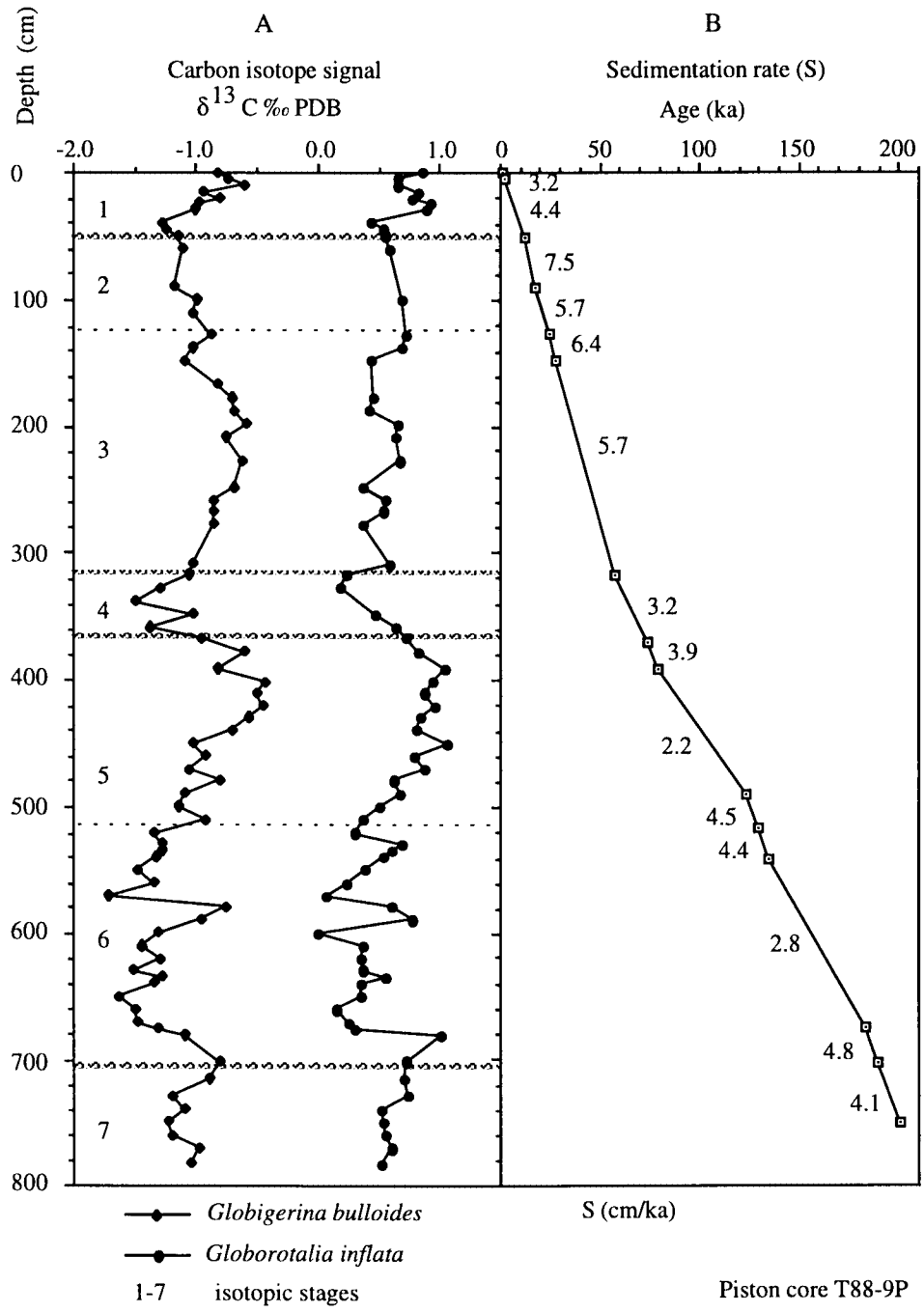

Fig. 5. (A) Carbon isotope ratios of *Globigerina bulloides* and *Globorotalia inflata* versus depth. Depth to age plot showing the sedimentation rate (cm/ka) between age control points.

assumption is supported by more detailed dating in nearby cores (Bond et al., 1992; Francois & Bacon, 1994) of the upper three Heinrich layers, which show similar or only slightly higher sedimentation rates.

The non-Heinrich layers of isotopic stages 7, 5 and 1 will subsequently be referred to as interglacial, and that of isotopic stages 6 and 4-2 as glacial.

>125 μm planktic foraminiferal frequencies and accumulation rates

The total planktic foraminiferal absolute frequencies (number of planktic foraminiferal specimens per gram bulk sediment) are generally higher in interglacial than in glacial sediments, averaging 36 800 and 21 200 specimens/g, respectively (Table 1; Fig. 6A). An interval in h4 was even devoid of Foraminifera. The highest absolute frequency is found in isotopic stage 5.

The total planktic foraminiferal accumulation rates show a similar pattern, which is higher in interglacial than glacial sediments, with a mean of 105 700 and 84 500 specimens/cm²ka, respectively (Table 1; Figs. 6B and 7B).

The planktic foraminiferal assemblage in piston core T88-9P sediments is dominated by seven species, viz. *N. pachyderma* (s), *Turborotalita quinqueloba*, *Globigerina bulloides*, *Neogloboquadrina incompta*, *Globorotalia scitula*, *Globigerinita glutinata*, and *Globorotalia inflata* (Figs. 6C and 8). Interglacial deposits have a low average relative frequency of *Neogloboquadrina pachyderma* (s) and generally high to moderate percentages of the other species. Glacial sediments have high relative frequencies of *N. pachyderma* (s) and *T. quinqueloba*, and moderate to low percentages of the other species while Heinrich layers are dominated by *N. pachyderma* (s).

Nine other species which do not exceed 4% of the total, include *Globorotalia hirsuta*, *Globigerinella aequilateralis*, *Globigerinoides ruber*, *Orbulina universa*, *Globorotalia truncatulinoides*, *Globigerina rubescens*, *Globigerinoides tenellus*, *Turborotalita humilis* and *Globigerinita uvula* (Figs. 6C and 8). These species are generally found in interglacial sediments and are rarely present in glacial deposits and Heinrich layers.

Neogloboquadrina pachyderma (s) averages 8.7% of the total planktic foraminiferal assemblage in interglacial, 44.6% in glacial, and 57.7% in Heinrich layers, corresponding to mean absolute frequencies of 3300, 9000, and 4400 specimens/g, respectively (Table 1; Figs. 6A and C). Although *N. pachyderma* (s) dominates in Heinrich layers, its absolute frequency is generally lower than in glacial sediments. It does not exceed 2500 specimens/g in the upper five Heinrich layers (h1-h5) though it may comprise up to 95% of the total foraminiferal fauna (compare Figs. 8 and 9). The absolute frequency of *N. pachyderma* (s) is generally high immediately before and after a Heinrich layer. The accumulation rate of *N. pachyderma* (s) is at least three times lower in interglacial than in glacial sediments (Fig. 10).

Although the average absolute frequency and accumulation rate of *T. quinqueloba* are higher in interglacial than in glacial sediments, its average relative frequency is slightly higher in the latter (Table 1; compare Figs. 6A and C). The average frequencies of this species are low in Heinrich layers (Figs. 8 and 9).

The average relative frequencies of *G. bulloides* are high (16.7%), moderate (13.4%), and low (7.3%) in interglacial, glacial and Heinrich layers corresponding to mean absolute frequencies of 5900, 2900 and 900 specimens/g, respectively (Table 1;

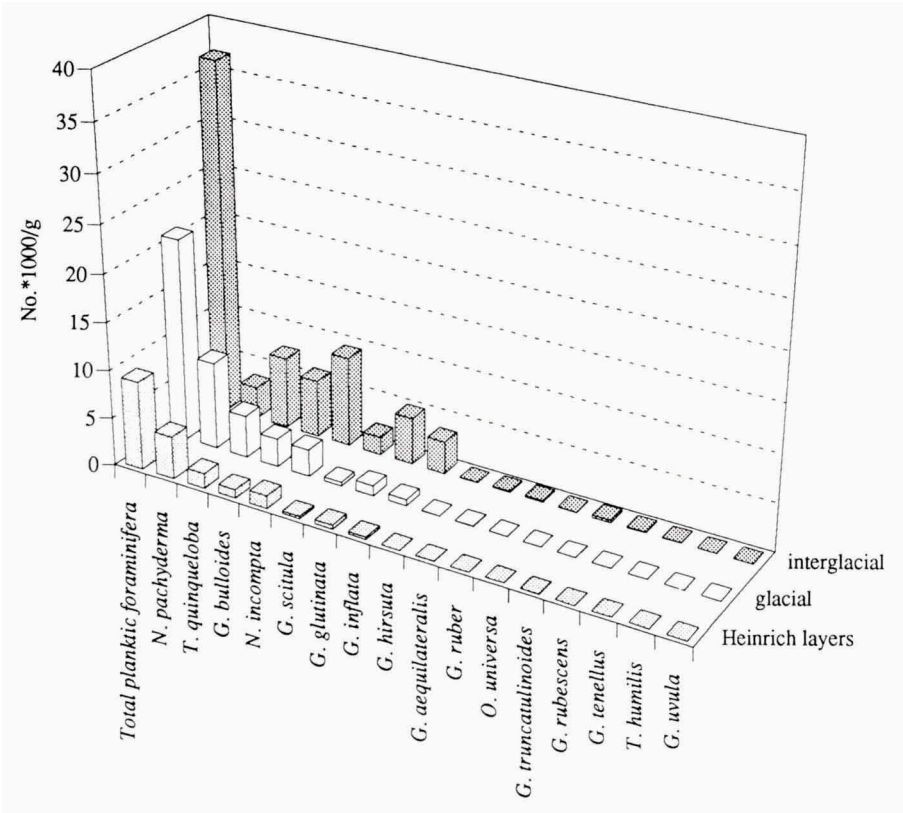

Fig. 6. (A) Absolute frequency (no.*1000/gram), (B) accumulation rate (no.*1000 /cm²ka) and (C) relative frequency (%) averages of the >125 μm planktic foraminifera in interglacial, glacial and Heinrich layers.

Figs. 6A and C). This species does not exceed 100 specimens/g in Heinrich layers h1-h5, even though it may comprise up to 20% of the planktic foraminiferal assemblage (Figs. 8 and 9). *G. bulloides* has a higher interglacial than glacial accumulation rate (Fig. 10).

Of all the planktic Foraminifera, *N. incompta* has the highest average frequencies and accumulation rate in interglacial sediments. Its average accumulation rate is more than two times higher in interglacial than in glacial layers (Table 1; Figs. 6B and 10).

Among the seven dominant species, *G. scitula* has the lowest average frequencies of only 5% and 1800 specimens/g in interglacial layers (Table 1, Figs. 6A and C). It is less frequent in glacial and Heinrich layers. The average accumulation rate of *G. scitula* is at least three times higher in interglacial than in glacial sediments (Figs. 6B and 10).

Both average relative and absolute frequencies of *G. glutinata* are moderate, low and very low in interglacial, glacial and Heinrich deposits, respectively (Table 1; Figs. 6A and C). The average accumulation rate of this species is about three times higher in interglacial than in glacial sediments (Figs. 6B and 10).

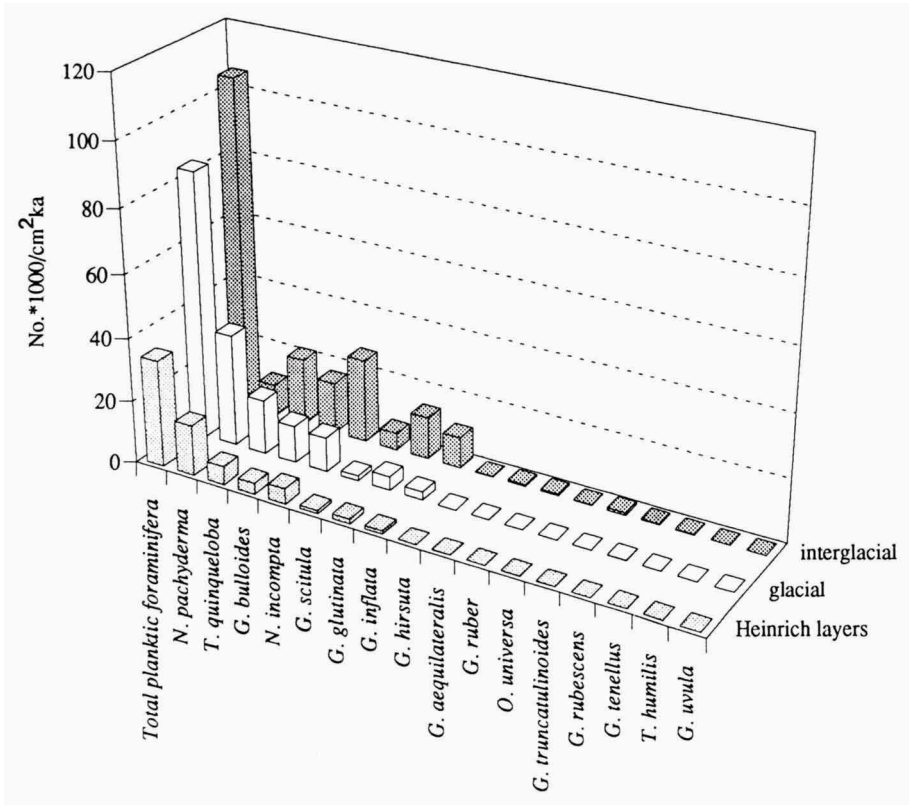

Globorotalia inflata shows decreasing average relative and absolute frequencies from interglacial, glacial to Heinrich layers of 9.7%, 2.9%, 1.8% and 3400, 600, 200 specimens/g, respectively (Table 1; Figs. 6A and C). The average accumulation rate of this species is about a factor four higher in interglacial than in glacial sediments.

Organic carbon

The total organic carbon content of the bulk sediment is very low, varying only from 0.06 to 0.22 % (Fig. 11). It is generally higher during isotopic stages 4 to 2 than in the other stages. Across Terminations I and II, and in most of the Heinrich layers the total organic carbon is low, except for Heinrich layers 3 and 6 which show peak maxima.

Cluster and correspondence analyses

Cluster analysis of the relative frequency data matrix shows five species clusters, I: *N. pachyderma* (s); II: *T. quinqueloba*; III: *G. bulloides, N. incompta, G. scitula, G. glutinata*, and *G. inflata*;IV: *G. ruber, G. aequilateralis*, and *G. hirsuta*; V: *G. truncatulinoides, G. rubescens, G. tenellus*, and *O. universa* (Fig. 12). Species with frequencies lower than 0.2% and the sample at 238 cm, which did not contain planktic Foraminifera, were excluded from all the analyses.

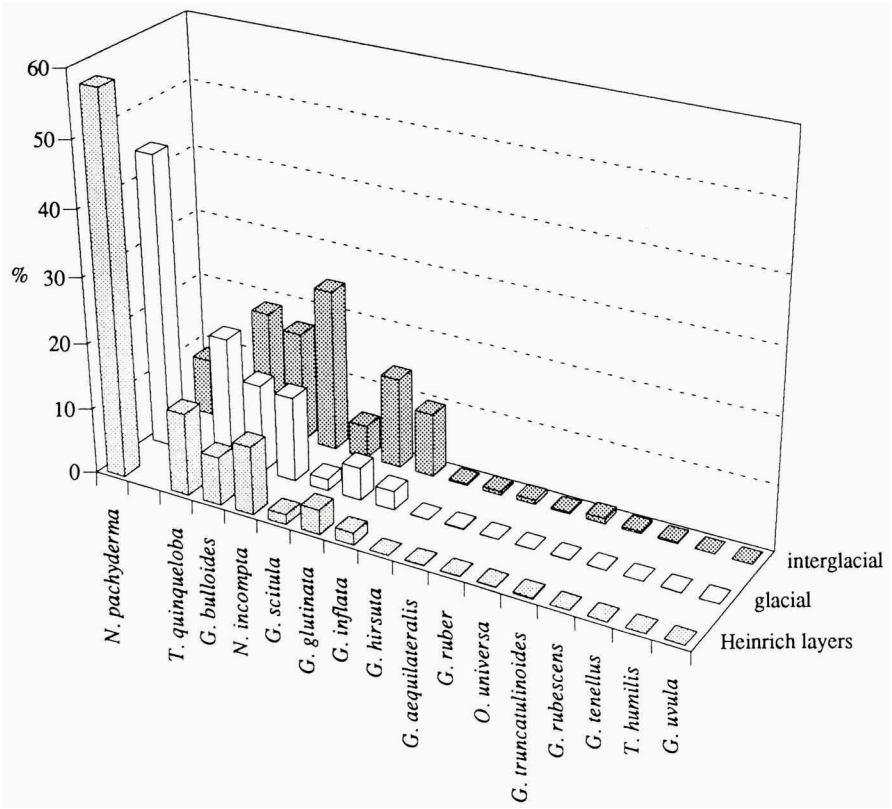

Sample clustering also showed five groups (Figs. 13 and 14A-B). Cluster A consists mostly of Heinrich and isotopic stages 2 and 6, with some stage 3 samples. Cluster B mostly combines samples from isotopic stages 3 and 6, with some from 4 and Heinrich layers. Clusters C and E generally consist of samples from isotopic stages 5 and 7 while cluster D is dominantly made up of isotopic stage 1 samples. These five sample clusters, represent 34, 11, 19, 8, and 10 of the total 82 samples corresponding to 42, 13, 23, 10, and 12%, respectively.

To relate species to sample clustering, the sum of the relative frequency of the species clusters in a sample (Fig. 14A) and the sample cluster designation (Fig. 14B) were plotted against time. In glacial intervals, cluster A is generally succeeded by cluster B and vice versa while during interglacial intervals, cluster C may either be succeeded by clusters D or E. Across Termination II, there is a drastic change from cluster I to V.

Figure 14A also shows that the sum of the relative frequency of the species clusters IV and V in a sample is only <10%. Therefore, clusters IV and V are of less importance and the interpretations are concentrated on clusters I to III.

The correspondence analysis more or less confirms the results of the cluster analysis though it is more difficult to interpret. The first correspondence analysis axis which is mainly controlled by *N. pachyderma* (s), explains 69% of the total variation (Figs. 15A and 16A). All other axes have only minor contributions (Figs. 15 B-C and 16A-B) although they distinguish groups that are similar to the clusters.

Table 1. Average relative frequency in %, absolute frequency in no./g and accumulation rate in no./cm²ka of the dominant planktic foramiferal species in interglacial, glacial and Heinrich layers. Average frequencies and accumulation rates of the dominant >125 µm planktic foraminiferal species.

Average relative frequency (%)			
	interglacial	glacial	Heinrich layers
N. pachyderma (s)	8.7	44.6	57.7
T. quinqueloba	18.6	19.2	12.6
G. bulloides	16.7	13.4	7.3
N. incompta	24.5	12.9	10.4
G. scitula	5.0	1.7	1.5
G. glutinata	13.7	4.9	3.8
G. inflata	9.7	2.9	1.8
Average absolute frequency (no./g)			
	interglacial	glacial	Heinrich layers
Total planktic foraminifera	36 800	21 200	9 200
N. pachyderma (s)	3 300	9 000	4 400
T. quinqueloba	7 400	4 300	1 600
G. bulloides	5 900	2 900	900
N. incompta	9 300	2 800	1 300
G. scitula	1 800	400	200
G. glutinata	4 800	1 000	400
G. inflata	3 400	600	200
Average accumulation rate (no./cm²ka)			
	interglacial	glacial	Heinrich layers
Total planktic foraminifera	105 700	84 500	34 000
N. pachyderma (s)	10 000	35 600	16 100
T. quinqueloba	21 200	17 400	5 900
G. bulloides	16 200	11 800	3 500
N. incompta	26 400	11 000	4 800
G. scitula	5 500	1 500	1 000
G. glutinata	13 600	4 300	1 600
G. inflata	9 900	2 600	1 000

Figures 16 A-B show the plots of the first three main factors that control the data set. The coordinates of the individual species or samples are indicative of their contribution to the variation of the particular axis. Correspondence axes 1 vs 2 and axes 1 vs 3 show five distinct groups corresponding to the species cluster (compare Figs. 16 A-B and 12). Fig. 16B and 15C show high positive and negative loadings on axis 3 of the species belonging to clusters V and IV, respectively (compare with Fig. 12). However, because no samples fall within these species range, IV and V are only of minor importance.

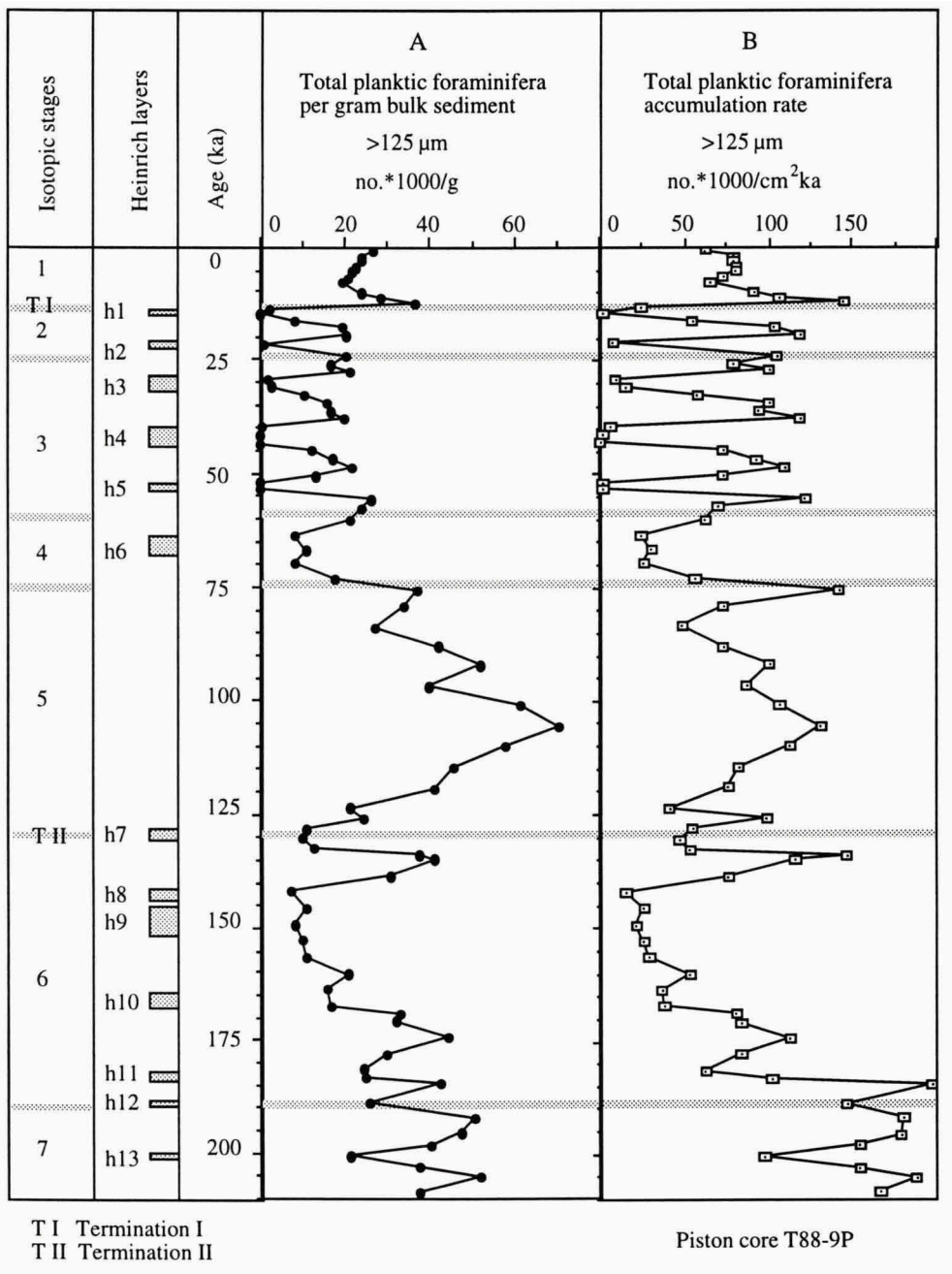

Fig. 7. (A) >125 µm total planktic foraminifera per gram bulk sediment and (B) accumulation rate in no.*1000/cm²ka plotted against age.

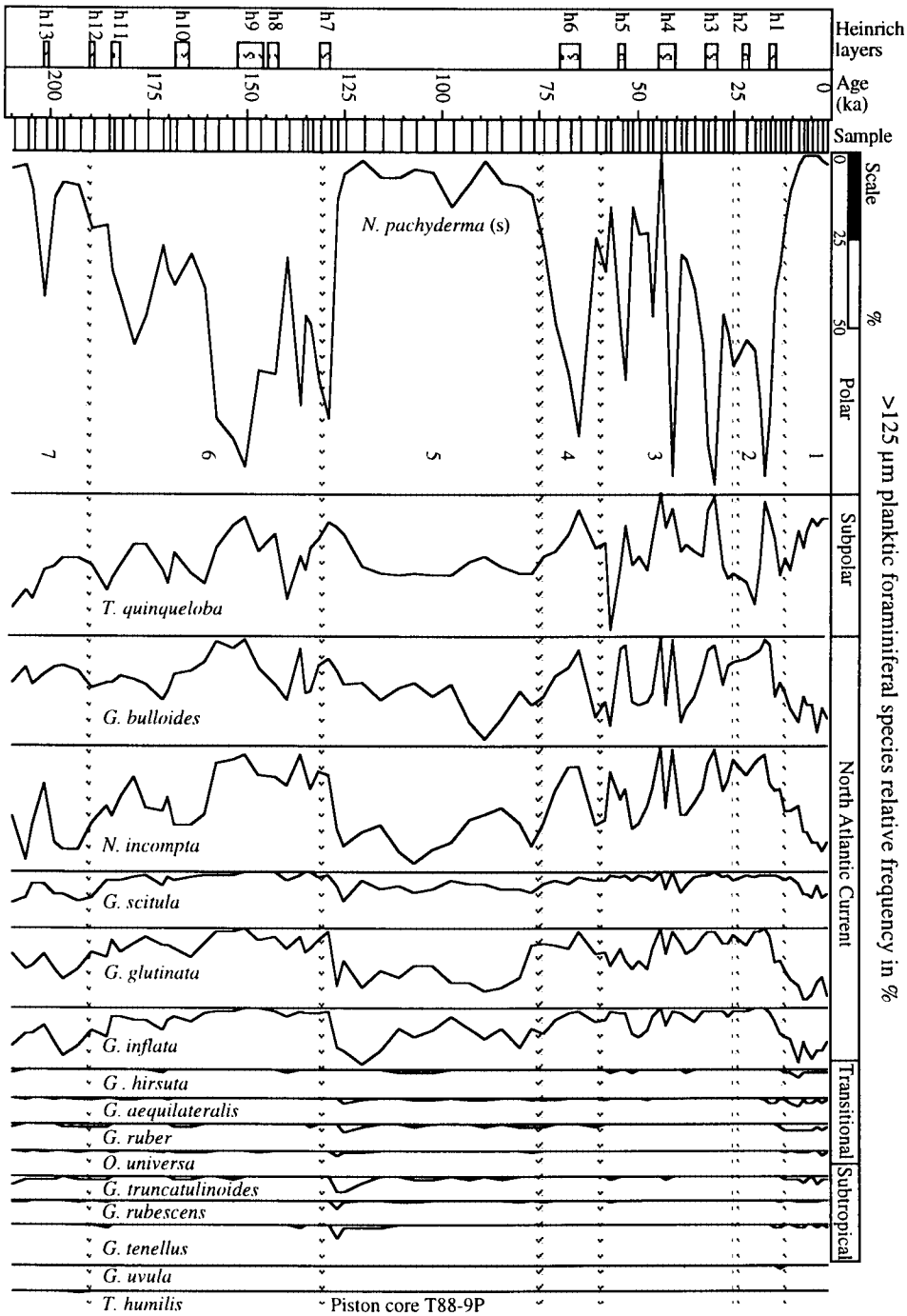

Fig. 8. >125 µm planktic foraminiferal species relative frequency in %, with the frequencies adding up to 100%. The water mass designation is based on clusters I-V of Fig. 12) with I-polar, II-subpolar, III-North Atlantic Current, IV- transitional, and V-subtropical. 1-7 are isotopic stages.

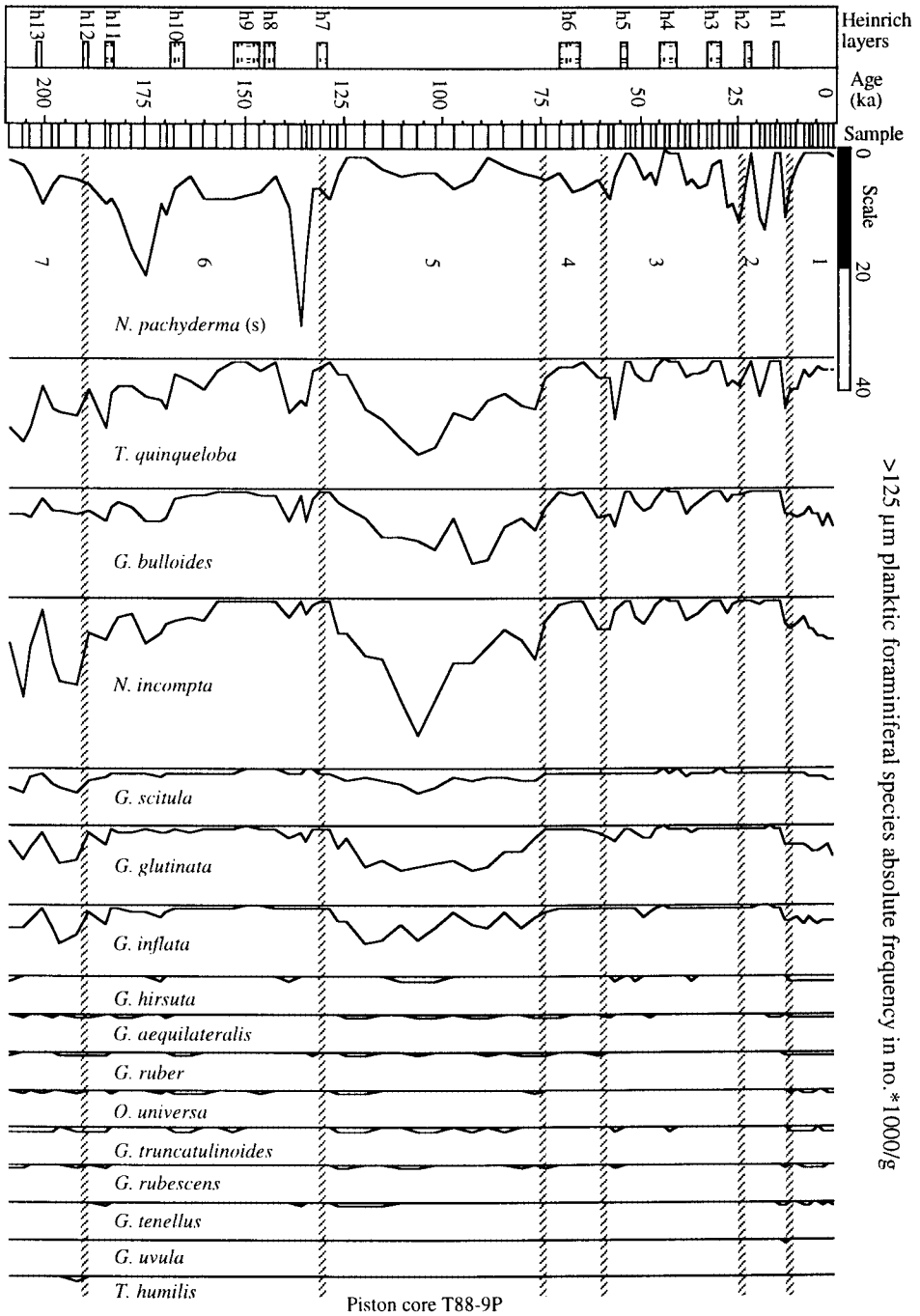

Fig. 9. >125 µm planktic foraminiferal species absolute frequency in no.*1000/g. 1-7 are isotopic stages.

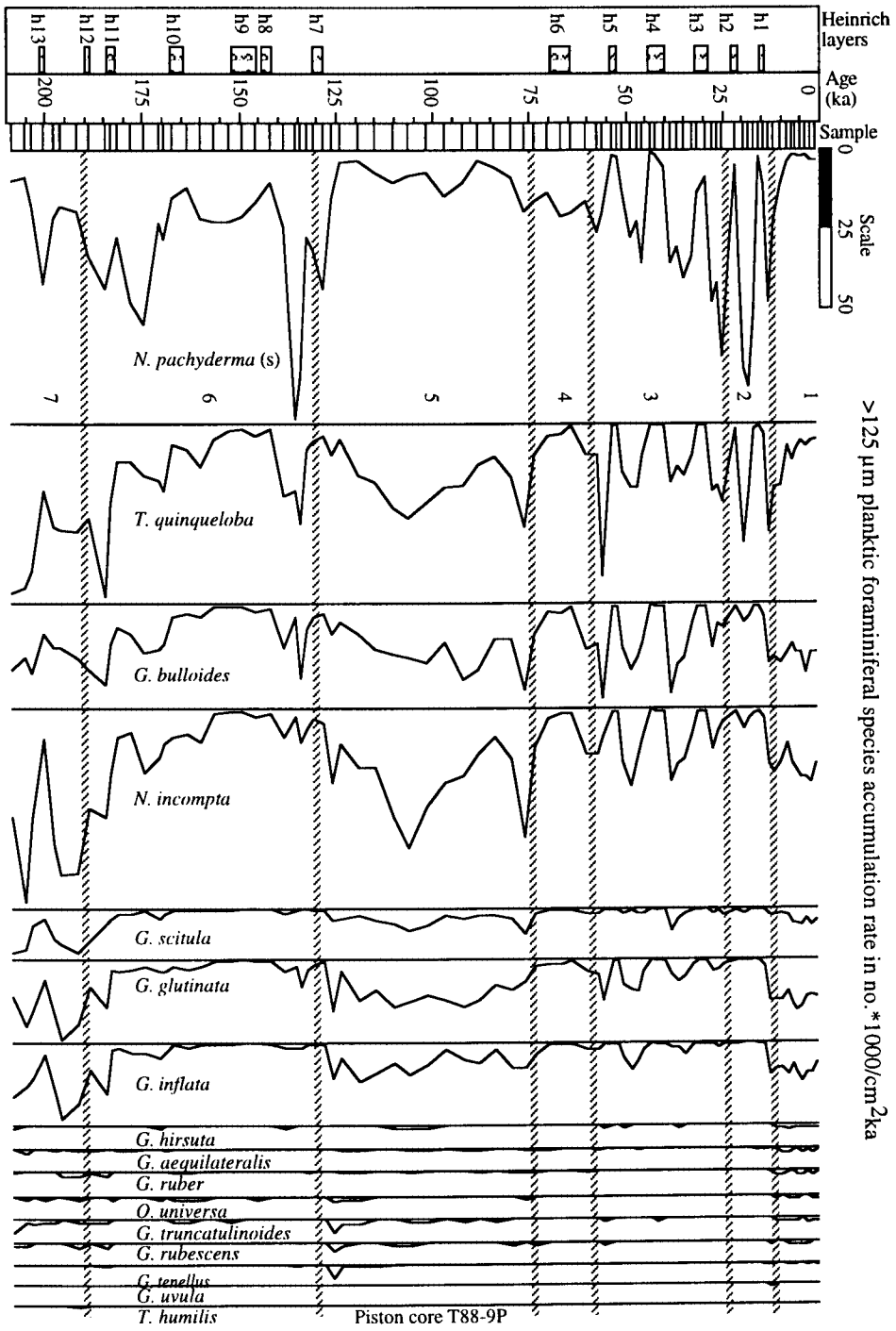

Fig. 10. >125 µm planktic foraminiferal species accumulation rate in no.*1000/cm²ka. 1-7 are isotopic stages.

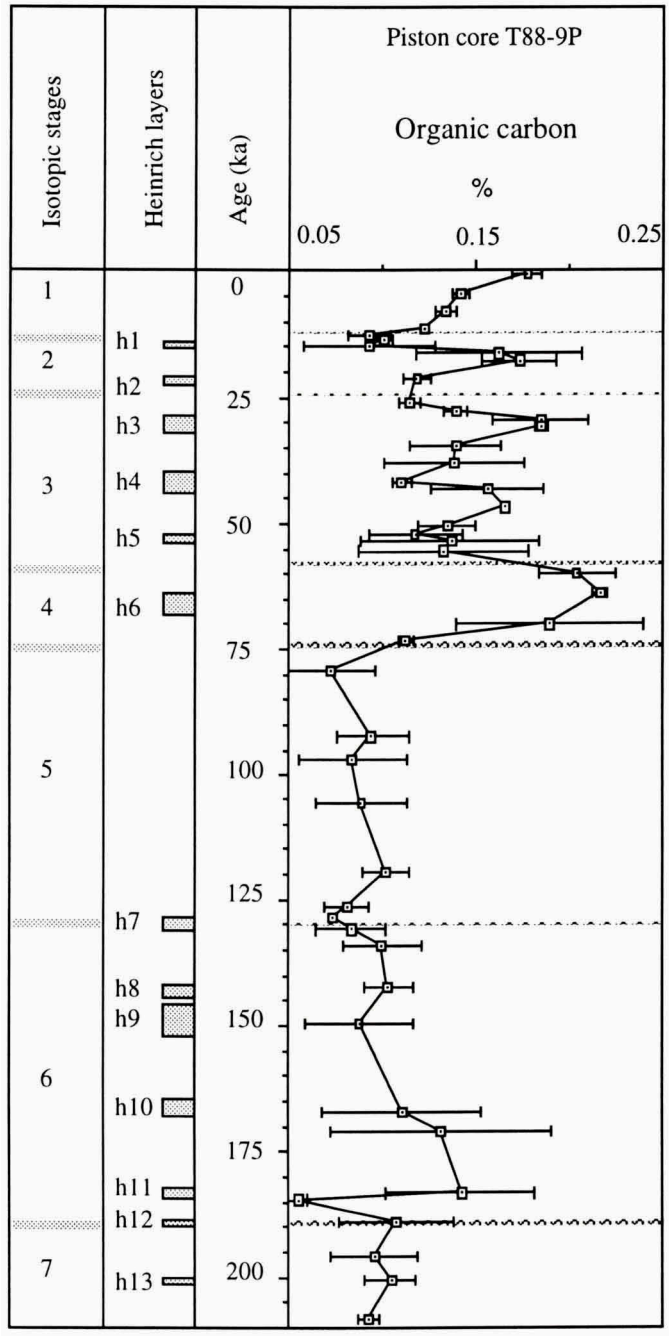

Fig. 11. Average weight percent organic carbon of the bulk sediment. Bars show duplicate measurements.

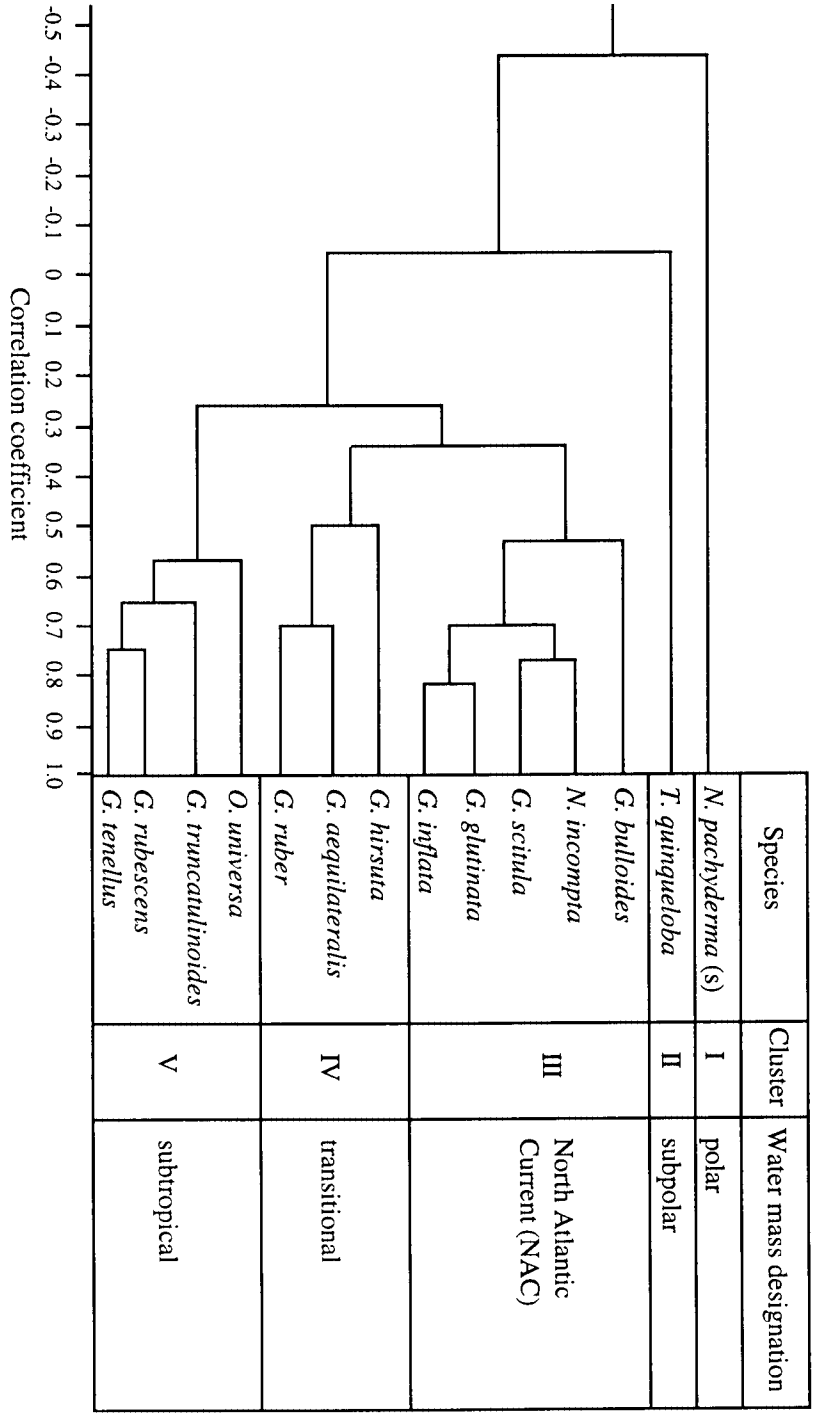

Fig. 12. Dendogram of the weighted pair group cluster analysis of the planktic foraminiferal species based on the correlation matrix of relative frequencies, excluding species lower than 0.2%. The five major clusters are interpreted to reflect water masses.

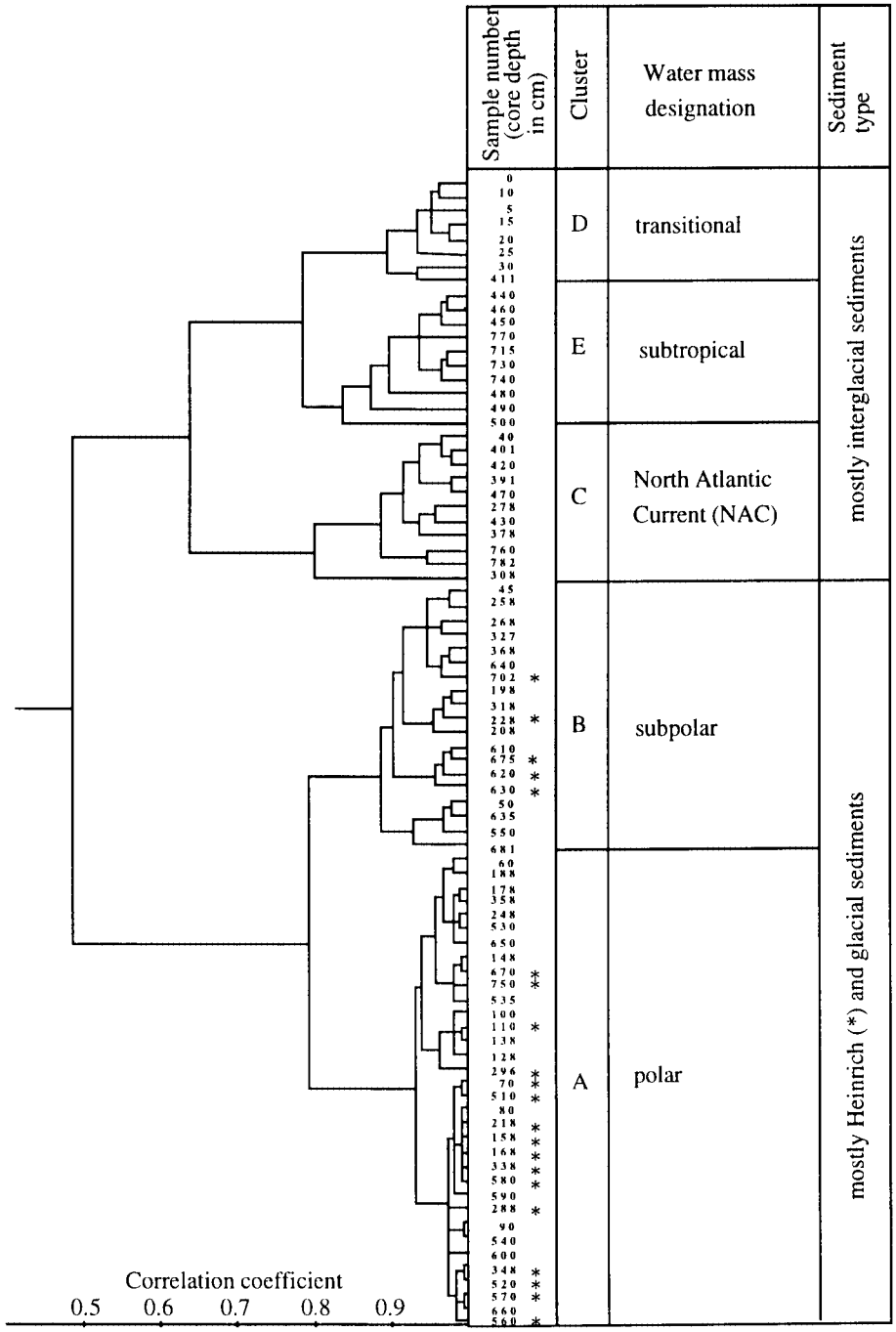

Fig. 13. Dendogram of the weighted pair group cluster analysis of the counted planktic foraminiferal samples from piston core T88-9P based on the correlation matrix of relative frequencies, excluding sample number 238, which did not contain planktic foraminifera. Sample numbers give depth below the mudline in cm. Asterisks (*) mark Heinrich intervals.

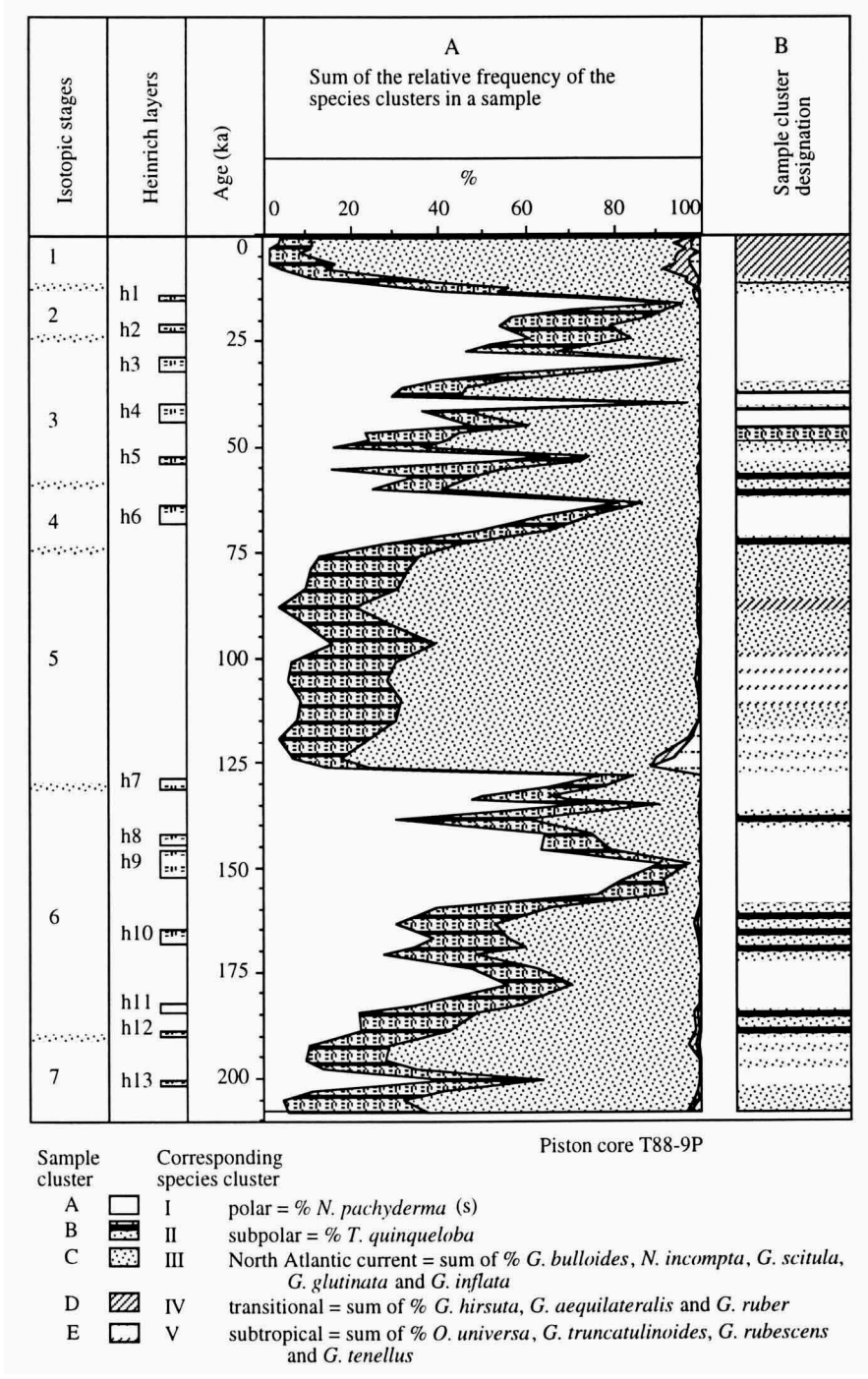

Fig. 14. (A) Sum of the relative frequency of the species clusters in a sample and (B) the sample cluster designation plotted against time.

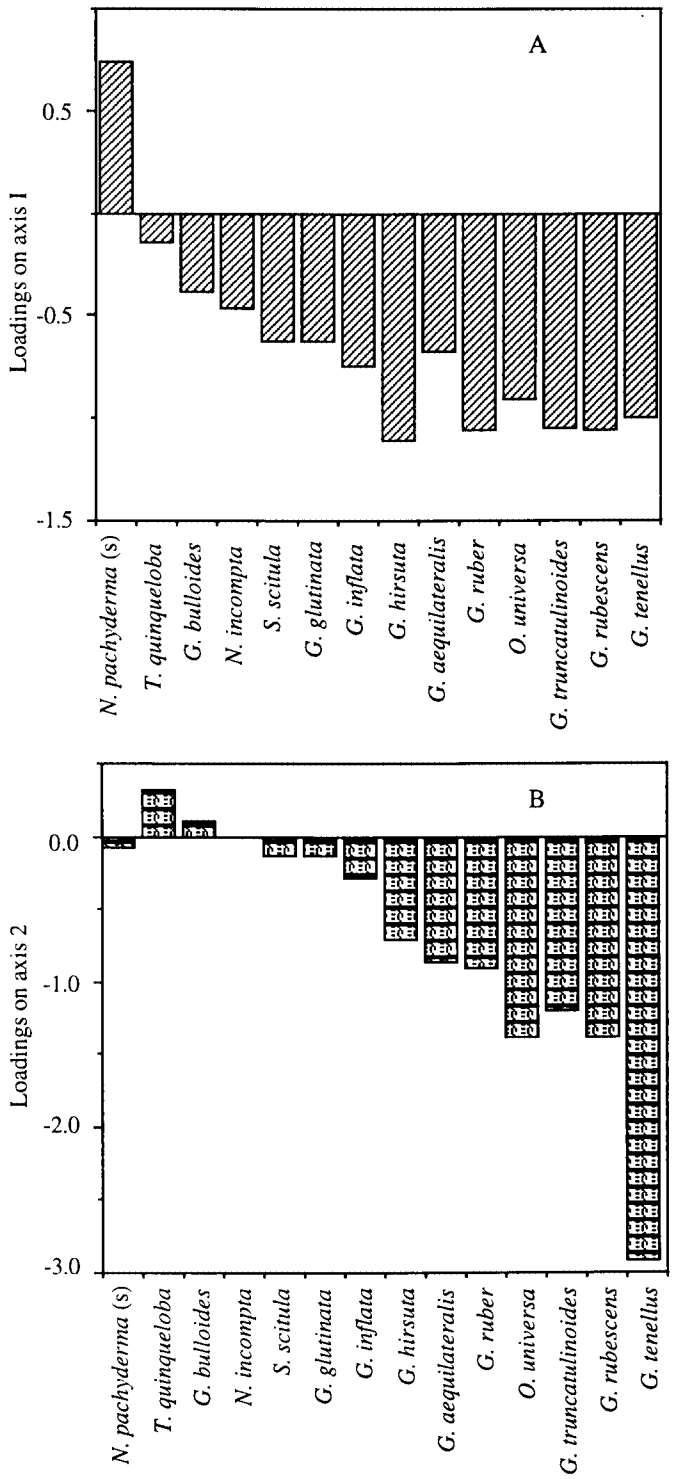
A
Loadings on axis 1
0.5
-0.5
-1.5
B
Loadings on axis 2
0.0
-1.0
-2.0
-3.0
N. pachyderma (s)
T. quinqueloba
G. bulloides
N. incompta
S. scitula
G. glutinata
G. inflata
G. hirsuta
G. aequilateralis
G. ruber
O. universa
G. truncatulinoides
G. rubescens
G. tenellus

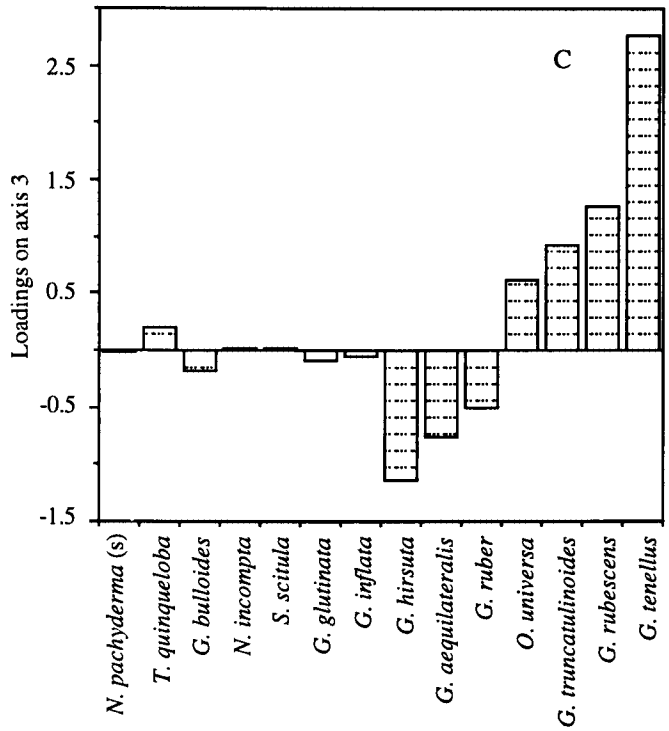

Fig. 15. Loadings of the different species on the first (A), second (B) and third (C) correspondence axes.

Diversity indices

In the past 208 ka, diversity was generally high except in Heinrich layers when simple diversity, Shannon and equitability indices have low values (Fig. 17). Both simple and Shannon diversity indices are generally slightly higher in interglacial than in glacial sediments. This trend is not reflected in the equitability.

Figure 18 shows the inverse relationship between % *N. pachyderma* (s) and the Shannon diversity index. It also shows that the Shannon index is low to very low for species cluster I, moderate for cluster II and high for clusters III-V.

Discussion and interpretation

Palaeo Primary Productivity

Planktic Foraminifera

Although the sedimentary record of planktic foraminiferal assemblages represents a composite mixture of different seasons over many years, it is still possible to link it to general primary productivity patterns in the surface ocean. Food supply is crucial to foraminiferal abundance, therefore, variations in frequencies and accumu-

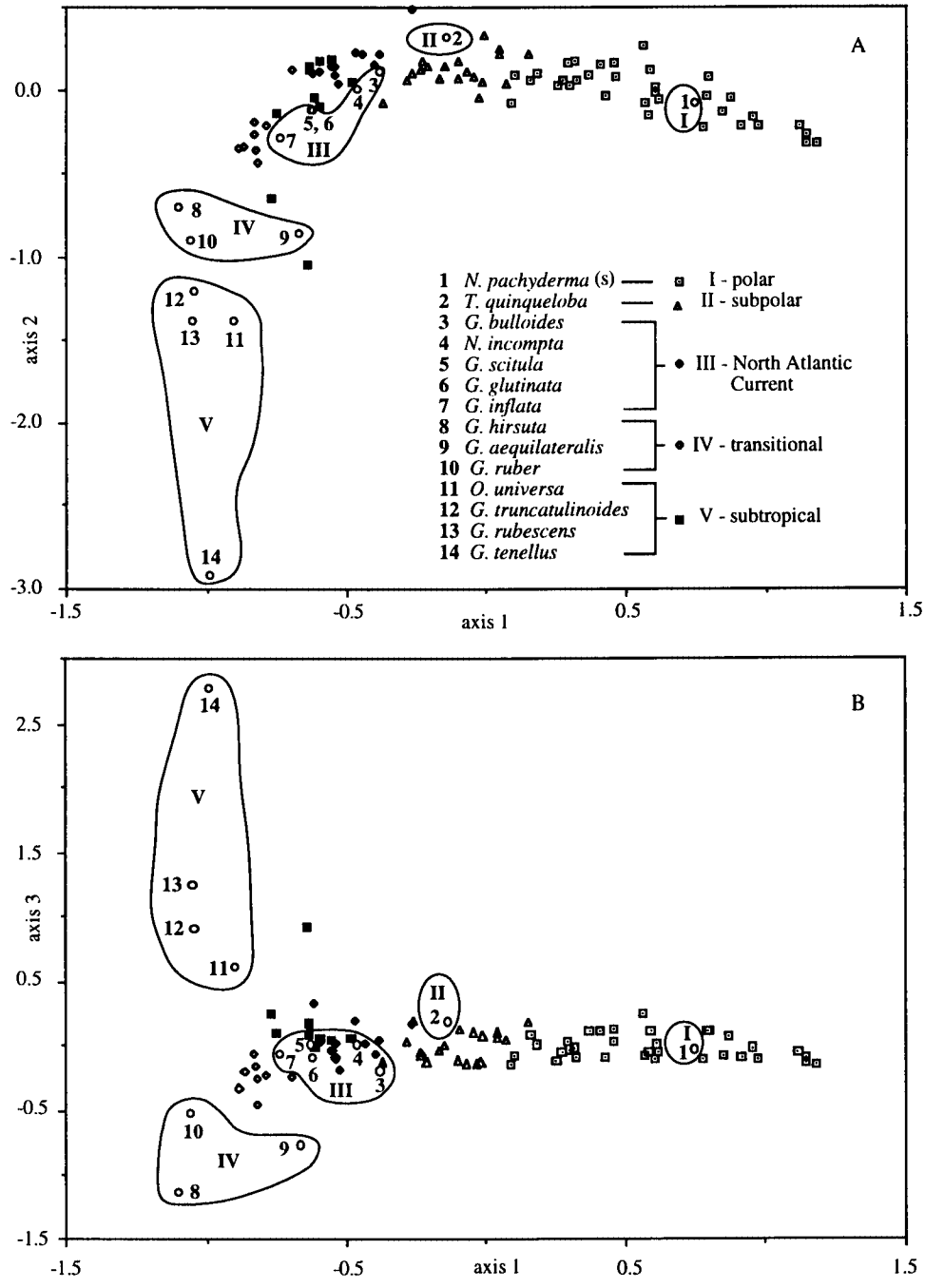

Fig. 16. Plot of samples and species on the (A) first vs second and (B) first vs third correspondence analysis axes. The first three axes explain 69, 10 and 6% of the total variation in the data set. Samples belonging to the same cluster (also see Fig. 12) are given an identical symbol.

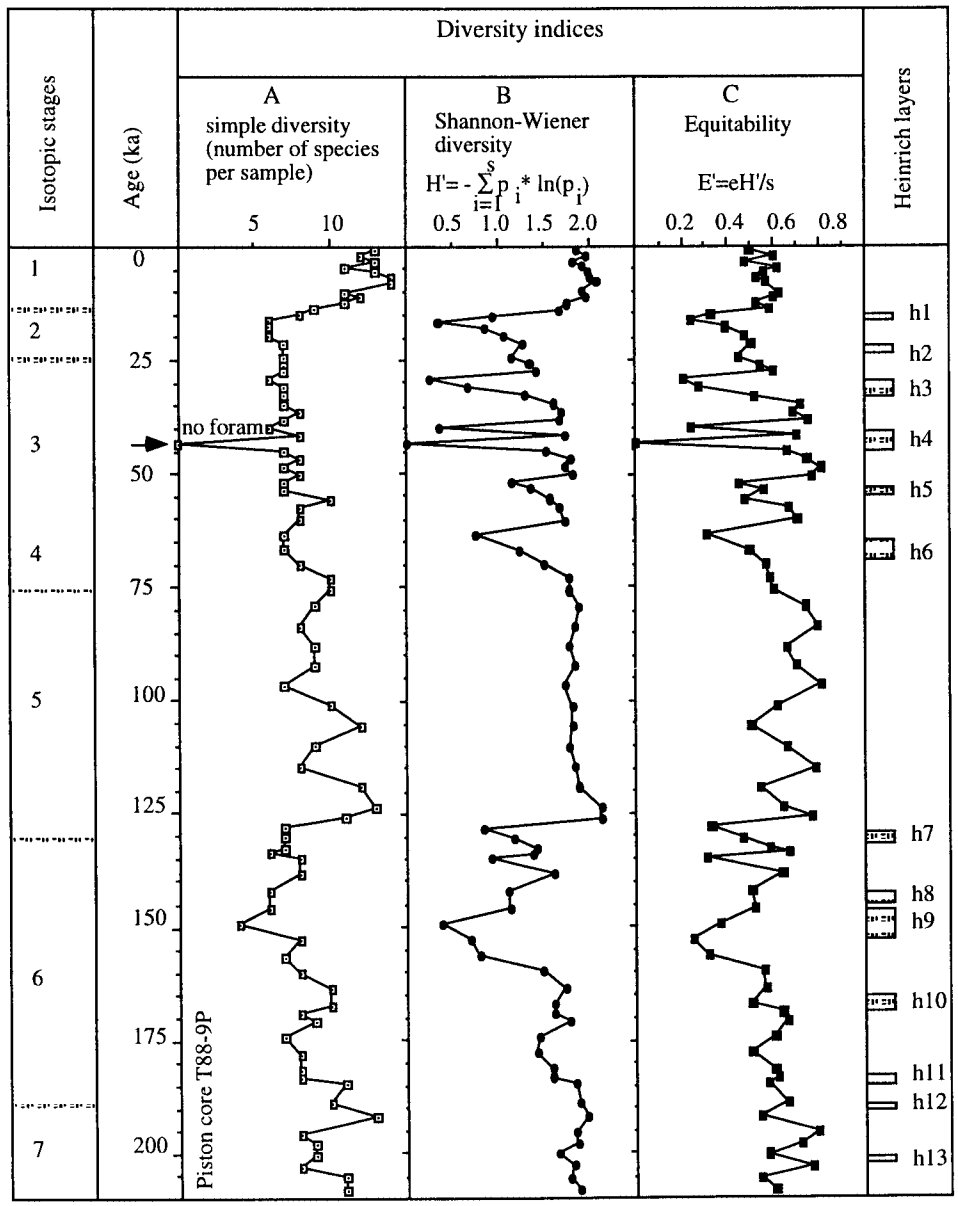

Fig. 17. Diversity indices (A) simple, (B) Shannon and (C) equitability of planktic foraminifera, after (Buzas & Gibson, 1969). Diversity is generally very low in Heinrich layers. One sample at about 43 ka is devoid of foraminifera, thus the diversity indices are indeterminate.

lation rates of planktic Foraminifera can be interpreted to reflect variations in primary productivity. This reasoning is supported by experimental data which showed increased food availability to enhance foraminiferal population growth (Bradshaw, 1955; Lipps & Valentine, 1970; Anderson et al., 1979; Bé et al., 1981; Caron et al., 1981, 1987). Additionally, planktic Foraminifera are plentiful in modern surface oceans where nutrients and biomass concentrations are high (compare Bé & Tolderlund, 1971 with Koblents-Mishke et al., 1970 and Berger et al., 1987 productivity maps; compare Bradshaw, 1959 with the productivity maps of Reid, 1962). The same phenomenon is observed in upwelling areas of the northern Indian Ocean (Kleijne et al., 1989). Sediment trap data also show that the fluxes of planktic Foraminifera are often strongly correlated with surface ocean productivity (Thunell et al., 1983; Thunell & Reynolds, 1984; Reynolds & Thunell, 1985; Thunell & Honjo, 1987).

In this study, the generally higher total planktic foraminiferal absolute frequencies and accumulation rates during interglacial than during glacial periods are interpreted to reflect higher production of planktic Foraminifera in the surface waters due to increased primary productivity. Indeed, the estimate for the top sediment (60 000 specimens of planktic Foraminifera >125 µm/cm²ka) compares well with flux data for one year (40 000 specimens of planktic Foraminifera >150 µm/cm²ka) from a sediment trap near the studied site (Wolfteich, 1994). These two estimates are comparable despite the 20 000 difference because the number of planktic Foraminifera in the 125-150 µm fraction constitutes on average one third of the total planktic Foraminifera larger than 125 µm (see Peeters et al., in prep.). In the trap, the fluxes of planktic Foraminifera exhibit sharp increases during the spring bloom period with *G. bulloides* being the most dominant planktic foraminiferal species (Wolfteich, 1994).

The coccolith carbonate accumulation rate is higher during interglacial than during glacial periods, which is similar to the pattern shown by the planktic Foraminifera (van Kreveld et al., 1996). These coccoliths are formed by coccolithophorids, which abound during phytoplankton blooms presently occurring in surface waters overlying the site in response to seasonal development and decay of the thermocline, and local upwelling within cyclonic eddies generated from meandering current systems of the North Atlantic Current (Wolfteich, 1994).

The generally low total planktic foraminiferal absolute frequencies and low accumulation rates in Heinrich layers are interpreted to reflect depressed planktic foraminiferal productivity as a consequence of limited food supply in the photic zone. This interpretation is supported by the very low coccolith carbonate accumulation rate in the Heinrich layers, particularly in h1 to h5 which are almost devoid of coccoliths (van Kreveld et al., 1996). During these events, the iceberg-laden waters probably blocked sunlight, slowing down algal and hence planktic foraminiferal production. Additionally, the lowered salinity due to the meltwater influx (Bond et al., 1992) and the cooling (Maslin et al, 1995; Madureira et al., in press) may have been unfavourable for the growth of coccolithophorids and Foraminifera. Thomas et al. (1995) also showed Heinrich events as periods of low primary productivity based on the very low benthic foraminiferal accumulation rates, and absolute and relative frequencies of the phytodetritus feeding species of benthic Foraminifera. Broecker et al. (1992) and Bond et al. (1992) also interpret Heinrich events to be periods of low primary productivity.

Aside from depressed primary productivity, they also give ice-rafted debris dilution as a possible alternative explanation for the lowered abundance of planktic Foraminifera in Heinrich layers. If so, then the sedimentation rate should at least be an order of magnitude higher than my estimates of between 5.7 to 7.5 cm/ka for the intense Heinrich events 1-3. However, detailed Th/U (Francois & Bacon, 1994) and radiocarbon dating (Bond et al., 1992) of cores recovered in the vicinity give similar values or just about 2 times higher, therefore dilution is unlikely to be the sole cause for planktic foraminiferal sparseness in these layers and decreased surface water productivity must have played a role. Moreover, the lateral extent of the area low in planktic Foraminifera exceeds that of the path of the Canada-derived debris (Broecker et al., 1992; Bond et al., 1992), supporting this contention.

Higher interglacial than glacial primary productivity was also observed in the mid- to high-latitude North Atlantic using benthic Foraminifera (Thomas et al., 1995), carbonate mass accumulation rates (van Kreveld et al., 1996), and organic carbon content (Stein & Stax, 1991; van Weering & de Rijk, 1991) proxies. At high latitudes in the Southern Oceans productivity was also higher during interglacials (Berger & Wefer, 1991; Charles et al., 1991; Mortlock et al., 1991; Kumar et al., 1993; Francois et al., 1993; Shemesh et al., 1993). To the contrary, primary productivity was higher during glacial than interglacial periods in low latitude regions and upwelling areas of the Atlantic (Müller et al., 1983; Pokras, 1987; Sarnthein et al., 1992) and the Pacific (Pederson, 1983; Pederson et al., 1988; Herguera & Berger, 1991; Herguera, 1992;1994; Thunell et al., 1992; Berger et al., 1994). In the more complex monsoon-influenced, upwelling area of the Northern Indian Ocean, primary productivity was higher during interglacial than glacial periods of isotopic stages 11 until 2 but the signal was reversed during isotopic stages 13 and 12 (Steens et al., 1992). With these geographic differences in glacial/interglacial primary productivity estimates, it is important to have a global ocean coverage to come up with a primary productivity signal to be used in global carbon models.

Organic carbon

Although organic carbon is extensively used as a primary productivity proxy in upwelling areas, it is unreliable in the studied open-ocean area because of the very low organic carbon content of the sediments and the contamination by terrigenous organic carbon.

The very low organic carbon, in addition to the high carbonate content of the sediments resulted to the poor reproducibility of the data (Fig. 11) even though the method adapted for this study (Nieuwenhuize et al., in press), eliminates reweighing and therefore minimises losses of organic compounds.

Aside from being low, the total organic carbon is contaminated by terrestrial organic material. The high weight percent total organic carbon in stages 4-2 coincides with high abundances of land-derived biomarkers consisting of *n*-alkanes (C_{27}, C_{29} and C_{31}), *n*-alkanoic acids (C_{24}, C_{26} and C_{28}) and *n*-alkanols (C_{24}, C_{26} and C_{28}) analysed in the same core (Madureira et al., in press). There is also a maximum in terrestrial biomarker abundances in h3 and h6, corresponding to high organic carbon content. This reflects increased input of terrigenous organic matter partly by icebergs which are known to have brought in material from Canada during Heinrich events h1, h2,

h4, and h5 (Grousset et al., 1993). During h3, the land-derived organic matter may have been transported by icebergs originating from Europe (Grousset et al., 1993). Aside from icebergs, the stronger winds during glacial periods (Fuhrer et al., 1993, GRIP Members, 1993) may have also brought in land-derived organic matter to the area (Madureira et al., in press).

The high weight percent organic carbon in stages 4-2 may also reflect better preservation rather than productivity variation. Organic carbon is severely affected by heterotrophic activity such that only a very small portion of the primary production in the euphotic zone is eventually preserved in the sediments. The lowered concentration of bottom water oxygen during the last glacial period (Boyle & Keigwin, 1982; Curry & Lohmann, 1983), likewise lowered heterotrophic activity on the seafloor and possibly enhanced organic carbon preservation (Emerson, 1985). Better preservation by rapid burial may also account for the higher glacial organic carbon content (Müller & Suess, 1979), as the sedimentation rate for this core is about 2 to 3 times higher in isotopic stages 4-2 than the other stages.

Organic carbon preservation is highly complex and has the potential for contamination by terrestrial organic matter making interpretations difficult, particularly in this open-ocean site.

Water masses

Since water masses have characteristic assemblages of biota, it is possible to recognise water mass variations based on changes in these organisms (Boltovskoy, 1959, 1962). Bé & Tolderlund (1971) and Bradshaw (1959), who studied the distribution of planktic Foraminifera in more than 700 plankton tows in the Atlantic and Pacific oceans showed that assemblages of planktic Foraminifera indeed characterise ocean water masses as defined by temperature and salinity. Ottens (1991) used cluster analyses and diversity indices to relate foraminiferal assemblages to hydrographically defined water masses.

The distribution and abundance of planktic Foraminifera in sediment core top samples by analogy with modern distributions, also reflect water masses (Imbrie & Kipp, 1971; Kipp, 1976), therefore, planktic Foraminifera were used to trace water mass movements in the Quaternary (Ruddiman & McIntyre, 1976; McIntyre et al., 1972). Planktic Foraminifera species are used to trace water mass changes during the past 208 ka by grouping the species using cluster and correspondence analyses, then comparing these groups to living plankton distributions. Although there are some detailed dissimilarities, the observed groups are similar to the distribution of living plankton reported by Bé & Tolderlund (1971), Bé (1977) and Ottens (1991). Clusters I to III are interpreted to reflect polar, subpolar, and North Atlantic Current (NAC) water masses, respectively. Species of clusters IV and V, which constitute <4% of the total foraminiferal assemblage, may reflect transitional and subtropical water masses.

Neogloboquadrina pachyderma (s), which is interpreted to indicate polar water masses, dominates present day polar waters of the Arctic and the Antarctic oceans. This species can live in sea ice in both the northern (Carsola, 1953) and the southern (Spindler & Dieckmann, 1986; Dieckmann et al., 1991) hemispheres, and can tolerate

temperatures of -1.4 °C though it favours temperatures between 0-9 °C (Bé & Tolderlund, 1971). It dominates, reaching between 95-100 % of the foraminiferal assemblage, in net tow samples from the Nansen Basin (Carstens & Wefer, 1992) and sediment samples from Greenland Sea (Bauch, 1993), Fram Strait and Central Arctic Ocean (Ericson, 1959).

Turborotalita quinqueloba, which is designated as a subpolar species, has the highest absolute and relative frequencies in present day subpolar waters (Bé & Hamlin, 1967; Bé & Tolderlund, 1971; Ottens, 1991). It also dominates sediment trap samples (Reynolds & Thunell, 1985) and surface sediments in subarctic regions (Kipp, 1976). This species prefers surface temperatures between 12° and 15°C (Bé & Hamlin, 1967).

Cluster III species are interpreted to indicate the NAC water mass (similar to 'transitional' of Bé & Hamlin, 1967), which can be further subdivided into two subclusters; (1) *G. bulloides*, *N. incompta* and *G. scitula* and (2) *G. glutinata* and *G. inflata*. Present day NAC water is a mixture of cold and warm waters which is reflected in the fauna. Aside from being prolific in NAC, cool water species *G. bulloides*, *N. incompta* and *G. scitula* also abound in subpolar waters while *G. glutinata* is quite common in subtropical waters (Bé & Hamlin, 1967; Bé & Tolderlund, 1971).

Globorotalia inflata is also interpreted as a NAC indicator, agreeing with its living distribution, being abundant in the boundary region between Labrador Current and the Gulf Stream-North Atlantic Current, and common in northern east Atlantic (Bé & Hamlin, 1967; Bé & Tolderlund, 1971).

Species of clusters IV and V are found in present day transitional to subtropical water masses.

Discrepancies between my Foraminifera-based water mass designations, and the living and sea-bed plankton distributions can be explained by differences in sieve size and depth habitats sampled. I analysed the >125 µm fraction while Bé & Tolderlund (1971), and Bé & Hamlin (1967), examined the >200 µm fraction, therefore underestimating the contribution of smaller Foraminifera such as *G. scitula* and *T. quinqueloba* while overestimating larger ones. Kipp (1976) analysed the >150 µm while Barash (1971) counted the >100 µm fraction of sediment samples.

Since Foraminifera live at different depths in the water column (Vincent & Berger, 1981), species distributions based on surface plankton only (e.g. Bé & Tolderlund, 1971; Ottens, 1991) underrepresents deep-living species such as *G. scitula* which is well represented in sediment samples (Kipp, 1976).

Moreover, data on living plankton represent only several hours to days while sediment data record an average signal over at least hundreds or even thousands of years incorporating both seasonal and interannual variations. This is illustrated in the transitional boundaries between the designated water masses (Fig. 16A-B).

Although plankton tow and sediment data are not directly comparable, the broad patterns are very similar. Therefore, Foraminifera in the sediments can still be used to reconstruct past water mass changes.

Diversity indices are also used to characterise present day water masses (Ottens, 1991). The Shannon diversity index for polar samples is low to very low, for subpolar samples moderate, and high for NAC to subtropical samples (Fig. 18). The overall pattern is comparable to box-core top data which show a decrease in planktic foraminiferal diversity from low to high latitudes in the Atlantic Ocean, generally agreeing

with modern sea-surface temperature and circulation (Balsam et al., 1980).

All three diversity indices, simple, Shannon, and equitability, are distinctly low during Heinrich events coinciding with the dominance of polar waters. The low equitability values are due to the almost monospecific planktic foraminiferal assemblage of *N. pachyderma* (s).

The foraminiferal assemblages characteristic of particular water masses have shifted through time in relation to the location of the piston core (Figs. 14A-B). The area is interpreted to be dominantly bathed by NAC with minor incursions of transitional and subtropical waters in interglacial periods and by polar waters during Heinrich events. During glacial periods, the area was covered by polar waters succeeded by subpolar waters and vice-versa.

The water mass reconstructions agree well with those of McIntyre et al. (1972), Ruddiman & McIntyre (1976), CLIMAP (1981), and Crowley (1981).

Productivity and water masses

The reconstructions generally show moderate to high primary productivity during interglacial periods when NAC water predominantly covered the area (compare Figs. 7 and 14A-B). At present, this site is mostly bathed by the NAC, the westerly wind-driven Gulf Stream extension. When the westerlies are strong during the cold season, they induce vertical mixing, bringing nutrients to surface waters. Enough nutrients and optimal light support algal spring blooms (Holligan et al., 1983; Brown & Yoder, 1994a, b) and high concentrations of planktic Foraminifera (Bé & Hamlin, 1967) currently observed in this area.

Modern polar waters in the Arctic as well as Antarctic generally have low productivities (Platt & Subba Rao, 1975; Subba Rao & Platt, 1984) which are comparable to those during Heinrich events. Icebergs probably blocked sunlight and caused a strong salinity stratification in the surface water suppressing admixture of nutrients and plankton productivity.

The moderate productivity during glacial periods may be due to localised blooms when the ice thawed, similar to present day ice-edge environments (Hebbeln & Wefer, 1991).

Conclusions

Piston core T88-9P was recovered from the Northeast Atlantic at 48°23'2"N, 25°05'6"W and provides a continuous pelagic record unaffected either by carbonate dissolution or by turbidity currents because the core site lies well above the lysocline at 3193 m water depth and on the east flank of the mid-Atlantic ridge, far from continental slopes where turbidity currents are common.

The age model for this core reveals a 208 ka stratigraphic record back to the beginning of isotopic stage 7, based on dates assigned to isotopic stage boundaries and events, calendar-calibrated radiocarbon ages, and tephrochonology.

The average total planktic Foraminifera are generally higher in interglacial (36 800 specimens/g and 105 700 specimens/cm²ka) than in glacial sediments (21 200 specimens/g and 84 500 specimens/cm²ka, maximum estimate), and low (9200 spec-

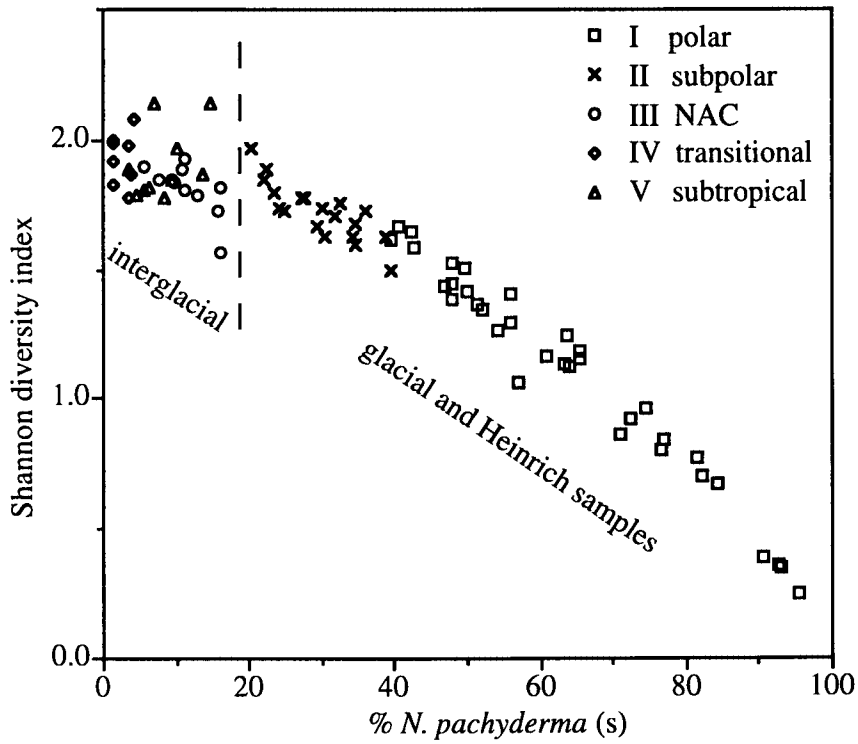

Fig. 18. Scatter plot of % *Neogloboquadrina pachyderma* (s) against Shannon diversity index, with species clusters (I-V). NAC stands for North Atlantic Current.

imens/g and 34 000 specimens/cm²ka, minimum estimate) in Heinrich layers. This pattern is interpreted to reflect variations in foraminiferal productivity as a consequence of changes in surface water primary productivity. In general, primary productivity variations during the past 208 ka coincide with water mass changes. As in the modern oceans, primary productivity is generally higher in NAC and subpolar than in polar waters.

The high average primary productivity during interglacials coincides with times when NAC water mostly covered the area as shown by the dominance of *G. bulloides*, *N. incompta*, *G. scitula*, *G. glutinata*, and *G. inflata* group in the sediments, while the photic zone had a low fertility during Heinrich events, when polar waters penetrated the area as reflected by the low diversity indices and the predominance of *N. pachyderma* (s). Productivity was moderate during glacial periods when polar, subpolar and NAC waters, probably in seasonal alternation, covered the area as reflected by the abundance of subpolar species *T. quinqueloba* as well as polar and NAC indicator species in the sediments.

The very low weight percent total organic carbon and the contamination by land-derived organic matter limit the use of organic carbon as a primary productivity proxy in the study area. In contrast, planktic Foraminifera are useful tracers for past

primary productivity and water mass changes in the carbonate-dominated, open-ocean, mid-latitude Northeast Atlantic site.

Acknowledgements

I am grateful to L. Labeyrie and E. Cortijo for digitising the core photograph. J.E. van Hinte and G.M. Ganssen initiated this research. They are also thanked for critically reviewing several versions of this manuscript along with M. Knappertsbusch and J.J. Ottens. I thank S. Kars for taking the Scanning Electron Micrographs and A.J. Nederbragt for providing the cluster and correspondence analyses programs and for her useful suggestions. Thanks are also due to M. Konert, R. van Elsas and P. Willekes for analysing the organic carbon.

This study is a part of the GEM program (Global *Emiliania* Modelling Initiative) coordinated by P. Westbroek and is financed by the 'Nederlandse Onderzoek Project'. The APNAP II expedition which collected the studied piston core was sponsored by the 'Stichting Onderzoek der Zee'. This is publication number 950705 of the Netherlands Research School of Sedimentary Geology, Center for Marine Earth Sciences, Free University, Amsterdam.

References

Abrantes, F., K. Winn & M. Sarnthein, 1994. Late Quaternary palaeoproductivity variations in the NE and equatorial Atlantic: diatom and C_{org} evidence. In: R. Zahn, T.H. Pederson, M.A. Kaminski, and L. Labeyrie (eds.). Carbon cycling in the glacial ocean: constraints on the ocean's role in global change. — NATO ASI Series, I17: 425-441.

Anderson, O.R., M. Spindler, A.W.H. Bé & C. Hemleben, 1979. Trophic activity of planktonic Foraminifera. — J. Mar. Biol. Assoc. U.K., 59: 791-799.

Andrews, J.T. & K. Tedesco, 1992. Detrital carbonate-rich sediments, northwestern Labrador Sea: implications for ice-sheet dynamics and iceberg rafting (Heinrich) events in the North Atlantic. — Geology, 20: 1087-1090.

Balsam, W.L., K.W. Flessa, N.G. Kipp & L.G. Dubois, 1980. Planktonic foraminiferal diversity in the interglacial and glacial North Atlantic: a test of diversity gradients as a paleoceanographic technique. — Geology, 8: 582-585.

Barash, M.S., 1971. The vertical and horizontal distribution of planktonic Foraminifera in Quaternary sediments of the Atlantic ocean. In: B.M. Funnel & W.R. Riedel (eds.). The Micropaleontology of the oceans. — Cambridge Univ. Press, London: 433-442.

Bard, E., 1988. Correction of accelerator mass spectrometry ^{14}C ages measured in planktonic Foraminifera: paleoceanographic implications. — Paleoceanogr., 3, 6: 635-645.

Bard, E., M. Arnold, R. Fairbanks & B. Hamelin, 1993. ^{230}Th-^{234}U and ^{14}C ages obtained by mass spectrometry on corals. — Radiocarbon, 35: 191-199.

Bard, E., B. Hamelin, R. Fairbanks & A. Zindler, 1990. Calibration of the ^{14}C timescale over the past 30,000 years using mass spectrometric U-Th ages from Barbados corals. — Nature, 345: 405-409.

Barnola, J.M., D. Raynaud, Y.S. Korotkevich & C. Lorius, 1987. Vostok ice core provides 160,000-year record of atmospheric CO_2. — Nature, 329: 408-414.

Bauch, H., 1993. Planktische Foraminiferen im europäischen Nordmeer - ihre Bedeutung für die paläo-ozeanographische Interpretation während der letzten 600.000 Jahre. — Sonderforschungsbereich, 313, Univ. Kiel, Germany, 40: 1-129.

Bé, A.W.H., 1959. Ecology of Recent planktonic Foraminifera 1. Areal distribution in the western North Atlantic. — Micropaleontology, 5: 77- 100.

Bé, A.W.H., 1977. An ecological, zoogeographic, and taxonomic review of recent planktonic Foraminifera. In: A.T.S. Ramsay (ed.). Oceanic Micropaleontology, 1. — Academic Press, London: 1-100.

Bé, A.W.H., D.A. Caron & O.R. Anderson, 1981. Effects of feeding frequency on life processes of the planktonic foraminifer *Globigerinoides sacculifer* in laboratory culture. — J. Mar. Biol. Assoc. U. K., 61: 73-86.

Bé, A.W.H. & W.H. Hamlin, 1967. Ecology of Recent planktonic foraminifera 3. Distribution in the North Atlantic during the summer of 1962. — Micropaleontology, 13: 87-106.

Bé, A.W.H., C. Hemleben, O.R. Anderson & M. Spindler, 1980. Pore structures in planktonic foraminifera. — J. Foram. Res., 10: 117-128.

Bé, A.W.H. & D.S. Tolderlund, 1971. Distribution and ecology of living planktonic foraminifera in surface waters of the Atlantic and Indian Oceans. In: B.M. Funnel & W.R. Riedel (eds.). The micropaleontology of the oceans. — Cambridge Univ. Press, London: 105-149.

Bénzecri, J.P., 1992. Correspondence analysis handbook. — M. Dekker, New York: 1-665.

Berger, W.H., K. Fischer, C. Lai & G. Wu, 1987. Ocean productivity and organic carbon flux. Part I. Overview and maps of primary production and export production. — Scripps Inst. Oceanogr., Univ. Calif., SIO 87-30: 1- 67.

Berger, W.H., J.C. Herguera, C.B. Lange & R. Schneider, 1994. Paleoproductivity: flux proxies versus nutrient proxies and other problems concerning the Quaternary productivity record. In: R. Zahn, T.H. Pederson, M.A. Kaminski & L. Labeyrie (eds.). Carbon cycling in the glacial ocean: constraints on the ocean's role in global change. — NATO ASI Series, I17: 387-412.

Berger, W.H. & J. Killingley, 1977. Glacial-Holocene transition in deep-sea carbonates: selective dissolution and stable isotope signal. — Science, 197: 563-566.

Berger, W.H. & G. Wefer, 1991. Productivity of the oceans: discussion of the iron hypothesis. — Paleoceanography, 36: 1899-1918.

Betzer, P.R., W.J. Showers, E.A. Laws, C.D. Winn, G.R. DiTullio & P.M. Kroopnick, 1984. Primary productivity and particle fluxes on a transect of the equator at 153°W in the Pacific Ocean. — Deep-Sea Res., 31: 1-11.

Boltovskoy, E., 1959. Foraminifera as biological indicators in the study of ocean currents. — Micropaleontology, 5: 473-481.

Boltovskoy, E., 1962. Planktonic Foraminifera as indicators of different water masses in the South Atlantic. — Micropaleontology, 8: 403-408.

Bond, G., H. Heinrich, W. Labeyrie, J. McManus, J. Andrews, S. Huon, R. Jantschik, S. Clasen, C. Simet, K. Tedesco, M. Klas, G. Bonani & S. Ivy, 1992. Evidence for massive discharges of icebergs into the North Atlantic ocean during the last glacial period. — Nature, 360: 245-249.

Boyle, E. & L. Keigwin, 1982. Deep circulation of the North Atlantic over the last 200,000 years: geochemical evidence. — Science, 218: 784-787.

Bradshaw, J.S., 1955. Preliminary laboratory experiments on ecology of foraminiferal populations. — Micropaleontology, 1: 351-358.

Bradshaw, J.S., 1959. Ecology of living planktonic Foraminifera in the North and Equatorial Pacific Ocean. Cushman Found. Foram. Res., 10, 2: 25-64.

Broecker, W., G. Bond, M. Klas, D. Clark & J. McManus, 1992. Origin of the northern Atlantic's Heinrich events. — Climate Dynamics, 6: 265-273.

Broecker, W.S., 1992. The glacial world according to Wally. — Lamont-Doherty Geol. Observatory, Columbia Univ., New York: 1-207.

Brown, C.W. & J.A. Yoder, 1994a. Coccolithophorid blooms in the global ocean. — J. Geophys. Res., 99: 7467-7482.

Brown, C.W. & J.A. Yoder, 1994b. Distribution pattern of coccolithophorid blooms in the western North Atlantic Ocean. — Continental Shelf Research, 14: 175-197.

Bruin, P., 1937. Enige ervaringen bij de bepaling van het gehalte van grond aan koolzure kalk volgens de methode Scheibler. — Chemisch Weekblad, 34: 755-759.

Brummer, G.J.A. & A.J.M. van Eijden, 1992. 'Blue-ocean' paleoproductivity estimates from pelagic carbonate mass accumulation rates. — Mar. Micropal., 19: 99-117.

Brummer, G.J.A. & D. Kroon, 1988. Planktonic foraminifera as tracers of ocean-climate history: ontogeny, relationships and preservation of modern species and stable isotopes, phenotypes and assemblage distribution in different water masses. Doctor's Theses, Vrije Univ., Amsterdam: 1-346.

Buzas, M.A. & T.G. Gibson, 1969. Species diversity: benthonic foraminifera in Western North Atlantic. — Science, 163: 72-75.

Bijma, J., W.W. Faber Jr & C. Hemleben, 1990. Temperature and salinity limits for growth and survival of some planktonic foraminifers in laboratory cultures. — J. Foram. Res., 20: 95-116.

Caron, D.A., A.W.H. Bé & O.R. Anderson, 1981. Effects of temperature and salinity on the growth and survival of the planktonic foraminifer *Globigerinoides sacculifer*. — J. Mar. Biol. Assoc. U. K., 62: 435-452.

Caron, D.A., W.W. Faber Jr & A.W.H. Bé, 1987. Growth of the spinose planktonic foraminifer *Orbulina universa* in laboratory culture and the effect of temperature on the life processes. — J. Mar. Biol. Assoc. U. K., 67: 343-358.

Carsola, A.J., 1953. Possible planktonic occurrence of *Globigerina pachyderma*. — J. Paleont., 27: 742-752.

Carstens, J. & G. Wefer, 1992. Recent distribution of planktonic foraminifera in the Nansen Basin, Arctic Ocean. — Deep-Sea Res., 39: S507-S524.

Charles, C.D., P.N. Froelich, M.A. Zibello, R.A. Mortlock & J.J. Morley, 1991. Biogenic opal in Southern Ocean sediments over the last 450,000 years: implications for surface water chemistry and circulation. — Paleoceanography, 6, 6: 697-728.

Cifelli, R., 1961. A new species of pelagic foraminifera from the North Atlantic. — Cushman Found. Foram. Res. Contr., 12: 83-86.

Cifelli, R., 1973. Observations on *Globigerina pachyderma* (Ehrenberg) and *Globigerina incompta* Cifelli from the North Atlantic. — J. Foram. Res., 3: 157-166.

CLIMAP, 1976. The surface of the ice-age earth. — Science, 191: 1131-1137.

CLIMAP, 1981. Seasonal reconstruction of the earth's surface at the last glacial maximum. — Geol. Soc. Am., Map Chart Ser., MC-36.

CLIMAP, 1984. The last interglacial ocean. — Quat. Res., 21: 123-224.

Crowley, T.J., 1981. Temperature and circulation changes in the Eastern North Atlantic during the last 150,000 years: evidence from the planktonic foraminiferal record. — Mar. Micropal., 6: 97-129.

Curry, W. & P. Lohmann, 1983. Reduced advection into Atlantic Ocean deep eastern basin during the last glaciation maximum. — Nature, 306: 577- 579.

Dale, B. & A. Fjellså, 1994. Dinoflagellate cysts as paleoproductivity indicators: state of the art, potential, and limits. In: R. Zahn, T.H. Pederson, M.A. Kaminski & L. Labeyrie (eds.). Carbon cycling in the glacial ocean: constraints on the ocean's role in global change. — NATO ASI Series, I17: 521-537.

Davis, J.C., 1986. Statistics and Data Analysis in Geology. — J. Wiley, New York: 1-646.

Delmas, R.J., J.M. Ascencio & M. Legrand, 1980. Polar ice evidence that atmospheric CO_2 20,000 BP was 50% of present. — Nature, 284: 155-157.

Dieckmann, G.S., M. Spindler, M.A. Lange, S.F. Ackley & H. Eicken, 1991. Antarctic sea ice: a habitat for the foraminifer *Neogloboquadrina pachyderma*. — J. Foram. Res., 21: 182-189.

Dietrich, G., K. Kalle, W. Krauss & G. Siedler, 1975. General Oceanography. — J. Wiley, New York: 1-626.

Dymond, J., E. Suess & M. Lyle, 1992. Barium in deep-sea sediments: a geochemical indicator of paleoproductivity. — Paleoceanography, 7: 163- 181.

Emerson, S., 1985. Organic carbon preservation in marine sediments. In: E.T. Sundquist & W.S. Broecker (eds.). The carbon cycle and atmospheric CO2: natural variation Archean to Present. — Amer. Geophys. Union, Washington, DC, Geophys. Mon., 32: 78-87.

Ericson, D.B., 1959. Coiling direction of *Globigerina pachyderma* as a climatic index. — Science, 130: 219-221.

Francois, R. & M.P. Bacon, 1994. Heinrich events in the North Atlantic: radiochemical evidence. — Deep-Sea Res., 41: 315-332.

Francois, R., M.P. Bacon & M.A. Altabet, 1993. Glacial/interglacial changes in sediment rain rate in the SW Indian sector of Subantarctic waters as recorded by ^{230}Th, ^{231}Pa, U and $d^{15}N$. — Paleoceanography, 8: 611-629.

Fuhrer, R., A. Neftel, M. Anklin & V. Maggi, 1993. Continuous measurements of hydrogen peroxide, formaldehyde, calcium and ammonium concentrations along the GRIP ice core from Summit, central Greenland. Atmos. Environ., 27A: 1873-1880.

Giraudeau, J. & J. Rogers, 1994. Phytoplankton biomass and sea-surface temperature estimates from sea-bed distribution of nannofossils and planktonic foraminifera in the Benguela upwelling system. — Micropaleontology, 40: 275-285.

GRIP Members, 1993. Climate instability during the last interglacial period recorded in the GRIP ice core. — Nature, 364: 203-207.

Grousset, F.D., L. Labeyrie, J.A. Sinko, M. Cremer, G. Bond, J. Duprat, E. Cortijo & S. Huon, 1993. Patterns of ice-rafted detritus in the glacial North Atlantic (40-55°N). — Paleoceanography, 8, 2: 175-192.

Hebbeln, D. & G. Wefer, 1991. Effects of ice coverage and ice-rafted material on sedimentation in the Fram Strait. — Nature, 350: 409-411.

Heinrich, H., 1988. Origin and consequences of cyclic ice rafting in the Northeast Atlantic ocean during the past 130,000 years. — Quat. Res., 29: 142-152.

Hemleben, C., M. Spindler & O.R. Anderson, 1989. Modern Planktonic Foraminifera. — Springer-Verlag, New York: 1-363.

Herguera, J.C., 1992. Deep-sea benthic foraminifera and biogenic opal: glacial to postglacial productivity changes in the western Equatorial Pacific. — Mar. Micropal., 19: 79-98.

Herguera, J.C., 1994. Nutrient, mixing and export indices: a 250 Kyr paleoproductivity record from the western equatorial Pacific. In: R. Zahn, T.H. Pederson, M.A. Kaminski & L. Labeyrie (eds.). Carbon cycling in the glacial ocean: constraints on the ocean's role in global change. — NATO ASI Series, I17: 481-519.

Herguera, J.C. & W.H. Berger, 1991. Paleoproductivity from benthic foraminifera abundance: glacial to post-glacial change in the west- equatorial Pacific. — Geology, 19: 1173-1176.

Hill, M.O., 1974. Correspondence analysis: a neglected multivariate method. — J. R. Stat. Soc. Ser., C23: 340-354.

Holligan, P.M., M. Viollier, D.S. Harbour, P. Camus & M. Champagne-Philippe, 1983. Satellite and ship studies of coccolithophore production along a continental shelf edge. — Nature, 304: 339-342.

Imbrie, J. & N.G. Kipp, 1971. A new micropaleontologic method for quantitative paleoclimatology: application to a late Pleistocene Caribbean core. In: K.K. Turekian (ed.). Late Cenozoic glacial ages. — Yale Univ. Press, New Haven, Conn: 71-191.

Käse, R. & G. Siedler, 1984. Meandering of the subtropical front south-east of the Azores. — Nature, 300: 245-246.

Kipp, N.G., 1976. New transfer-function for estimating past sea-surface conditions from sea-bed distributions of planktonic foraminiferal assemblages in the North Atlantic. In: R. Cline & J. Hays (eds.). Investigation of Late Quaternary paleoceanography and paleoclimatology. — Geol. Soc. Amer. Mem., 145: 3-41.

Kleijne, A., D. Kroon & W. Zevenboom, 1989. Phytoplankton and foraminiferal frequencies in northern Indian Ocean and Red Sea surface waters. — Neth. J. Sea Res., 24: 531-539.

Koblents-Mishke, O.I., V.V. Volkovinsky & Y.G. Kabanova, 1970. Plankton primary production of the World Ocean. In: W. Wooster (ed.). Scientific Exploration of the South Pacific. — Nat. Acad. Sci., Washington, DC: 183- 193.

Krauss, W., 1986. The North Atlantic Current. — J. Geophys. Res., 91: 5061- 5074.

Kreveld, S.A. van, M. Knappertsbusch, J.J. Ottens, G. Ganssen & J.E. van Hinte, 1996. Biogenic carbonate and ice-rafted debris (Heinrich layer) accumulation in deep-sea sediments from a Northeast Atlantic piston core. — Marine Geol., 131:21-46.

Kumar, N., R. Gwiazda, R.F. Anderson & P.N. Froelich, 1993. $^{231}Pa/^{230}Th$ ratios in sediments as a proxy for past changes in Southern Ocean productivity. — Nature, 145: 3-4.

Lipps, J.H. & J.W. Valentine, 1970. The role of foraminifera in the trophic structure of marine communities. — Lethaia, 3: 279-286.

Lourens, L.J., F.J. Hilgen, L. Gudjonsson & W.J. Zachariasse, 1992. Late Pliocene to early Pleistocene astronomically-forced sea surface productivity and temperature variations in the Mediterranean. — Mar. Micropal., 19: 49-78.

Madureira, L.A.S, S.A. van Kreveld, G. Eglinton, M.H. Conte, G.M. Ganssen, J.E. van Hinte & J.

Ottens, in press. Late Quaternary high-resolution biomarker and other sedimentary climate proxies in a Northeast Atlantic core. — Paleoceanography.

Mann, C.R., 1967. The termination of the Gulf Stream and the beginning of the North Atlantic Current. — Deep-Sea Res., 14: 337-359.

Martinson, D.G., P.G. Pisias, J.D. Hays, J. Imbrie, T.C. Moore Jr & N.J. Shackleton, 1987. Age dating and the orbital theory of the ice ages: development of a high-resolution 0 to 300,000-year chronostratigraphy. - - Quat. Res., 27: 1-29.

Maslin, M.A., N.J. Shackleton & U. Pflaumann, 1995. Surface water temperature, salinity, and density changes in the northeast Atlantic during the last 45,000 years: Heinrich events, deep water formation, and climatic rebound. — Paleoceanography, 10(3): 527-544.

McIntyre, A., W.F. Ruddiman & R. Jantzen, 1972. Southward penetrations of the North Atlantic Polar Front: faunal and floral evidence of large-scale surface water mass movements over the last 225,000 years. — Deep-Sea Res., 19: 61-77.

Milliman, J.D., 1993. Production and accumulation of calcium carbonate in the ocean: budget of a nonsteady state. — Glob. Biogeochem. Cyc., 7: 927- 957.

Mix, A.C., 1989. Pleistocene paleoproductivity: evidence from organic carbon and foraminiferal species. In: W.H. Berger, V.S. Smetacek & G. Wefer (eds.). Productivity of the Ocean: Present and Past. — J. Wiley, Chichester: 313-340.

Mortlock, R.A., C.D. Charles, P.N. Froelich, M.A. Zibello, J. Saltzman, J.D. Hays & L.H. Burckle, 1991. Evidence for lower productivity in the Antarctic Ocean during the last glaciation. — Nature, 351: 220-222.

Müller, P.J., H. Erlenkeuser & R. von Grafenstein, 1983. Glacial-interglacial cycles on oceanic productivity inferred from organic carbon contents in eastern North Atlantic sediment cores. In: J. Thiede & E. Suess (eds.). Coastal upwelling, Part B. — Plenum, New York: 365-398.

Müller, P.J. & E. Suess, 1979. Productivity, sedimentation rate, and sedimentary organic matter in the oceans-I. Organic carbon preservation. — Deep-Sea Res., 26: 1347-1362.

Neftel, A., H. Oeschger, T. Staffelbach & B. Stauffer, 1988. CO_2 record in the Byrd ice core 50,000-5,000 years BP. — Nature, 331: 609-611.

Nieuwenhuize, J., Y. Maas & J. Middelburg, in press. Rapid analysis of organic carbon and nitrogen in particulate materials. — Mar. Chem.

Ottens, J.J., 1991. Planktic foraminifera as North Atlantic water mass indicators. — Oceanol. Acta, 14: 123-140.

Ottens, J.J., 1992. April and August Northeast Atlantic surface water masses reflected in planktic foraminifera. — Neth. J. Sea Res., 28: 261-283.

Parker, F.L., 1962. Planktonic foraminiferal species in Pacific sediments. — Micropaleontology, 8: 219-254.

Pederson, T.F., 1983. Increased productivity in the eastern equatorial Pacific during the last glacial maximum (19,000 to 14,000 year BP). — Geology, 11: 16-19.

Pederson, T.F., M. Pickering, J.S. Vogel, J.N. Southon & D.E. Nelson, 1988. The response of benthic foraminifera to productivity cycles in the eastern equatorial Pacific: faunal and geochemical constraints on glacial bottom water oxygen levels. — Paleoceanography, 3: 157-168.

Peeters, F.J.C., E. Ivanova, S. Conan, G.J. Brummer, G. Ganssen, S. Troelstra, T. van Weering & J.E. van Hinte, in prep. Size analysis of planktic foraminifera from the Arabian Sea.

Platt, T. & D.V. Subba Rao, 1975. Primary production of marine microphytes. In: J.P. Cooper (ed.). Photosynthesis and productivity in different environments. — Cambridge Univ. Press, Cambridge: 249-280.

Pokras, E.M., 1987. Diatom record of the late Quaternary climatic change in the eastern equatorial Atlantic and tropical Africa. — Paleoceanography, 2: 273-286.

Prell, W.L., 1984a. Monsoonal climate of the Arabian Sea during the late Quaternary: a response to changing solar radiation. In: A. Berger, J. Imbrie, J. Hays, G. Kukla & B. Saltzman (eds.). Milankovitch and Climate. — Reidel, Dordrecht: 349-366.

Prell, W.L., 1984b. Variation of monsoonal upwelling: a response to changing solar radiation. In: J.E. Hansen & T. Takahashi (eds). Climate processes and climate sensitivity. Amer. Geophys. Union, Washington, DC, Geophys. Monogr., 29: 48-57.

Prell, W.L. & W.B. Curry, 1981. Faunal and isotopic indices of monsoonal upwelling: Western Arabian Sea. — Oceanol. Acta, 4: 91-98.

Pujos, A., 1992. Calcareous nannofossils of Plio-Pleistocene sediments from the northwestern margin of tropical Africa. In: C.P. Summerhayes, W.L. Prell & K.C. Emeis (eds.). Upwelling systems: evolution since the Early Miocene. — Geol. Soc. Spec. Publ., 64: 343-359.

Rea, D.K., N.G. Pisias & T. Newberry, 1991. Late Pleistocene paleoclimatology of the central equatorial Pacific: flux patterns of biogenic sediments. — Paleoceanography, 6, 2: 227-244.

Reid, J.L., 1962. On the circulation, phosphate-phosphorus content and zooplankton volumes in the upper part of the Pacific Ocean. — Limnol. Oceanogr., 7: 287-306.

Reynolds, L.A. & R.C. Thunell, 1985. Seasonal succession of planktonic foraminifera in the subpolar North Pacific. — J. Foram. Res., 15: 282-301.

Reynolds, L.A. & R.C. Thunell, 1986. Seasonal production of morphologic variation of *Neogloboquadrina pachyderma* (Ehrenberg) in the northeast Pacific. — Micropaleontology, 32: 1-18.

Ruddiman, W.F. & A. McIntyre, 1976. Northeast Atlantic paleoclimatic changes over the past 600,000 years. In: R. Cline & J. Hays (eds.). Investigation of Late Quaternary paleoceanography and paleoclimatology. — Geol. Soc. Amer. Mem., 145: 199-214.

Saager, P.M., 1994. On the relationships between dissolved trace metals and nutrients in sea water: implications for the use of cadmium as a paleoceanographic tracer. — Doctor's Thesis, Vrije Univ., Amsterdam: 1- 240.

Saito, T., P.R. Thomson & D. Breger, 1981. Systematic index of Recent and Pleistocene planktonic Foraminifera. — Univ. Tokyo Press: 1-190.

Sancetta, C., 1992. Primary production in the glacial North Atlantic and North Pacific oceans. — Nature, 360: 249-250.

Sarnthein, M., U. Pflaumann, R. Ross, R. Tiedemann & K. Winn, 1992. Transfer functions to reconstruct ocean palaeoproductivity: a comparison. In: C.P. Summerhayes, W.L. Prell & K.C. Emeis (eds.). Upwelling systems: evolution since the Early Miocene. — Geol. Soc. Spec. Publ., 64: 411-427.

Schrader, H., 1992. Peruvian coastal primary palaeo-productivity during the last 200,000 years. In: C.P. Summerhayes, W.L. Prell & K.C. Emeis (eds.). Upwelling systems: evolution since the Early Miocene. — Geol. Soc. Spec. Publ., 64: 391-409.

Shannon, C.E., 1949. The mathematical theory of environments. In: C.E. Shannon & W. Weaver (eds.). The mathematical theory of communication. — Univ. Illinois Press, Urbana: 1-93.

Shemesh, A., S.A. Macko, C.D. Charles & G.H. Rau, 1993. Isotopic evidence for reduced productivity in the glacial Southern Ocean. — Science, 262: 407-410.

Siedler, G., W. Zenk & J. Emery, 1985. Strong-current events related to a subtropical front in the Northeast Atlantic. — J. Phys. Oceanogr., 15: 885- 897.

Spindler, M. & G.S. Dieckmann, 1986. Distribution and abundance of the planktic foraminifer *Neogloboquadrina pachyderma* in the sea ice of the Weddell Sea (Antarctica). — Polar Biol., 5: 185-191.

Srinivasan, M.S. & J.P. Kennett, 1974. Secondary calcification of the planktonic foraminifer *Neogloboquadrina pachyderma* as a climatic index. — Science, 186: 630-632.

Steens, T.N.F., G. Ganssen & D. Kroon, 1992. Oxygen and carbon isotopes in planktonic foraminifera as indicators of upwelling intensity and upwelling induced high productivity in sediments from the Northwestern Arabian Sea. In: C.P. Summerhayes, W.L. Prell & K.C. Emeis (eds.). Upwelling systems: evolution since the Early Miocene. — Geol. Soc. Spec. Publ., 64: 107-119.

Stein, R. & R. Stax, 1991. Late Quaternary organic carbon cycles and paleoproductivity in the Labrador Sea. — Geo-Marine Letters, 11: 90-95.

Stuiver, M. & T. Braziunas, 1993. Modeling atmospheric ^{14}C influences and ^{14}C ages of marine samples to 10,000 BC. In: M. Stuiver, A. Long & R.S. Kra (eds.). Calibration 1993. — Radiocarbon, 35,1: 137-189.

Stuiver, M. & P. Reimer, 1993. Extended ^{14}C data base and revised CALIB 3.0 ^{14}C age calibration program. In: M. Stuiver, A. Long & R.S. Kra (eds.). Calibration 1993. — Radiocarbon, 35, 1: 215-230.

Subba Rao, D.V. & T. Platt, 1984. Primary production of Arctic waters. — Polar Biol., 3: 191-201.

Takahashi, K., 1994. From modern flux to paleoflux: assessment from sinking assemblages to thanato-

coenosis. In: R. Zahn, T.H. Pederson, M.A. Kaminski & L. Labeyrie (eds.). Carbon cycling in the glacial ocean: constraints on the ocean's role in global change. — NATO ASI Series, I17: 413-424.

Thomas, E., L. Booth, M. Maslin & N.J. Shackleton, 1995. Northeastern Atlantic benthic foraminifera during the last 45,000 years: changes in productivity seen from the bottom up. Paleoceanography, 10, 3: 545-562.

Thunell, R.C., W.B. Curry & S. Honjo, 1983. Seasonal variation in the flux of planktonic foraminifera: time series sediment trap results from the Panama Basin. — Earth Planet. Sci. Lett., 64: 44-55.

Thunell, R.C. & S. Honjo, 1987. Seasonal and interannual changes in planktonic foraminiferal production. — Nature, 328: 335-337.

Thunell, R.C., Q. Miao, S.E. Calvert & T.F. Pederson, 1992. Glacial-Holocene biogenic sedimentation patterns in the South China Sea: productivity variations and surface water pCO_2. — Paleoceanography, 7, 2: 143-162.

Thunell, R.C. & L.A. Reynolds, 1984. Sedimentation of planktonic foraminifera: seasonal changes in species flux in the Panama Basin. — Micropaleontology, 30: 241-260.

Versteegh, G.J.M., 1995. Paleoenvironmental changes in the Mediterranean and North Atlantic in relation to the onset of northern hemisphere glaciations (2.5 Ma B.P.) -a palynological approach-. — Doctor's Thesis Univ. Utrecht: 1-134.

Vincent, E. & W.H. Berger, 1981. Planktonic foraminifera and their use in paleoceanography. In: C. Emiliani (ed.). The oceanic lithosphere: the sea. — J. Wiley, New York, vol. 7: 1025-1119.

Wolfteich, C.M., 1994. Satellite-derived sea surface temperature, mesoscale variability, and foraminiferal production in the North Atlantic. — M.Sc., Mass. Inst. Techn./Woodshole Oceanogr. Inst.: 1-80.

Weering, T.C.E. van & S. de Rijk, 1991. Sedimentation and climate-induced sediments on Feni Ridge, Northeast Atlantic Ocean. — Marine Geol., 101: 49-69.

Manuscript received 28 July 1995, revised version accepted 13 June 1996.

Appendix 1

Annotated alphabetical species list

Plates 1-12 represent Scanning Electron Micrographs of foraminifera specimens from the Northeast Atlantic piston core T88-9P. RGM stands for the National Museum of Natural History, Palaeontology Department, formerly Rijksmuseum van Geologie en Mineralogie, Leiden.

I follow the taxonomy of Bé & Tolderlund (1971) with some modifications by Saito et al. (1981).

Globigerina bulloides d'Orbigny, 1826
Pl. 1, figs. 1-7.

In the North Atlantic, *G. bulloides* is a dominant species in NAC waters (Ottens, 1991, 1992) and abounds in subpolar waters as well, from New York to Portugal and from the Labrador to the Norwegian Sea (Bé & Hamlin, 1967; Bé & Tolderlund, 1971). It has a similar distribution in surface sediment samples (Kipp, 1976). *G. bulloides* is also a characteristic species in upwelling regions (Prell & Curry, 1981; Prell, 1984a,b). It occurs over a surface temperature range of 0°C to 27°C (Bé & Tolderlund, 1971).

G. bulloides has high (up to 29%), moderate and low accumulation rates, relative and absolute frequencies in interglacial, glacial and Heinrich layers, respectively. The species is about twice as frequent in interglacial as in glacial sediments.

Globigerina rubescens Hofker, 1956
Pl. 1, figs. 8-13.

Most specimens were white although some had a pink/orange pigmentation. This species is distinguished from *G. tenellus* by its pigmentation and by the absence of a secondary aperture(s).

This species may comprise up to 2.3% in interglacial, is seldom present in glacial and absent in Heinrich layers. In the 208 ka record, the maximum relative and absolute frequencies and accumulation rate of *Globigerina rubescens* are noted immediately after Termination II, just like those of the other warm-water species such as *Globigerinoides tenellus* and *Orbulina universa*.

Globigerinella aequilateralis (Brady, 1879)
Pl. 2, figs. 1-7.

G. aequilateralis is only present in low frequencies not exceeding 2.3% in interglacial, seldom present in glacial and generally absent in Heinrich sediments. There are two forms, the loosely-coiled being more common than the involute and tightly-coiled tests. Peak absolute frequency of 490 specimens/g is noted in isotopic stage 7.

Globigerinita glutinata (Egger, 1893)
Pl. 3, figs. 1-18.

The supplementary features like bullae and secondary apertures give *G. glutinata* many morphologic variations even within a single sample.

The relative frequency of this species is high (reaching 20%) in interglacial, moderate in glacial and very low in Heinrich layers. The mean absolute frequency is 4800, 1000 and 400 specimens/g, respectively. The interglacial accumulation rate is generally higher than the glacial.

Globigerinita uvula (Ehrenberg, 1861)

This very small microperforate species with a high trochospiral and translucent, smooth test is identified only in sample 50 at about 12.5 ka. The accumulation rate, relative and absolute frequencies are 3090 specimens/cm²ka, <1%, and 780 specimens/g, respectively.

Globigerinoides ruber (d'Orbigny, 1839)
Pl. 4, figs. 1-14.

There are three *G. ruber* forms: (1) a small, compact, low-spired, thick- walled form; (2) a bigger, moderately high-spired and lobular variant; and (3) a high-spired and thin-walled form. *G. ruber* also exhibits two colour varieties, pink and white. The pink form is generally larger than the white one and usually occurs in warmer waters in the Atlantic, whereas the white form prefers lower temperatures (Hemleben et al., 1989). Most specimens are white except for a few pink ones in isotopic substage 5.5.

This species is absent from isotopic stages 2 and 3, and does not exceed 3% of the total planktic foraminiferal assemblage in the other isotopic stages. Both the average absolute frequency and the accumulation rate are higher in interglacial than in glacial periods.

Globigerinoides tenellus Parker, 1958
Pl. 5, figs. 1-4.

G. tenellus was distinguished from *G. rubescens* by the presence of dorsal supplementary aperture(s) and from *G. ruber* by its more lobulate periphery.

This species may comprise up to 3.7% of the planktic foraminiferal assemblage in interglacial sediments. It is absent from Heinrich and most glacial sediments.

Globorotalia hirsuta (d'Orbigny, 1839)
Pl. 6, figs. 1-4.

G. hirsuta is a cool subtropical species (Ruddiman & McIntyre, 1976). Like *Globorotalia truncatulinoides* it reproduces at the surface and then sinks to deeper waters where it prefers to live (Hemleben et al., 1989).

This species can be big with a relatively high spire, pustulate surface and a weakly lobulate periphery in interglacial sediments while glacial specimens are small with a relatively lower spire. *G. hirsuta* is absent from Heinrich layers and isotopic stages 2 and 4, and occurs in relatively low amounts (not exceeding 3%) in the other stages. Its average absolute frequency and accumulation rate are about four times higher in interglacial than in glacial sediments.

Globorotalia inflata (d'Orbigny, 1839)
Pl. 7, figs. 1-11.

G. inflata abounds in the Gulf Stream and the North Atlantic Current (Bé & Hamlin, 1967; Bé & Tolderlund, 1971) but inhabits subpolar waters as well. It is a deep-dweller preferring depths between 100-150 m (Bé, 1977).

Most specimens in the core have a smooth and shiny outer layer with a convex spiral side and rounded periphery. However, some specimens have a granular texture and subangular periphery.

This species has high, moderate and low frequencies and accumulation rates in interglacial, glacial and in Heinrich layers, respectively. *G. inflata* may comprise up to 16.0 % of the foraminiferal assemblage with a maximum absolute frequency of 4170 specimens/g in interglacial sediments.

Globorotalia scitula (Brady, 1882)
Pl. 2, figs. 8-13.

G. scitula is found in subpolar waters in rather high frequencies (Rea et al., 1991; Reynolds & Thunell, 1985) and in subtropical waters (Bé & Hamlin, 1967).

The relative frequency of *G. scitula* is higher (reaching 8.5%) in interglacial than in glacial sediments. Both absolute frequency and accumulation rate are also generally higher in the former than in the latter. It occurs in very low frequencies or may be absent in Heinrich layers.

Globorotalia truncatulinoides (d'Orbigny, 1839)
Pl. 6, figs. 5-8.

G. truncatulinoides is a subtropical species (Bé & Tolderlund, 1971). It is common in the Sargasso Sea where it reaches a maximum abundance during winter (Bé, 1959; Bé & Tolderlund, 1971).

This species occurs in low accumulation rates, absolute and relative frequencies (not exceeding 3.7%) in interglacial layers. Its peak absolute frequency is at 126 ka, immediately after Termination II. It is absent from isotopic stage 2 and in most of stages 6, 4 and 3.

Neogloboquadrina incompta (Cifelli, 1961)
Pl. 8, figs. 1-12.

N. incompta has been regarded as a dextral ecophenotype of *N. pachyderma* or a

dextral-coiling subspecies thereof (Parker, 1962; Reynolds & Thunell, 1986). I followed the classification of Ciffeli (1961, 1973) and distinguished *N. incompta* by its dextral coiling, more pustulate surface and more lobulate form compared to *N. pachyderma*.

The relative frequency of *N. incompta* is high (reaching 33% in isotopic stage 5), moderate (up to 23 %) and very low in interglacial, glacial and Heinrich layers, respectively. Both absolute frequency and accumulation rate are higher in interglacial than in glacial sediments.

Neogloboquadrina pachyderma (Ehrenberg, 1861)
Pl. 9, figs. 1-15.

This species inhabits polar as well as subpolar waters (Bé & Hamlin, 1967), can live within sea ice and tolerates salinities of up to 82‰ (Hemleben et al., 1989).

N. pachyderma was initially separated into two groups A and B, with group A consisting of crystalline forms which results from a secondary calcification process over a primary reticulate surface texture, and group B having reticulate textures (Srinivasan & Kennett, 1974). Reynolds & Thunell (1986) adapted the same classification and added that group A is predominantly sinistral while group B is predominantly dextral. For this study, Reynolds & Thunell's (1986) group A was identified as *N. pachyderma*.

Bé & Hamlin (1967) demonstrated that the distribution boundary between dextral and sinistral forms (according to my classification, *N. incompta* and *N. pachyderma*, respectively) is associated with the 7.2 °C surface isotherm. Aside from temperature changes, coiling patterns could also reflect availability of nutrients with dextral forms abundant when nutrient concentration is low and sinistral forms being abundant when nutrient concentration is high (Reynolds & Thunell, 1986). However, Brummer & Kroon (1988) showed that changes in coiling patterns reflect the dynamics of central water masses and polar fronts rather than the displacements of particular isotherms.

There are two major *N. pachyderma* forms in the core. One has a small compact test with a rounded outline, and has thick walls which tend to obscure the sutures and the aperture. The other has a large lobulate test and 4 to 5 discrete chambers separated by sutures, with the last chamber reduced or bullate, sometimes partially covering the aperture. Both forms are abundant in Heinrich and glacial layers while the former is more common in interglacial sediments.

The relative frequency of *N. pachyderma* is low (not exceeding 20%), moderate and very high (up to 95%) in interglacial, glacial and Heinrich layers, respectively. Despite its dominance in Heinrich layers, its absolute frequency is generally lower compared to glacial sediments. Its maximum absolute frequency and accumulation rate is in isotopic stage 6.

Orbulina universa d'Orbigny, 1830
Pl. 5, figs. 5-7.

The size of this species is correlated with the availability of food supply, the more

food, the larger the spherical shell and overfeeding results in a double sphere, a so-called *'Biorbulina'* (Hemleben et al., 1989). There are some large tests in interglacial sediments.

This species may comprise up to 2% of the total planktic foraminiferal assemblage in interglacial sediments. It is absent from glacial sediments except in isotopic stage 6 where it is occasionally present.

Turborotalita humilis (Brady, 1884)
Pl. 5, figs. 8-11.

T. humilis is found only in sample number 715 cm, at 192 ka. It has a very low frequency of 0.2 %, corresponding to 360 specimens/cm²ka. This species differs from *T. quinqueloba* by its smaller size and more numerous chambers.

Turborotalita quinqueloba (Natland, 1938)
Pl. 10, figs. 1-14; Pl. 11, figs. 1-18; Pl. 12, figs. 1-11.

This typically subpolar species (Bé & Hamlin, 1967; Bé & Tolderlund, 1971) shows considerable variation in the core. Numerous specimens have a bulla-like elongation of the final chamber which can partially or completely cover the aperture, others have an aperture without a lip, while some have a thickened rim-like basal lip.

The relative frequency of *T. quinqueloba* is high in interglacial (reaching 31.9%) and in glacial (reaching 38.8%) sediments while it is low in Heinrich layers. The average absolute frequency and accumulation rate of this species are higher in interglacial than in glacial sediments.

Plate 1

The 100 μm bar scale below fig. 2 applies to figs. 1-6; the scale on the lower left corner is for figs. 8-12; and the 10 μm bar is for figs. 7 and 13.

Figs. 1-7. *Globigerina bulloides* d'Orbigny, 1826
1-4. Umbilical views. Specimens of figs. 1, 5, and 6 are from sample 0, of figs. 2-4 and 7 are from sample 450.
1. Typical specimen with lobulated periphery and four spherical to subspherical chambers in the final whorl; RGM 360 200.
2. Common morphotype with wide apertural opening; RGM 360 201.
3. Thinner-shelled, smoother-surfaced specimen with chambers rapidly increasing in size; RGM 360 202.
4. Specimen with diminutive ultimate chamber in the final whorl; RGM 360 203.
5. Spiral view; RGM 360 204.
6. Side view; RGM 360 205.
7. Detail of surface wall structure showing large irregularly-spaced pores. Elevated areas are spine bases, disappearance of spine shafts reveal circular holes in the centre; RGM 360 206.

Figs. 8-12. *Globigerina rubescens* Hofker, 1956 from sample 500.
8. Spiral view; note absence of secondary aperture; RGM 360 207.
9. Side view; RGM 360 208.
10. Umbilical view of same specimen in fig. 8 showing wide highly-arched aperture.
11. Umbilical view of specimen with thick-wall, compact test and small aperture with distinct lip; RGM 360 209.
12. Spiral view; RGM 360 209.
13. Same specimen as in fig. 8 showing last chamber to have shallow depression leading to roughly equidistant pores. Pores are small and interpore areas are wide.

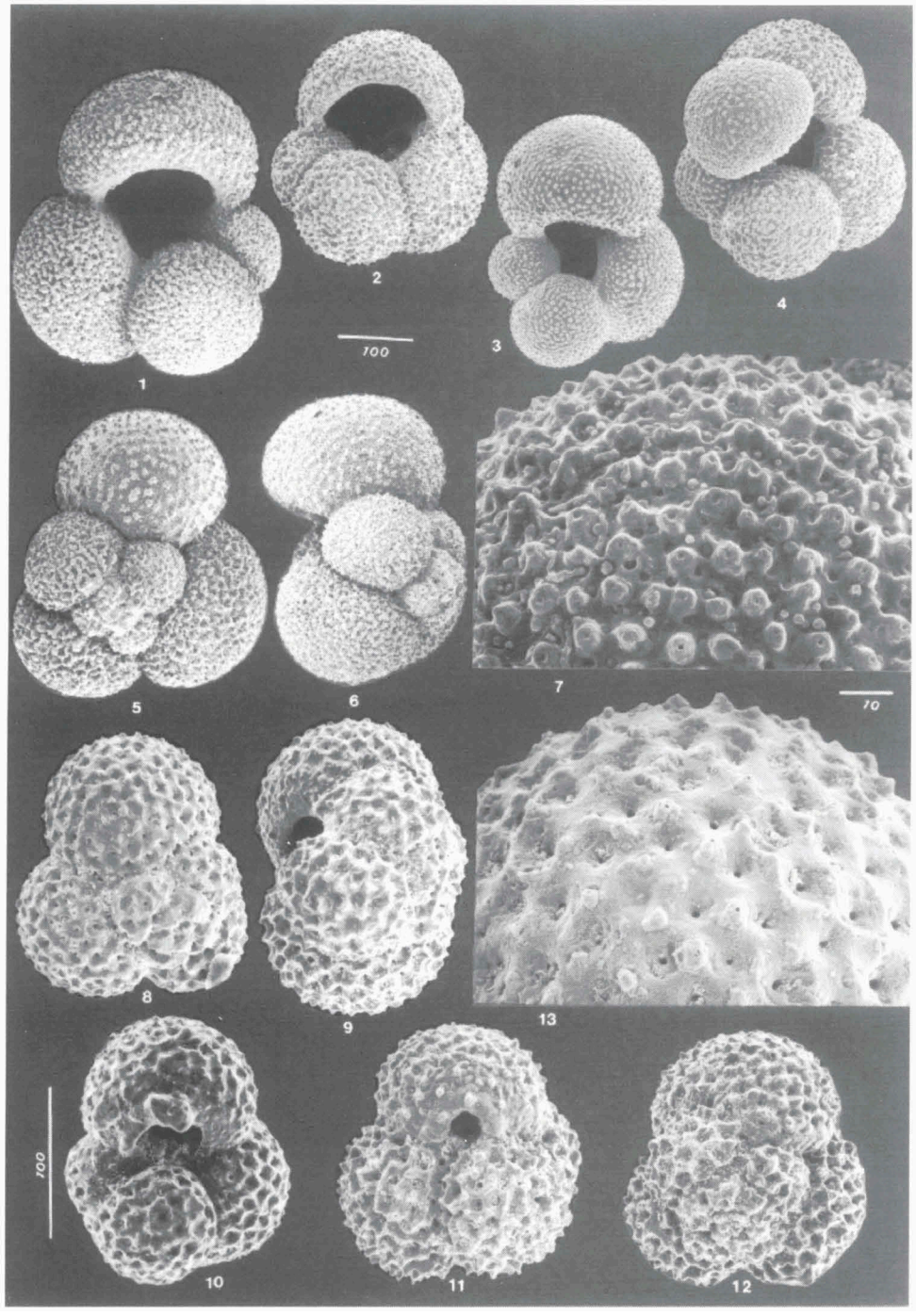
1
2
3
4
100
5
6
7
10
8
9
13
100
10
11
12

Plate 2

The 100 μm scale bar applies to figs. 1-9 and figs. 10-11, the 10 μm bar to figs. 7 and 12, and the 1 μm bar to fig. 13.

Figs. 1-7. *Globigerinella aequilateralis* (Brady, 1879). Specimens of figs. 1-3 and figs. 5-7 are from samples 0 and 500, respectively.
1. Umbilical view of large, loosely-coiled specimen; note smooth surface of last chamber compared to rest of test; RGM 360 210.
2. Spiral view showing partial separation of last two chambers; RGM 360 211. 3. Asymmetrically-coiled specimen with crescent-shaped aperture; RGM 360 212.
4. Umbilical view of small, tightly-coiled specimen; RGM 360 213.
5-6. Spiral and side views of small specimens displaying asymmetrical coiling; RGM 360 214-215.
7. Enlargement of last chamber of specimen in fig. 4 shows spine bases as upraised circular to triangular mounds with round holes. Living specimens have triradiate spines.

Figs. 8-13. *Globorotalia scitula* (Brady, 1882) specimens from sample 450.
8. Spiral view; note large pores with wide pore pits within and around the proloculus, decreasing in size in older chambers; RGM 360 216.
9. Side view showing irregularly-shaped lip; RGM 360 217.
10. Spiral view of specimen with slowly increasing chamber size giving a nearly circular peripheral outline; RGM 360 218.
11. Umbilical view of a specimen that is heavily pustulate near the apertural area; RGM 360 219.
12. Enlargement showing smooth finely perforate last chamber of specimen in fig. 8.
13. Further enlargement of a single pore of fig. 12 illustrates that widening of pore size as the wall thickens with age, results to a well-layered conical pit.

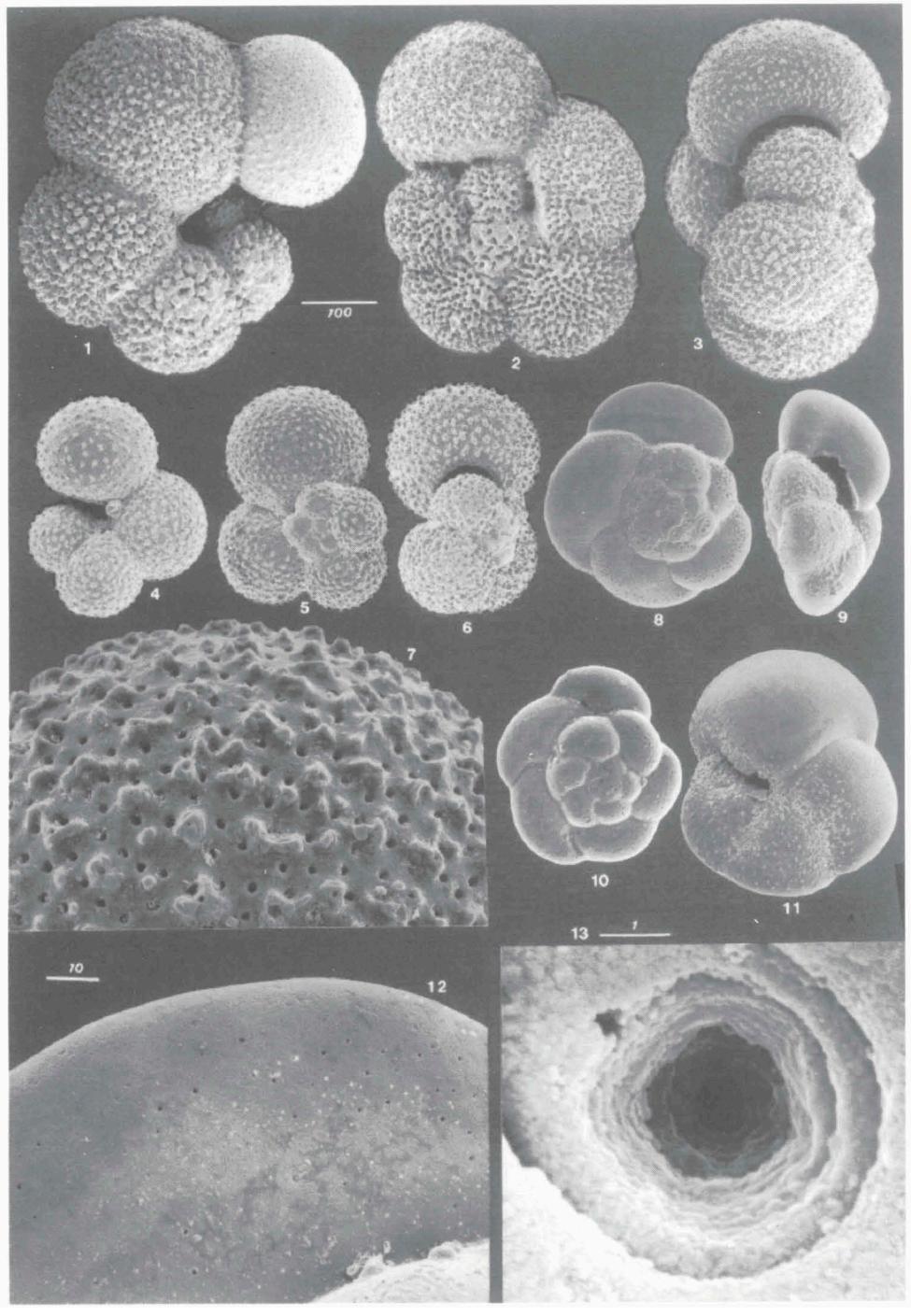
100
1
2
3
4
5
6
7
8
9
10
11
13
1
10
12

Plate 3

This plate illustrates the extreme variability in *Globigerinita glutinata* (Egger, 1893) test morphology. The 100 µm scale bar applies to figs. 1-15. Figs. 5, 11 and 15 are specimens from sample 0 while the rest are from sample 500.

Figs. 1-7. Umbilical views.
1. Simple primary aperture with thin lip; RGM 360 220.
2. Specimen with inflated last chamber and flap covering aperture; RGM 360 221.
3. Circular bulla covers aperture; RGM 360 222.
4. Specimen with dumbbell-shaped bulla; RGM 360 223.
5. Large inflated bulla with four infralaminal apertures; RGM 360 224.
6. Complex bulla with apertures at sutures of older chambers; RGM 360 225.
7. Intricate bulla with multiple apertures covering considerable part of test; RGM 360 226.

Figs. 8-12. Spiral views.
8. Specimen without secondary aperture; RGM 360 227.
9. Specimen with one secondary aperture. I consider this form to be synonymous to *Globigerinoides parkerae* Bermudez; RGM 360 228.
10. Specimen with large secondary aperture almost divided into two parts; RGM 360 229.
11. Infralaminal aperture of specimen extends to spiral side; RGM 360 230.
12. Part of bulla and two infralaminal apertures reach spiral side RGM 360 231.

Figs. 13-15. Side views.
13. Slit-like opening on the side; RGM 360 232.
14. Specimen with secondary aperture; RGM 360 233.
15. Smooth and thin-walled specimen with irregularly defined bulla that has multiple infralaminal apertures; RGM 360 234.

Figs. 16-18. Detailed views.
16. Specimen in fig. 13 showing bulla with smaller pustules than the remainder of the test.
17. Bulla of specimen in fig. 7 displaying conical pustules and small, dense but irregularly-spaced pores on their bases.
18. The two infralaminal apertures of fig. 12 specimen open beneath the bulla.

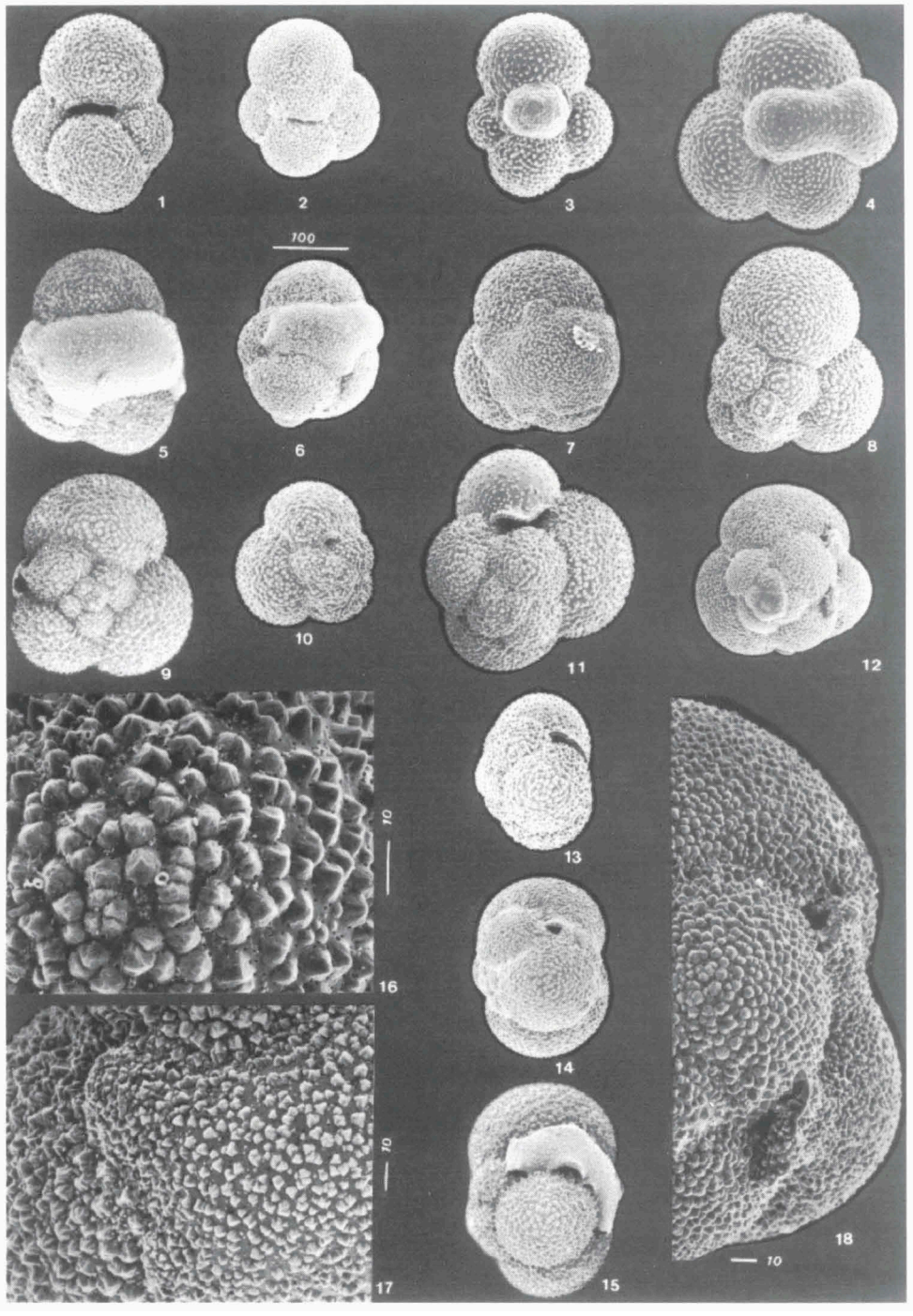
1
2
3
4
100
5
6
7
8
9
10
11
12
10
16
13
14
10
17
15
18
10

Plate 4

Test morphology and microstructure of *Globigerinoides ruber* (d'Orbigny, 1839). The 100 μm bar scale applies to figs. 1-10. Figs. 10 and 14 specimens are from sample 500 and the rest are from sample 15.

Figs. 1-3. Small, compact and thick-walled form.
1. Apertural view; RGM 360 235.
2. Spiral view showing one accessory aperture; RGM 360 236.
3. Side view; RGM 360 237.

Figs. 4-8. Larger, more lobulate form.
4-5. Umbilical views of specimens having circular apertures with and without a lip, respectively; RGM 360 238-239.
6-7. Specimens with one and two apertures on the spiral side, respectively; RGM 360 240-241.
8. Side view showing an accessory aperture; RGM 360 242.

Figs. 9-10. Large and high trochospiral form. Side views.
9. Specimen with small last chamber; RGM 360 243.
10. Thin-walled with inflated chambers rapidly increasing in size. Note same magnification as other *G. ruber* variants; RGM 360 244.

Fig. 11-14. Detailed views.
11. Penultimate chamber of fig. 1 specimen showing pores between mostly isolated and few interconnected spine bases with circular spine holes.
12. Last chamber of fig. 6 specimen illustrating big, inequidistant pores and spine bases.
13. Ultimate chamber of fig. 9 specimen shows large cone-shaped pores.
14. Last chamber of fig. 10 specimen showing rounded spine bases with circular holes.

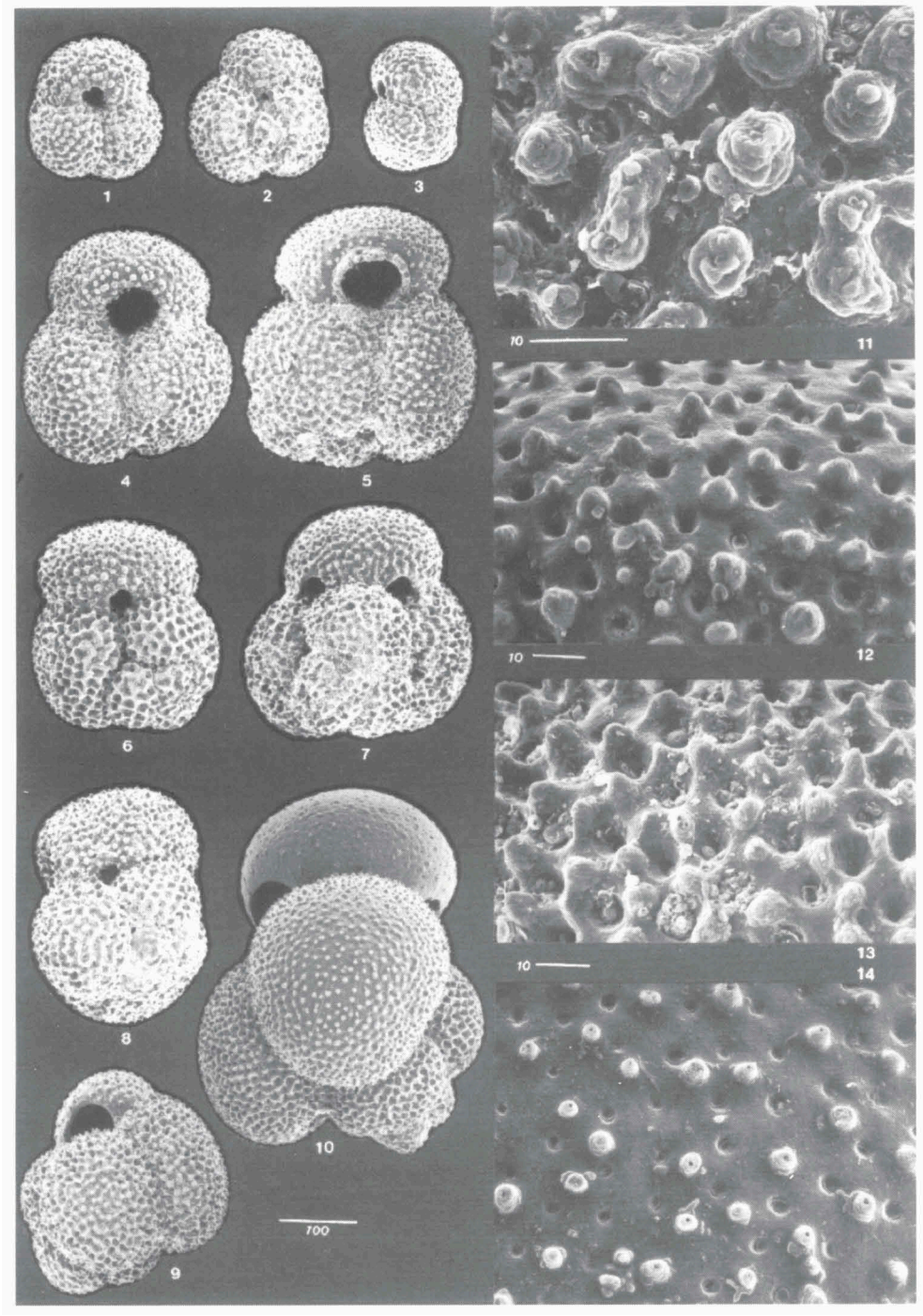
1
2
3
4
5
6
7
8
9
10
100
10
11
10
12
10
13
14

Plate 5

The 100 µm scale bar on the upper left applies to figs. 1-3 and 6-7 while the lower left one is for figs. 8-10. The 10 µm scale bar applies to figs. 4, 5 and 11.

Figs. 1-4. *Globigerinoides tenellus* Parker, 1958 specimen from sample 500.
1. Umbilical view of specimen with four spherical chambers in the final whorl and circular, highly-arched primary aperture with faint rim-like lip; RGM 360 245.
2. Spiral view of fig. 1, showing two accessory apertures, big and small.
3. The big accessory aperture is still visible from the side; RGM 360 246.
4. Detail of last chamber of fig. 1, illustrating coarsely perforated wall structure with large pores set in shallow depressions. Pore depressions are bounded by weakly developed polygonal ridges and spine bases are located at the junction between these ridges. Disappearance of the spine shafts show round spine holes.

Figs. 5-7. *Orbulina universa* d'Orbigny, 1830 specimens from sample 0.
5. Wall structure of fig. 6 specimen shows big and small pore openings of about 15 and 5 µm, respectively. The small pores of living specimens possess an inner organic lining and pore plates (Bé, et al., 1980) while the large pores lack these structures, and are therefore defined as apertures.
6. Big specimen with irregularly-spaced areal apertures; RGM 360 247.
7. Small specimen showing same feature; RGM 360 248.

Figs. 8-11. *Turborotalita humilis* (Brady, 1884) specimen from sample 715.
8. Umbilical view showing 6 1/2 chambers in the last whorl, with ultimate chamber extending basally to cover aperture; RGM 360 249.
9. Spiral view of fig. 8; note deeply-incised sutures.
10. Side view of fig. 8.
11. Enlargement of part of ultimate and penultimate chambers showing intergrowth of angular, euhedral calcite crystals to conceal some pores; same specimen.

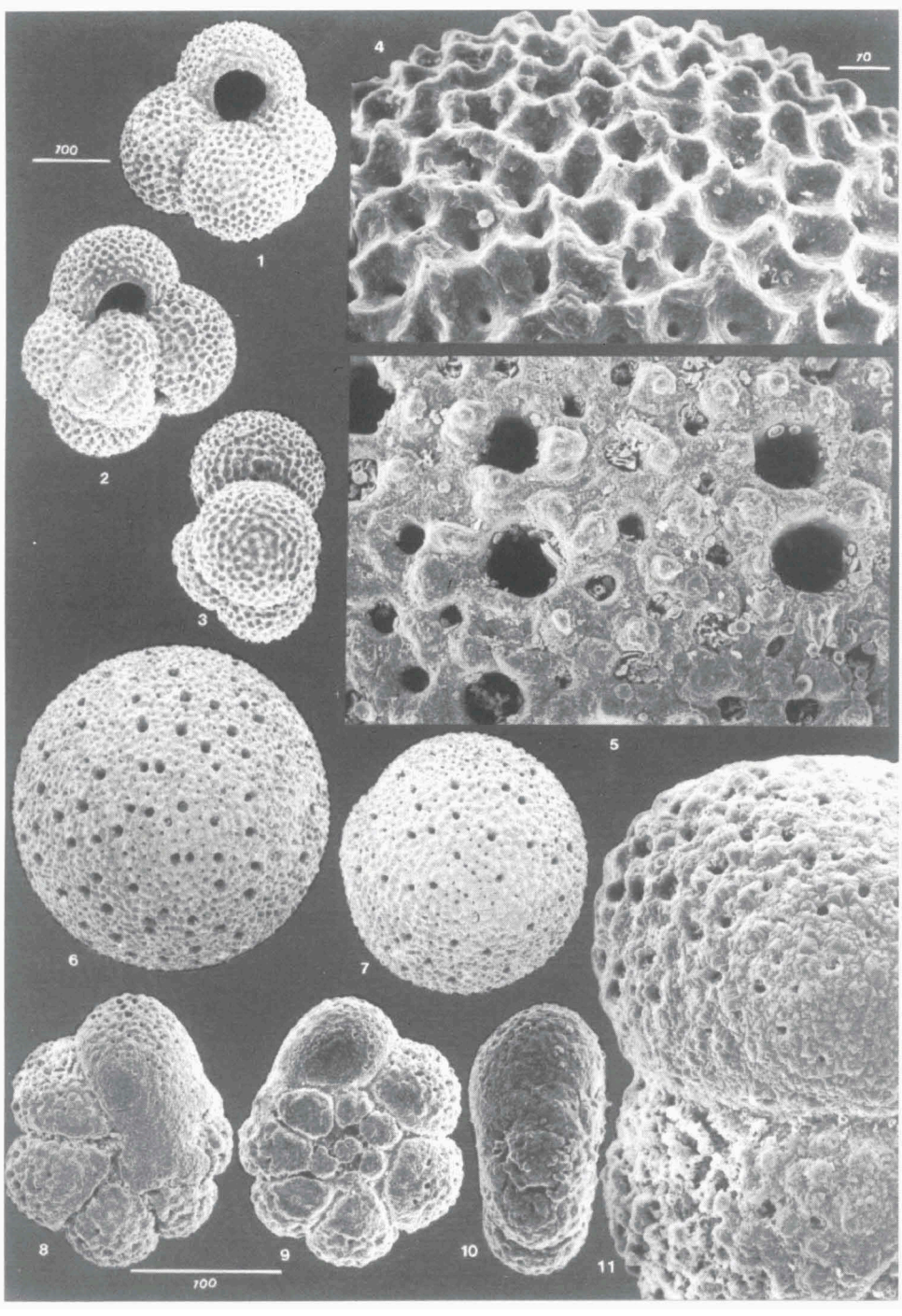
100
1
2
3
4
10
5
6
7
8
9
100
11

Plate 6

The 10 μm bar scale applies to figs. 4 and 5 while the 100 μm bar to the rest.

Figs. 1-4. *Globorotalia hirsuta* (d'Orbigny, 1839) from sample 15.
1. Umbilical view displaying intergrowth of nodelike pustules forming botryoidal surface near apertural area. Most pores in earlier chambers are obliterated by abundant interlocking pustules except in ultimate chamber; RGM 360 250.
2. Spiral view showing angular, platelike structures thickening prolocular area instead of knoblike pustules seen on spiral side; RGM 360 251.
3. Side view; RGM 360 252.
4. Close-up of last chamber of fig. 1 specimen showing only few isolated pustules. Note uneven surface texture due to partial calcite layer cover.

Figs. 5-8. *Globorotalia truncatulinoides* (d'Orbigny, 1839) from sample 0.
5. Enlargement of last chamber displaying medium-sized, dense pores and nodelike pustules in flat surface; RGM 360 253.
6. Umbilical view. As in *G. hirsuta*, test is very thick near aperture and thins in direction of growth, with little thickening in last chamber; RGM 360 254.
7. Spiral view; note big dense pustules in prolocular area and at keel junction; RGM 360 255. 8. Side view showing triangular peripheral outline and aperture with lip; RGM 360 256.

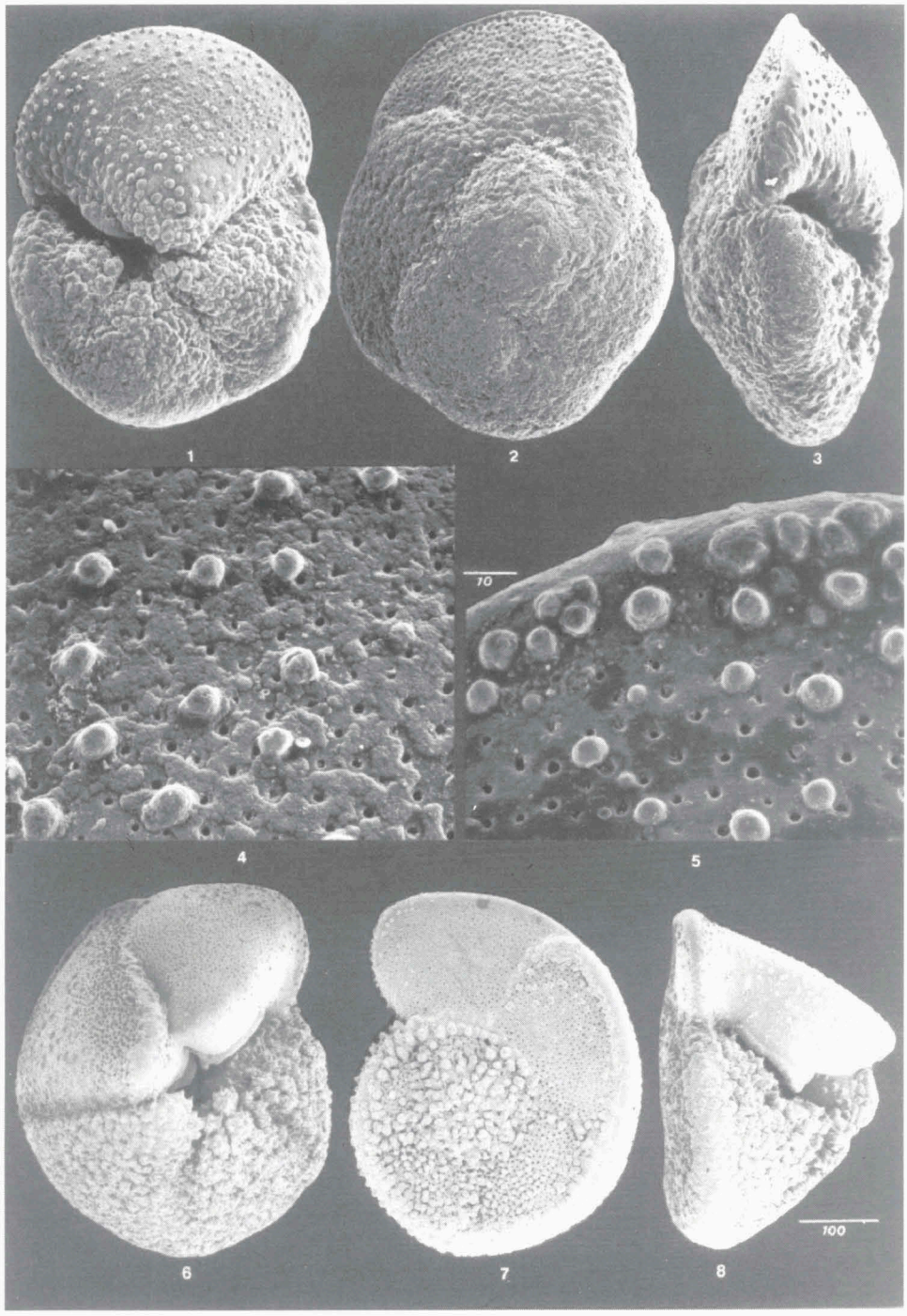
1
2
3
10
4
5
6
7
8
100

Plate 7

Test morphology and wall microstructure of *Globorotalia inflata* (d'Orbigny, 1839). The 10 μm bar scale applies to figs. 10 and 11 while the 100 μm bar to the rest. Figs. 1-3 are specimens from sample 0 while figs. 4-13 are from sample 450.

Figs. 1-3. Large thick-walled form.
1. Umbilical view of typical specimen which is coarsely granular in umbilicus and smooth in last chamber; RGM 360 257.
2. Spiral side has smooth wall structure; RGM 360 258.
3. Side view shows flatter spiral side of specimen compared to more convex ones of specimens in figs. 6 and 9; RGM 360 259.

Figs. 4-6. Large, thick-walled form with diminutive last chamber.
4. Umbilical view; note smooth diminutive and penultimate last chamber; RGM 360 260.
5. Spiral view showing almost rounded peripheral outline; RGM 360 261.
6. Side view displays large pustules around umbilicus; RGM 360 262.

Figs. 7-9. Small, thin-walled forms.
7. Umbilical view; RGM 360 263.
8. Spiral view illustrates rougher wall texture compared to specimens in figs. 2 and 5; RGM 360 264.
9. Side view shows more angular outline due to protrusion of last chamber; RGM 360 265.

Fig. 10-11. Enlarged views.
10. Penultimate chamber of specimen in fig. 5 has smooth, hummocky wall structure with constricted or obliterated pores. Most pores are on top of hummocks but few are located in depressions in between.
11. Last chamber of specimen in fig. 8 has porous surface with discrete nodelike pustules; note bigger irregularly-spaced pores compared to specimen with veneer of calcite crust (fig. 10).

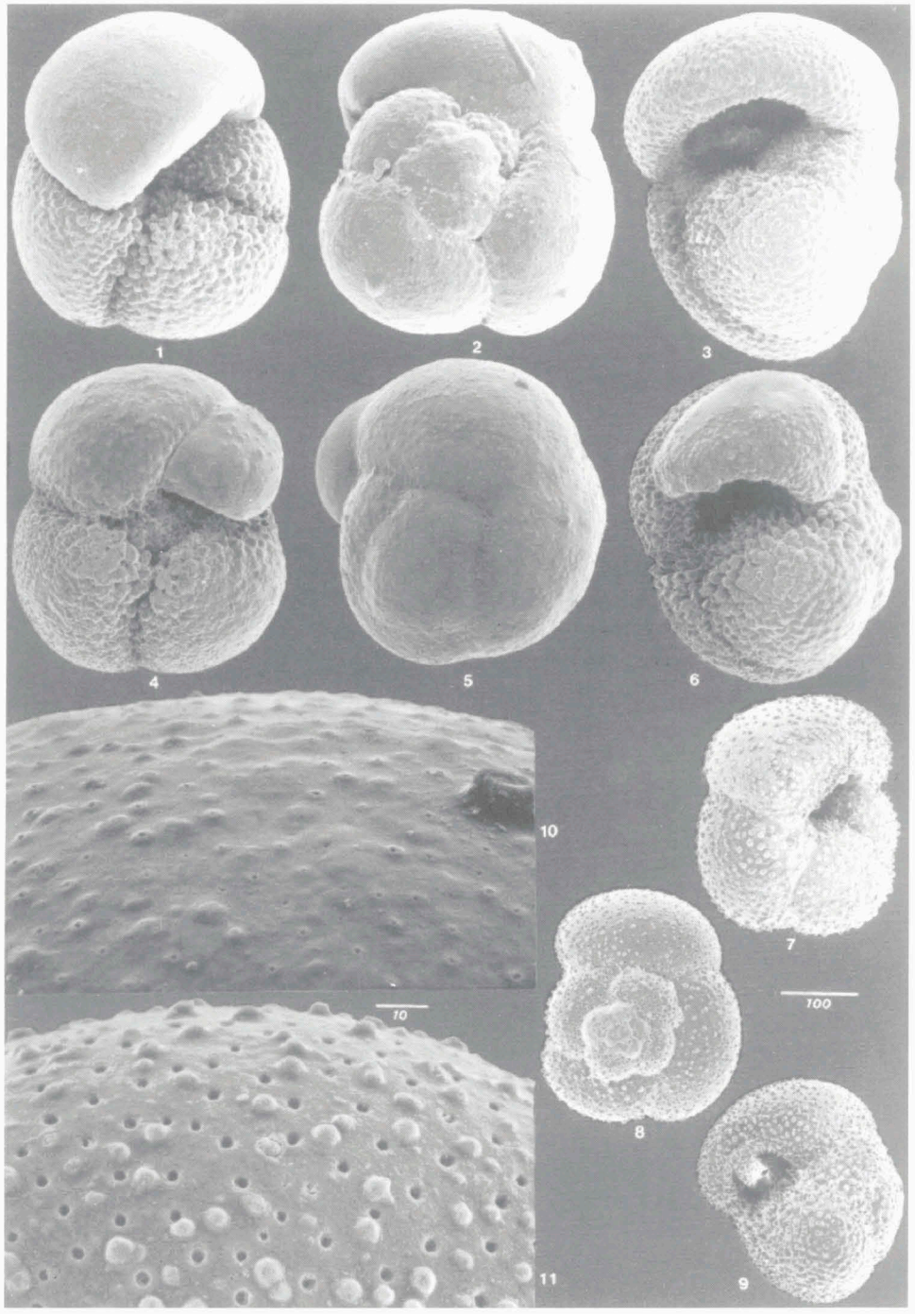
1
2
3
4
5
6
7
8
9
10
11
10
100

Plate 8

Morphological variants of *Neogloboquadrina incompta* (Cifelli, 1961) from samples 0 (fig. 2), 702 (figs. 1, 6 and 10) and 450 (figs. 3-5, 7-9 and 11-12). The 100 μm scale bar applies to all figures except for fig. 5.

Figs. 1-4. Umbilical views.
1. Lobulate specimen with 5 chambers in last whorl separated by distinct sutures. Chambers rapidly increase in size as added with last chamber partially covering aperture; RGM 360 266.
2. Less lobulate specimen with bean-shaped last chamber totally covering aperture; RGM 360 267.
3. Specimen has deep umbilicus and almost circular peripheral outline with the chambers slowly increasing in size as added (compare to fig. 1); RGM 360 268. 4. Specimen with four chambers in last whorl; ultimate chamber has flap with lip partially covering aperture; RGM 360 269.

Fig. 5. Enlarged view of penultimate chamber of specimen in fig. 7 showing large pores with calcite ridges surrounding individual pore pits. The sharp, uneven crystals of these ridges give an overall rough texture (compare with wall structure of *N. pachyderma* in Pl. 9, figs. 13-15).

Figs. 6-8. Spiral views.
6. Note the thickened prolocular area; RGM 360 271.
7. Specimen with quadrate peripheral outline and smaller ultimate than penultimate chamber; RGM 360 270.
8. Note large last chamber; RGM 360 272.

Figs. 9-12. Side views.
9. Note aperture with thick lip; RGM 360 273.
10. Specimen with wide apertural opening only partially covered by a lip; RGM 360 274.
11. Aperture without a lip; RGM 360 275.
12. Last chamber covers most of aperture; RGM 360 276.

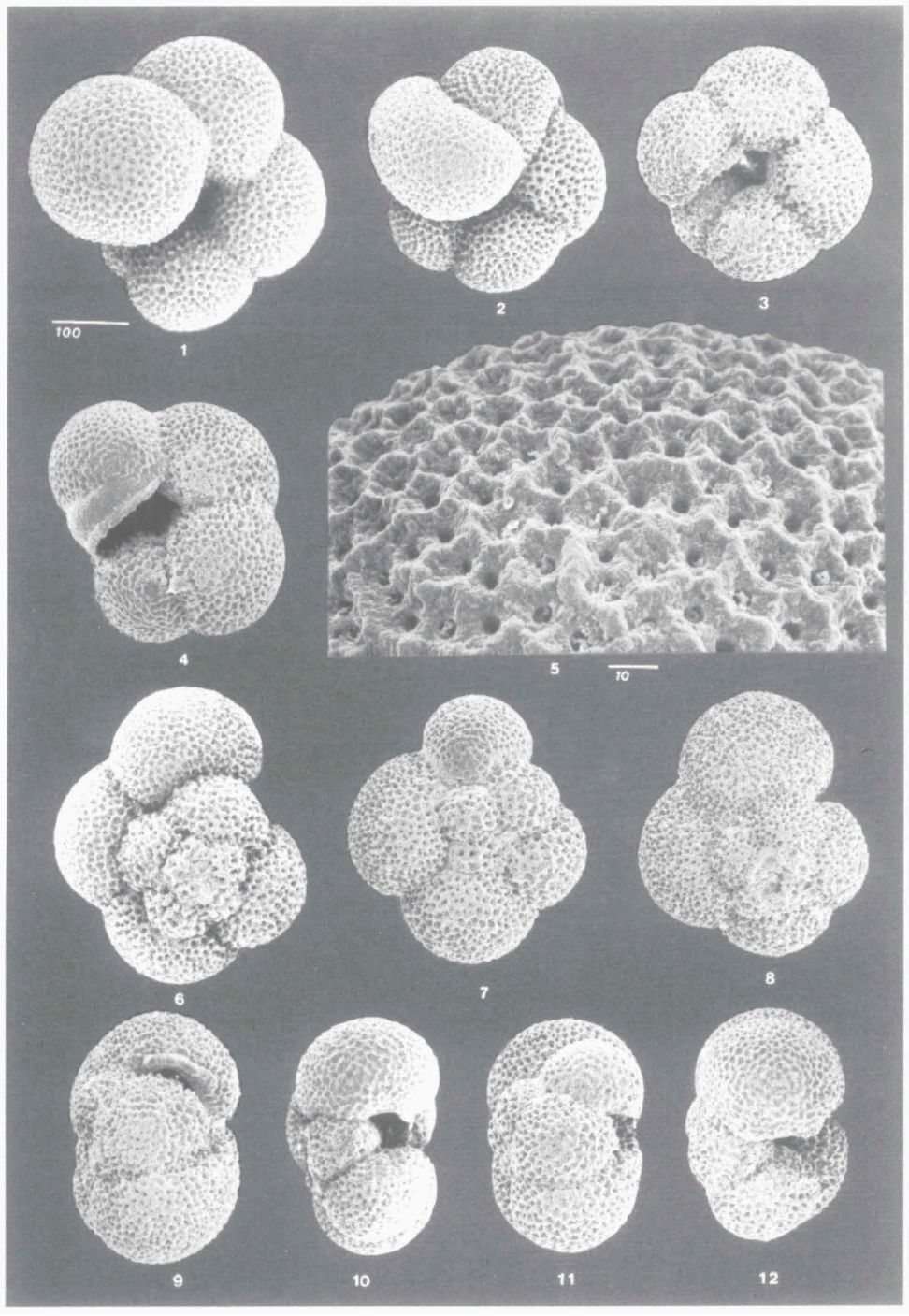
100
1
2
3
4
5
10
6
7
8
9
10
11
12

Plate 9

Neogloboquadrina pachyderma (Ehrenberg, 1861) specimens from samples 500 (figs. 1-3), 70 (figs. 4-6 and 13) 100 (figs. 7-12 and 14-15). The 100 µm scale bar applies to figs. 1-12 while the 10 µm bar to figs. 13-15.

Figs. 1-3. Small, very thick-walled, typical interglacial form.
1. Specimen with compactly arranged chambers. This is classified as *N. pachyderma*, group A by Reynolds & Thunell (1986); RGM 360 277.
2. Spiral view shows rounded test outline; RGM 360 278.
3. Side view. Note aperture is covered by last chamber; RGM 360 279.

Figs. 4-6. Large and very thick-walled specimens from a Heinrich layer.
4. Umbilical view. Although this form is similar to fig. 1, Heinrich layer and glacial specimens can attain big sizes. Note wide umbilicus surrounded by distinct calcite rhombs; RGM 360 280.
5. Spiral view showing sutures obliterated by heavy calcification; RGM 360 281. 6. Part of aperture still visible on side view; RGM 360 282.

Figs. 7-9. Quadrate morphotype typical of glacial sediments.
7. Umbilical view showing wide aperture covered by unornamented thin lip. A less encrusted specimen with similar form is classified by Reynolds & Thunell (1986) as *N. pachyderma*, group B; RGM 360 283.
8. Spiral view. Note sutures obliterated by calcite crust; RGM 360 284.
9. Side view showing wide apertural opening; RGM 360 285.

Figs. 10-12. Ovate morphotype common in glacial sediments.
10. Umbilical view of 4 1/2-chambered specimen with diminutive last chamber covering part of aperture; RGM 360 286.
11. Spiral view showing faint sutures; RGM 360 287.
12. Side view; note small last chamber; RGM 360 288.

Figs. 13-15. Enlarged views.
13. Last chamber of fig. 4 specimen showing calcite crust to obliterate some pores.
14. Wall structure and topography of penultimate chamber of fig. 8 specimen illustrating rugged ridges surrounding pores.
15. Penultimate chamber of fig. 11 specimen showing smoothened surface texture with most pores closed-off.

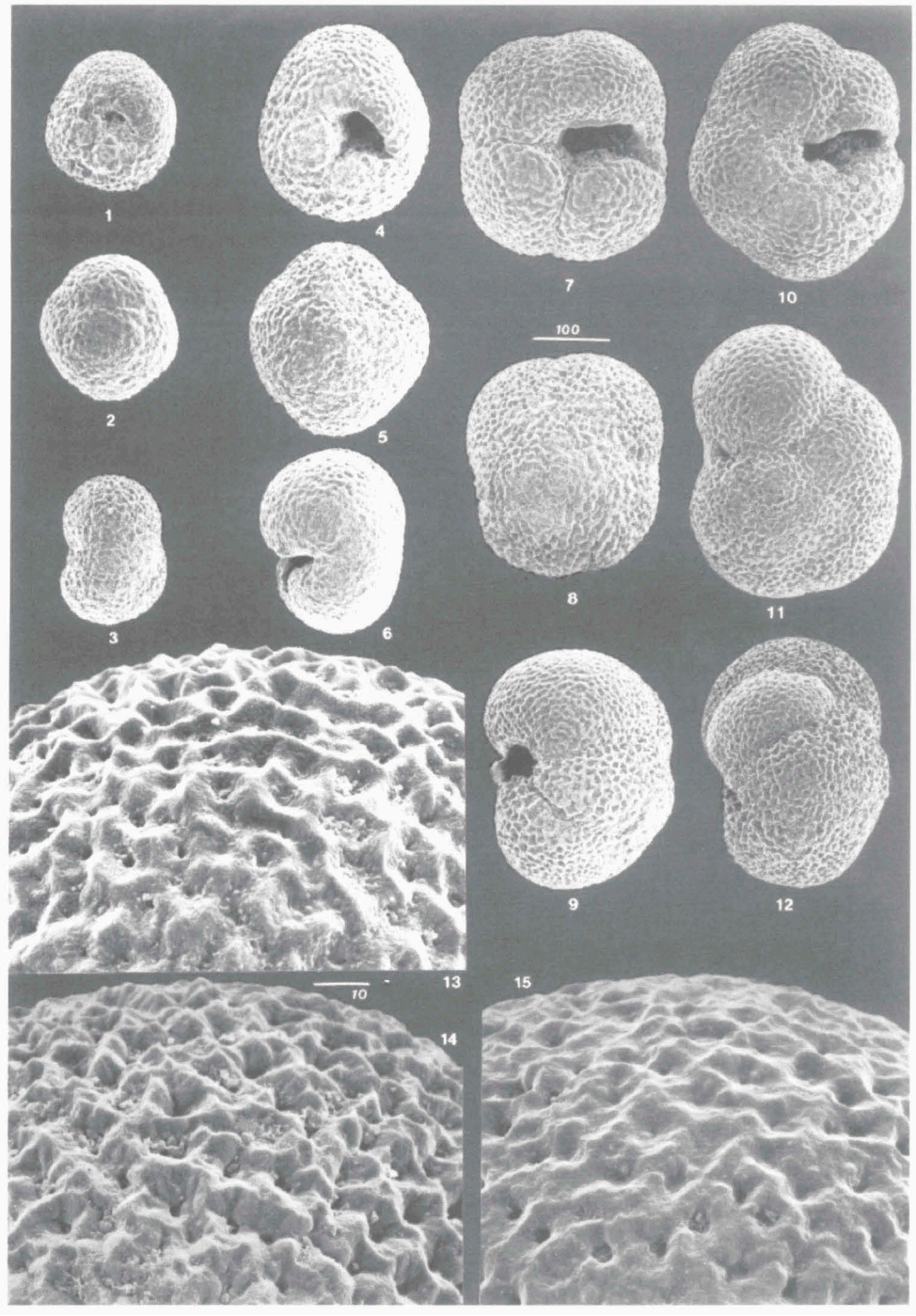
1
4
7
10
100
2
5
8
11
3
6
9
12
13
10
14
15

Plate 10

Extreme variability in *Turborotalita quinqueloba* (Natland, 1938) morphotypes due to differences in test thickening, shape of the chambers and aperture. All specimens are from interglacial sample 450 and are dextrally-coiled, except for those shown in figs. 5 and 13. The 100 μm bar scale applies to all figures.

Figs. 1-14. Umbilical views.
1. Typical specimen with five chambers in the last whorl and an umbilical aperture bordered by small lip; RGM 360 289.
2. More lobulate form with big aperture and no lip. This specimen has spine bases and holes distinguishing it from small specimens of *N. incompta*; RGM 360 290.
3. Umbilical aperture with small unornamented lip; RGM 360 291.
4. Flap partially covers aperture. Note less thickened, deeply-incised apertural area; RGM 360 292.
5. Slightly compressed specimen; RGM 360 293.
6. Flap-like extension of last chamber is partially fused to an earlier chamber in apertural area; RGM 360 294.
7. Large lobular variant; RGM 360 295.
8. Terminal chamber has two flap-like extensions; RGM 360 296.
9. Tear drop-shaped last chamber with irregular flap; RGM 360 297.
10. Tear drop-shaped last chamber with projecting lip covering aperture; RGM 360 298.
11. Six chambers in last whorl with diminutive ultimate chamber; RGM 360 299.
12. Aberrant terminal chamber is smaller than penultimate chamber; RGM 360 300.
13. Large specimen with bullate last chamber totally covering the aperture and parts of earlier chambers; RGM 360 301.
14. Huge and rare *T. quinqueloba* variant with exceptionally big last chamber and thick crescent-shaped ornamented lip; RGM 360 302.

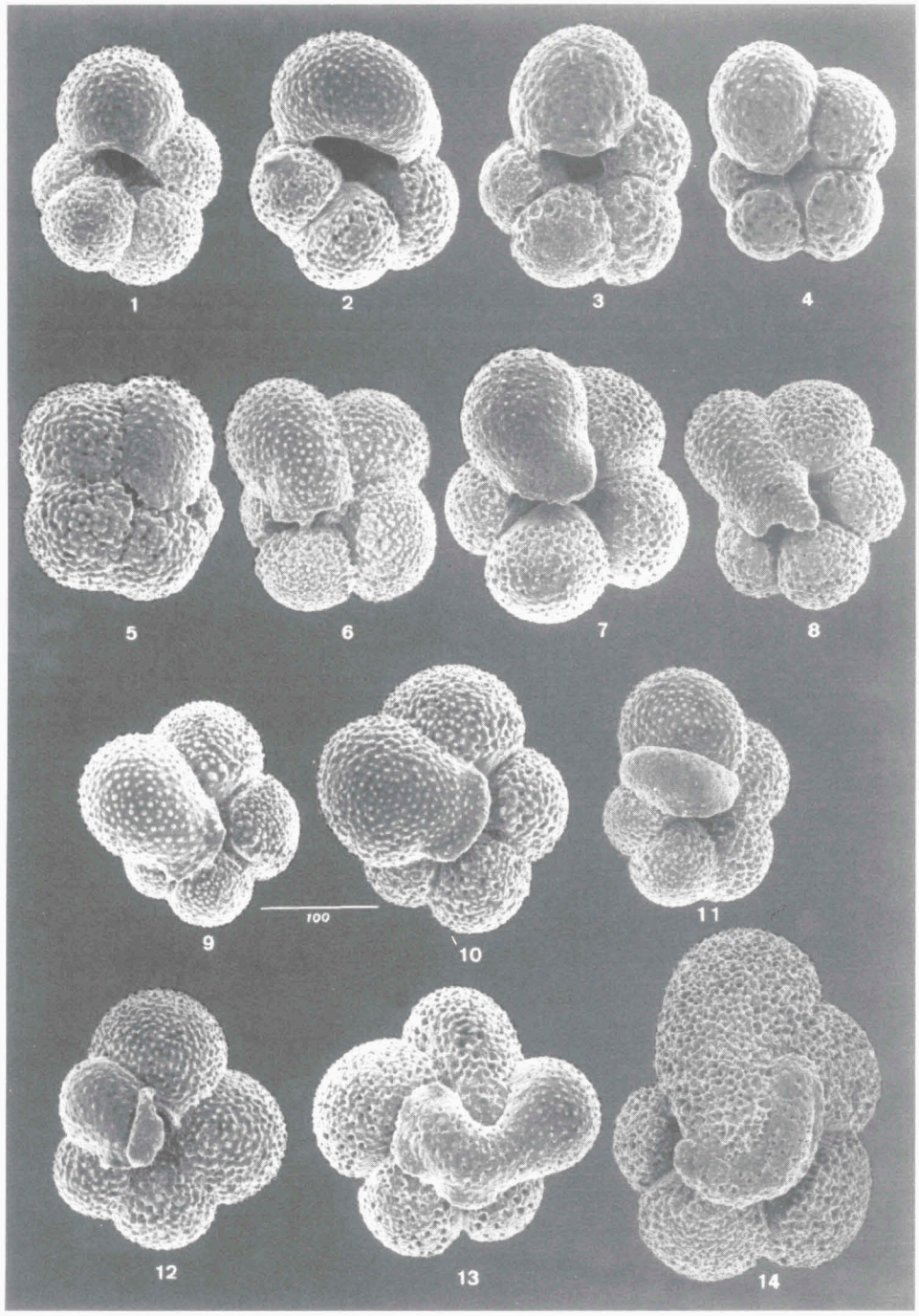
1
2
3
4
5
6
7
8
9
100
10
11
12
13
14

Plate 11

Turborotalita quinqueloba (Natland, 1938) morphotypes from glacial and Heinrich layers except for figs. 13 and 14 which are specimens from interglacial sediments (sample 450). Figs. 1-4 and 15; figs. 5-8, 11, 16 and 17; and figs. 9-10, 12 and 18 are specimens from samples 100, 70 and 702, respectively. Specimens shown in figs. 1-6, 9 13-15 and 17 are dextrally-coiled while the others are sinistrally-coiled. The 100 μm bar scale applies to all figures.

Figs. 1-12. Umbilical views.
1. Note triangular lip partially covering aperture; RGM 360 303.
2. Terminal chamber with flap-like extension; RGM 360 304.
3. Coalescence of some spine bases to form ridges gives this specimen a rough surface wall texture; RGM 360 305.
4. Large and lobular with intricate bulla; RGM 360 306.
5. Small compressed specimen with semi-circular aperture and thin lip; RGM 360 307.
6. Small with faint sutures due to calcite encrustation on surface; RGM 360 308.
7. Note wide aperture and irregularly-shaped unornamented lip; RGM 360 309.
8. Umbilical-interiomarginal aperture partially covered by an unornamented lip; RGM 360 310.
9. Small, lobulate with spherical chambers and circular umbilical aperture; RGM 360 311.
10. Note deeply-incised sutures particularly near the aperture; RGM 360 312.
11. Small specimen with big last chamber; RGM 360 313.
12. Note smooth surface compared to other specimens; RGM 360 314.

Figs. 13-18. Spiral views.
13. Large specimen with spherical chambers rapidly increasing in size as added; RGM 360 315.
14. Ultimate is smaller than penultimate chamber (compare with fig. 13); RGM 360 316.
15. Note distinctly smoother last chamber compared to other chambers; RGM 360 317.
16. Small specimen with smoother wall structure than those of figs. 13-15; RGM 360 318.
17. Small, compact specimen with large pores; RGM 360 319.
18. Note thickened prolocular area; RGM 360 320.

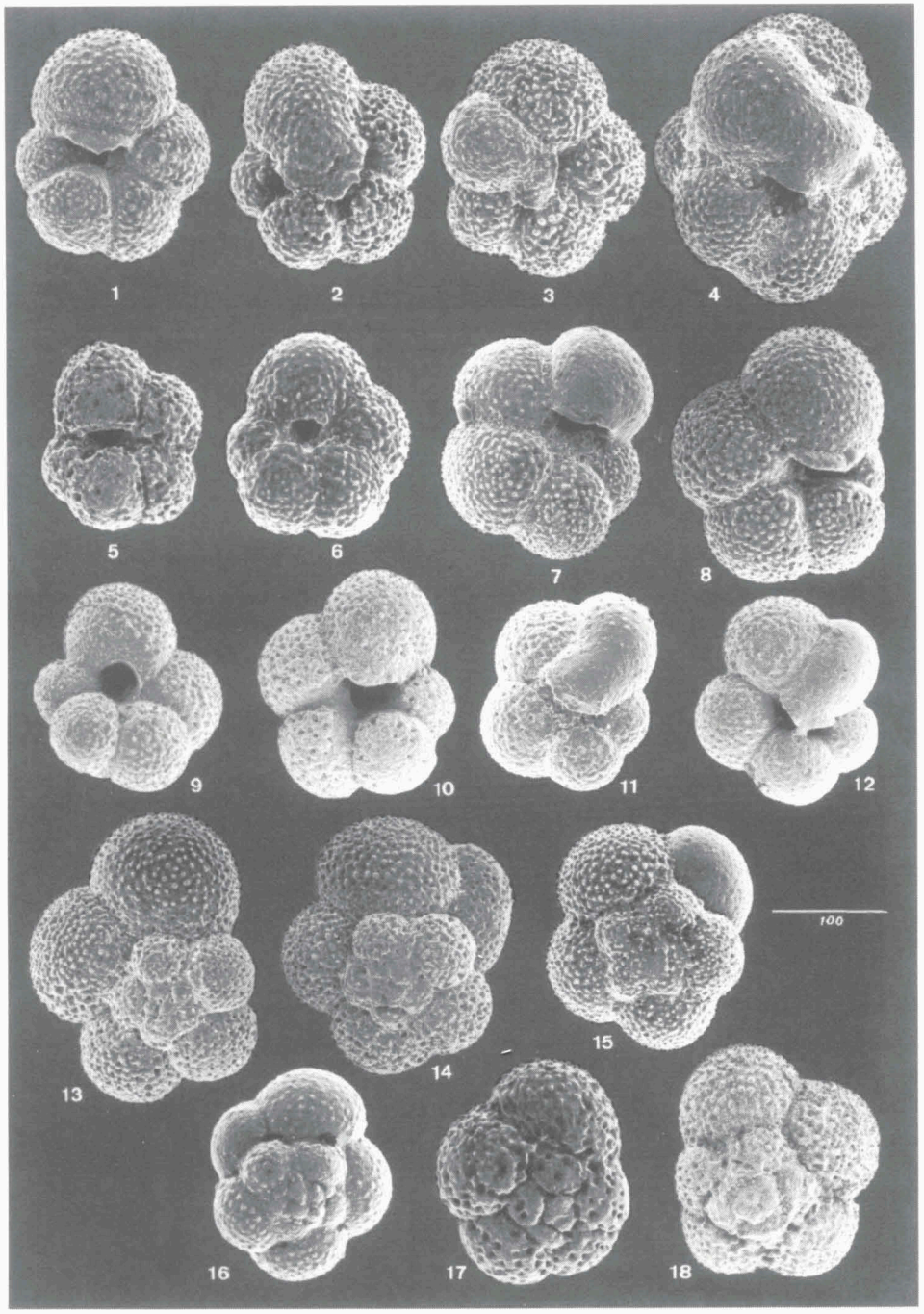
1
2
3
4
5
6
7
8
9
10
11
12
13
14
15
100
16
17
18

Plate 12

Turborotalita quinqueloba (Natland, 1938). Figs. 1-2, 3, 4 and 5 are specimens from sample 450, 100, 702 and 70, respectively. The 100 μm scale bar applies to figs. 1-5 while the 10 μm bar to figs. 6-14.

Figs. 1-5. Side views.
1. Large specimen with lip projecting away from aperture; RGM 360 321.
2. Part of lip is attached to an earlier chamber; RGM 360 322.
3. Lip projects inward partially closing aperture; RGM 360 323.
4. More oblong and less inflated specimen than those in figs. 1-3; RGM 360 324.
5. Small, compact with smooth texture; RGM 360 325.

Figs. 6-11. Enlarged views.
6. Penultimate chamber of specimen in Pl. 10, fig. 6 showing medium-sized, irregularly-spaced pores and spine bases.
7. Terminal chamber of specimen in Pl. 11, fig. 2; note pore doublets (a).
8. Less dense pores and spine bases in last chamber of specimen in Pl. 11, fig. 4; note uneven coating of calcite.
9. Penultimate chamber of specimen in Pl. 11, fig. 13 showing dense, medium- sized pores and rounded to subrounded spine bases with circular holes.
10. Ultimate and penultimate chambers of specimen in Pl. 11, fig. 5 shows calcite encrustation covered most spine holes and pores. Uncovered pores of this small specimen are big.
11. This small specimen (same as in Pl. 11, fig. 17; detail of penultimate chamber) has bigger and less dense pores than larger specimens of figs. 6 and 9.

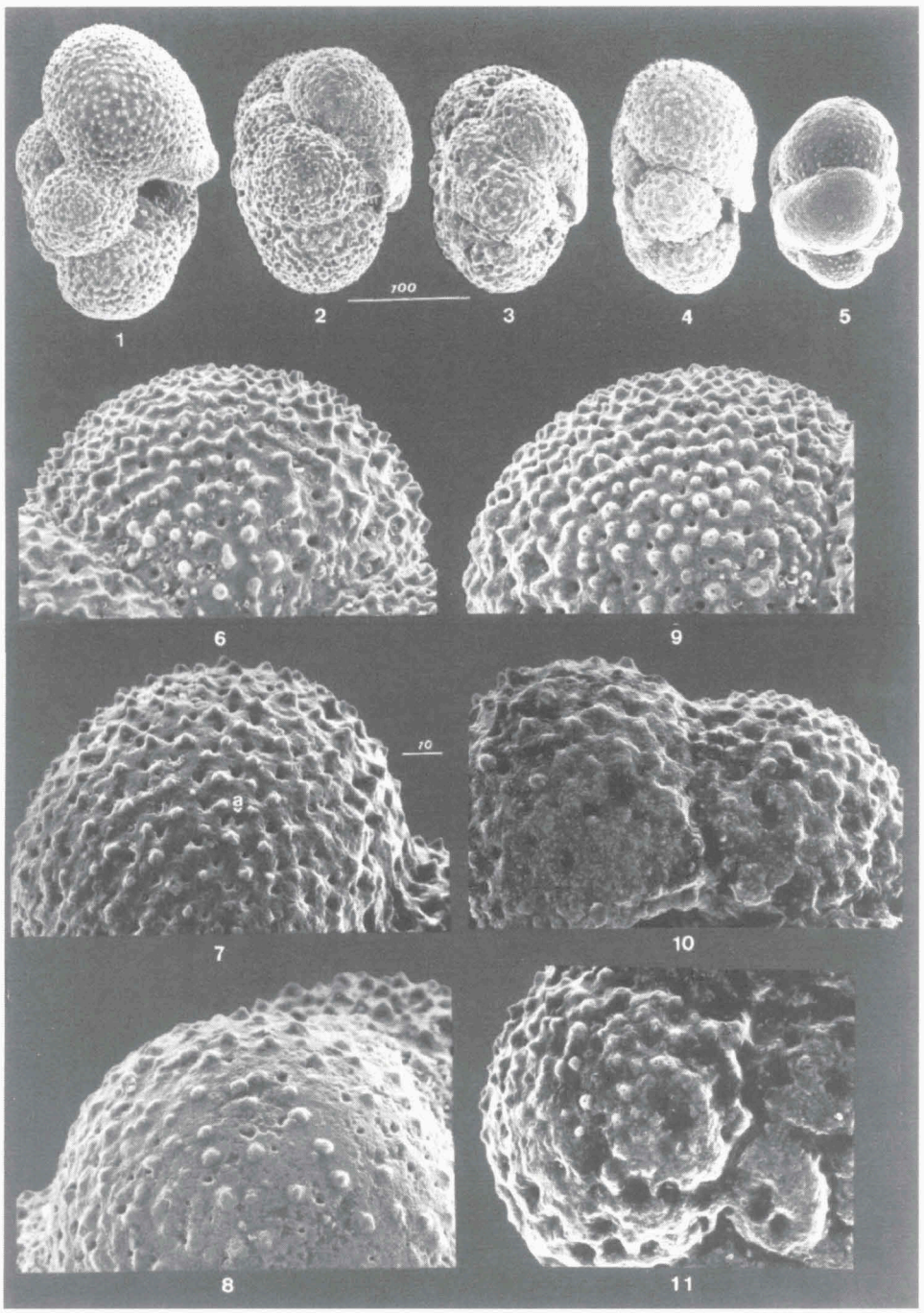
100
1
2
3
4
5
6
9
10
7
a
8
11